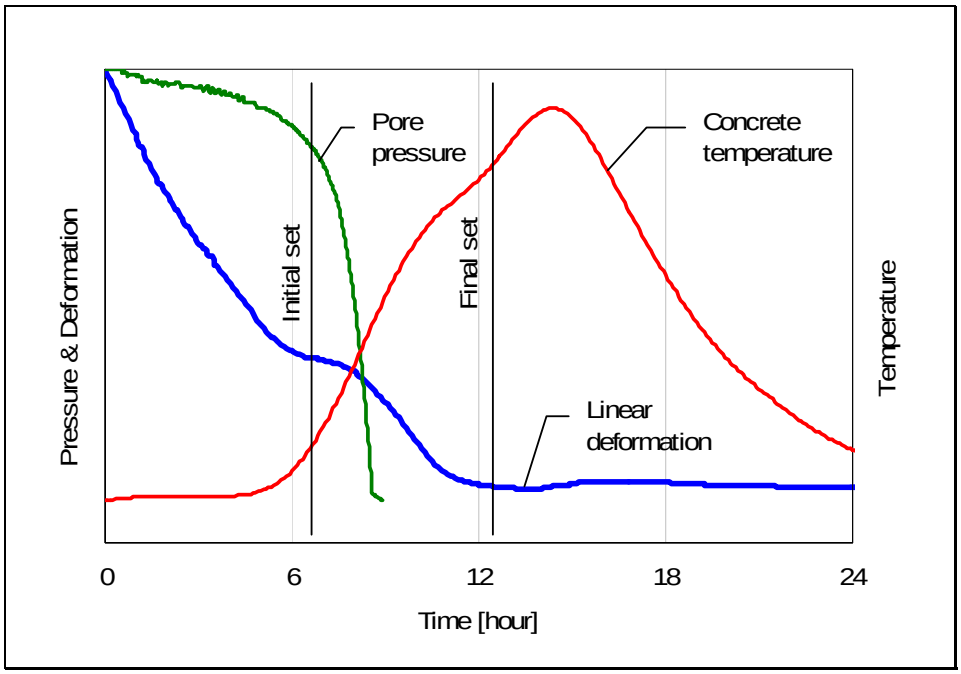

Cracking due to plastic and autogenous shrinkage - Investigation of early age deformation of self-compacting concrete

Experimental study

OSKAR ESPING
INGEMAR LÖFGREN

Department of Civil and Environmental Engineering
CHALMERS UNIVERSITY OF TECHNOLOGY
Göteborg, Sweden 2005

Report 2005:11

Cracking due to plastic and autogenous shrinkage - Investigation of early age deformation of self-compacting concrete

OSKAR ESPING & INGEMAR LÖFGREN

ISSN 1652-9162
Publication No Report 2005:11
Department of Civil and Environmental Engineering
Chalmers University of Technology
SE-412 96 Göteborg
Sweden
Telephone: +46 (0)31-772 1000
http://www.chalmers.se

Cover:
Picture showing the measures of autogenous linear deformation, temperature and pore pressure, of a SCC with w/c 0.45

Chalmers Reproservice
Göteborg, Sweden 2005

Abstract

Early-age shrinkage and cracking have become reoccurring problem in concrete construction. Conditions such as reduced maximum aggregate size, increased amount of fines, presence of retarding admixtures, increased binder content and deficient covering and curing all contribute to this problem. At early age, when the cement paste is young and has poorly developed mechanical properties, autogenous and evaporating shrinkage, both incorporated in the plastic shrinkage, are the two main driving forces for cracking. For modern concretes developing large autogenous shrinkage, as the high performance and self-compacting concrete (SCC), early-age cracking is a highly topical and important area.

When the concrete dries out due to evaporation there will be formation of water menisci near the concrete surface. The distance between the particles then tends to be reduced and the concrete will contract. These contracting capillary forces are in reverse ratio to the meniscus radius. The capillary tension stresses will therefore increase with decreasing interparticle spaces. For a concrete where the evaporation is prevented, the negative capillary pressure will also start to develop as the concrete sets. As a solid skeleton starts to form the chemical shrinkage is not totally transformed into external volume change and, if the water supply is restricted, empty pores will be formed inside the paste and water meniscus occurs.

In this work, early age (< 24 h) autogenous deformation and crack tendency due to plastic shrinkage was measured. For the autogenous deformation, a specially developed digital dilatometer was used with great satisfactory, generating accurately measures of the linear displacements of the concrete cast in a vapor proof flexible tube mould. The plastic shrinkage cracking tendency was evaluated, using a modified Nordtest method (NT BUILD 433), where the concrete sample was exposed to early drying conditions and where the restraining inner steel ring causes development of tangential stresses which if sufficiently high leads to cracking. As the underlying mechanisms are not quantified by the ring-test and as plastic shrinkage strongly are related to the negative capillary pressure in fresh concrete, the test was complimented with transducer recording the development of the pore pressure. In some cases, pore pressure development was also measured on sealed specimens, referring to the autogenous deformation tests.

A large number of different SCC constituents and mix compositions have been investigated; e.g. w/c-ratio from 0.38 to 0.67, coarse aggregate content, silica fume, fly ash, cement type, extra water and different admixtures (accelerator, retarder, shrinkage reducer, air entraining agent, superplasticizer dosage). For comparison, tests with standard concrete were made. The crack tendency test was also performed on mixes with different fibers and curing compounds.

The influence of different constituents and mixes on the autogenous deformation and plastic shrinkage crack tendency was significantly observed. The results indicated that:

- High crack tendency was generated when:
  - large autogenous shrinkage (silica addition, low w/c, high fineness)
  - high water evaporation (extra water, high w/c, low fineness)
  - retardation (retarder, slow hardening cement, high superplastisizer dosage),
  - low content of coarse aggregate
- Minimum crack tendency at w/c 0.55

- Reduced crack tendency by:
  - shrinkage reducing admixture (large positive effect on both autogenous shrinkage and evaporation, without influencing the time to initial- and final set)
  - acceleration (accelerator, rapid cement)
  - air entraining agent
  - fibers
  - wax membrane (effectively for concretes with high evaporation)

Finally the ring-test method and the experimental results were clearly verified by field studies.

Keywords: shrinkage, deformation, chemical, autogenous, drying, plastic, evaporation, early age, crack, pore pressure, self-compacting concrete.

Sammanfattning

Tidig krympning och sprickbildning är idag ett stort problem. Betong med minskad stenandel, ökad andel finmaterial, tillsatsmedel med retarderande effekt, ökad andel bindemedel samt brisfällig täckning och membranhärdning bidrar alla till problematiken. I tidig ålder när cementpastans mekaniska egenskaper fortfarande relativt lite utvecklade, är autogena och avdunstningskrympningen, vilka båda innefattas i den plastiska krympningen, de två främsta orsakerna till tidig sprickbildning. För moderna betonger som utvecklar stor autogen krympning, såsom högpresterande och självkompakterande betong (SKB), är tidig sprickbildning ett högaktuellt och viktigt område.

När avdunstningen får betongen att torka ut kommer vattenmenisker att bildas nära betongens yta. Avståndet mellan partiklarna tenderar att minska och betongen vill dra ihop sig. Dessa sammandragande kapillära krafter står i omvänd relation till meniskernas radier, och kommer därför att öka med minskat interpartikulärt avstånd. För betonger där avdunstningen är förhindrad kommer det kapillära undertrycket också att utvecklas så fort betongen hårdnar. Så fort ett fast skelett börjar bildas kan den kemiska krympningen inte direkt omsättas till en extern volymminskning och, om tillgången på vatten är begränsad, tomma porer med vattenmenisker kommer att bildas.

I detta arbete har mätningar gjorts på den tidiga (< 24 h) autogena deformationen och plastiska sprickbildningen. En speciellt utvecklad betongdilatometer har används för mätningen av den autogena deformationen, där längdförändringen hos de täta flexibla provkropparna med betong mättes med stor noggrannhet. Den plastiska spricktendensen utvärderades med en modifierad Nordtest metod (NT BUILD 433), där betongen exponerades för tidig uttorkning samtidigt som en inre mothålland stålring skapade tangentiella spänningar som om tillräckligt stora genererade sprickbildning. Eftersom de underliggande mekanismerna till krympning inte kvantifieras med ringtest-metoden, och eftersom den plastiska krympningen är starkt kopplad till det kapillära undertrycket i den färska betongen, kompletterades försöken med givare för portrycksmätning. I vissa fall mättes betongens portryck hos förseglade prover, för att kunna relatera till de autogena krympförsöken.

Ett stort antal försök med olika delmaterial och sammansättningar av SKB har gjorts, såsom vct från 0,38 till 0,67, varierande stenhalt, silika, flygaska, olika cementtyper, extra vattentillsats och olika tillsatsmedel (accelerator, retarder, krympreducerare, luftporbildare, flytmedelsdos). Som jämförelse, testades standardbetong. Ring-försöken kompletterades även med olika fibrer och membranhärdare.

De olika delmaterialen och sammansättningarna hade en tydlig påverkan på den autogena deformation och plastiska sprickbildningen. Resultaten indikerar att:

- Hög spricktendens genererades när betongen hade:
  - stor autogen krympning (silika tillsats, lågt vct, hög finhet)
  - hög avdunstning av vatten (extra vatten, högt vct, låg finhet)
  - retardation (retarder, långsamt hårdnande cement, hög flytmedelsdos),
  - låg stenhalt och liten maximal stenstorlek
- Vid vct 0,55 var sprickbildningen som minst.
- Minskad spricktendens vid:

- krympreducerare (positiv effekt på både autogena krympningen och avdunstningen, utan att påverka tidpunkten för betongens tillstyvnande)
- acceleration (accelerator, snabbhårnande cement)
- luftporbildare
- fibertillsats
- vaxbaserad membranhärdare (effektiv hos betonger med stor avdunstning)

Genom fältförsök kunde ringtest-metoden och de experimentella resultaten tydligt verifieras.

Nyckelord: krympning, deformation, kemisk, autogen, uttorkning, plastisk, avdunstning, spricka, portryck, självkompakterande betong.

Preface

In December 1995 SBUF granted Färdig Betong founds to a project where the aim was to develop a test method and a calculation tool to, at a given climate, determine the risk for early age cracking. The project was performed at the department of Building Material, at Chalmers University of Technology. For a number of reasons it was not finished according to the plan. A number of attempts have been made to restart the project with modified alignment, unfortunately without successful results. However the work performed has resulted in the two reports:

1. Dejke V., Radocea A., "Mätmetoder för bestämning av mekaniska egenskaper hos Betong i mycket tidig alder". Publication P-98:4, Chalmers University of Technology, 1998.

2. Rodhe M., Nilsson L-O., "Sprickbildning på grund av plastisk krympning – försök att reproducera sprickbildning i SKB", Work report, Chalmers University of Technology, 2002.

Cracking due to early age deformation still is a highly topical and important area, especially for self-compacting concrete, why it was important to bring the project to conclusions.

The present work is less theoretical and is a restart, rather then a continuation, of the previous work, where the aim of was to investigate early autogenous and drying shrinkage of self-compacting concrete and to evaluate and develop suitable test methods to monitor this. Guidelines and recommendations for mix design and curing actions in order to minimize the risk of early age cracking is published in a SBUF report (5038) as a extended outcome of this project.

The work has mainly been conducted at the main laboratory of AB Färdig Betong in Göteborg, during the period May 2004 - August 2005.

Grateful thanks are addressed to:

- ☺ Björn Andersson, AB Färdig Betong
- ☺ Martin Hansson, Sika AB
- ☺ Rolf Jonsson, Wäst-Bygg AB
- ☺ Rickard Jörgensen, AB Färdig Betong
- ☺ Mats Karlsson, Thomas Concrete Group AB
- ☺ Tomas Kutti, Thomas Concrete Group AB
- ☺ Marek Machowski, Chalmers University of Technology
- ☺ Sten Rodenstam, Nordkalk AB
- ☺ Mats Rodhe, Chalmers University of Technology
- ☺ Fredrik Svensson, AB Färdig Betong
- ☺ Pär Åhman, Swedish Construction Federation

Finally, we would like to direct a special thanks to SBUF and AB Färdig Betong for their generous donation and their confidence in us.

Göteborg, August 2005

Oskar Esping & Ingemar Löfgren

Contents

1 Introduction

A source of deleterious cracking already in the construction stage is the early age shrinkage due to evaporation (often referred to as plastic shrinkage) and the volume change related to hydration reactions and autogenous shrinkage phenomena. As the use of high-performance and self-compacting concrete has increased, early-age shrinkage and cracking have become a cause of great concern. Conditions such as reduced water-binder ratio (w/b), increased binder content, reduced maximum aggregate size, and increased amount of fines all contribute to this problem. Early age cracking due to evaporation occurs when the concrete is in its 'plastic stage'. In traditional concretes it is mainly caused by the loss of water from the fresh concrete, e.g. by evaporation of water from the surface or by suction of water by the formwork material or by the sub-base. Loss of water from the paste generates negative capillary pressures. This cause the paste to contract, which, in turn, can lead to cracks. To avoid this type of cracks, care has to be taken to protect the surface against drying. However, experience with the use of low w/b concretes have revealed that severe cracking may occur in spite of proper protection (curing membrane, plastic sheets, water spray, etc), see e.g. Bjøntegaard et al (1998). Furthermore, self-compacting concrete seems to be especially susceptible to early-age cracking since there is no separation of bleeding water on the surface. However, there are also other internal effects that could be contributing. These include: suction of water by the fine material (e.g. lime filler or manufactured sand) and the increased chemical shrinkage and autogenous deformation in the early age when the concrete is setting and starting to harden.

Cracking is a complex phenomenon dependent on several factors including the rate of shrinkage, degree of restraint, and stress relaxation. Compared with long term drying shrinkage, which generally develops from the surface of the concrete, autogenous shrinkage progresses uniformly through the concrete member and are more likely to cause cracking, because it develops more rapidly and occurs when the cement paste is young and has poorly developed mechanical properties (strain capacity, modulus of elasticity, fracture energy, etc.).

There are two main driving forces for early age shrinkage: (1) Early age drying shrinkage may develop due to loss of water from the fresh concrete, and (2) shrinkage due to hydration and chemical reactions produces autogenous shrinkage. Temperature dilation may also in some cases contribute (e.g. when cooling the surface). Accordingly, the cracking tendency in the initial phase is a product of several factors. Thus, it is important to separate the mechanisms into those that are dependent on environmental conditions (e.g. evaporation of water from the surface) and those that occur without moisture transfer to the environment and which are associated with the autogenous deformation of the material. The former may be controlled by an appropriate curing while the latter has to be tackled by proper mix design. Furthermore, this also suggests that for investigating the early-age deformations and the risks of cracking two methods should be used in parallel: one method for quantifying the autogenous deformation and another method to investigate the effects of moisture exchange. A test rig for early age cracking due to evaporation (the NORDTEST method "Concrete: Cracking tendency – Exposure to drying during the first 24 hours " NT BUILD 433) is alone not sufficient in order to approach a better understanding of the involved mechanisms. Therefore, the more fundamental factors with focus on the autogenous shrinkage have been investigated by using a concrete digital dilatometer developed by the authors.

1.1 Aim

The primary aim of the project was to investigate factors (materialparameters) which influence/effect autogenous shrinkage, evaporation, and development of early-age cracks. In addition, the aim was to increase the understanding of the underlying mechanisms.

The outcome of the project is to be used to provide guidelines for appropriate mix design (e.g. type and amount of filler material and the possible addition of fibres) and curing conditions in order to minimize the risk of early age cracking due to evaporation.

1.2 Terminology

Linear deformation; the relative change in length due to shrinkage or expansion, referred to the specimen origin length.

Autogenous deformation; the unrestrained, time-depending, bulk deformation of fresh and hardening sealed concrete at a constant temperature.

Shrinkage; when the deformation is a contraction, it may be referred to as shrinkage, e.g. autogenous shrinkage.

Chemical shrinkage; shrinkage due to cement hydration. The hydration products occupy less space than the original reactants. Chemical is the major factor causing autogenous shrinkage.

Drying shrinkage; shrinkage caused by loss of water (humidity) due to evaporation. When water evaporates from the fresh and hardening concrete, tensile stress build up in the capillaries causing the concrete to contract. In the fresh stage, defined as plastic shrinkage.

2 Background

2.1 Hydration and development of microstructure

The hydration of Portland cement is a complex sequence of overlapping chemical reactions between clinker components, calcium sulphate, and water, leading to setting and hardening. Immediately after mixing cement and water reactions starts to occur, which generates an outburst of heat (Stages 0 and I in Figure 1). After these initial stages an induction period, or dormant period, is entered (Stage II). During the induction period not much hydration takes place, but this does not mean that the paste is "dormant" with respect to volume changes. Setting (Stage III) is defined as the onset of rigidity in fresh concrete, see Figure 1. In Figure 2, the products associated with the stages of cement hydration and the change of porosity can be seen. The setting process is the consequence of a change from a concentrated suspension of flocculated particles to a viscoelastic skeletal solid capable of supporting an applied stress, see Figure 3. Setting is controlled primarily by the hydration of C_3S and occurs when the induction period is terminated by a rapid hydration of C_3S leading to a fast temperature rise of the concrete (Stage III), see Mindess at el. (2003). However, hydration is highly influenced by a number of parameters such as: (1) the water cement ratio; (2) the fines of the cement and its composition (the main clinker components); (3) addition of supplementary materials (such as fly ash and silica); (4) admixtures (super plasticizer, accelerator, retarder, etc.); and (5) the temperature.

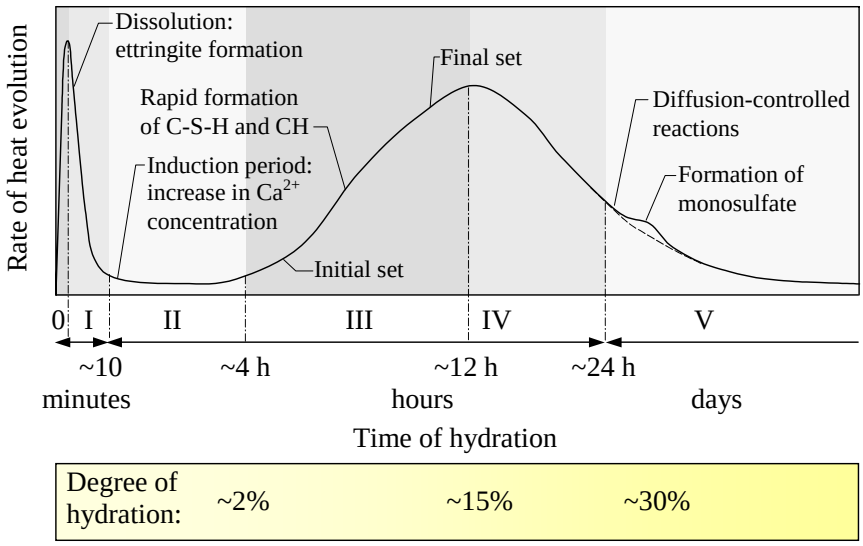

Figure 1. Schematic representation of heat evolution during hydration of a cement, based on Gartner at al. (2002).

As long as the concrete is fluid there will be a linear relationship between the linear shrinkage and the volumetric chemical shrinkage, see RILEM TC 181-EAS. However, once the self-supporting skeleton starts to form the chemical shrinkage will mainly result in internal voids and the linear deformation diverges from the chemical shrinkage. Moreover, when measuring the linear deformation the setting will be manifested as a change of the slope of the deformation (see Figure 4).

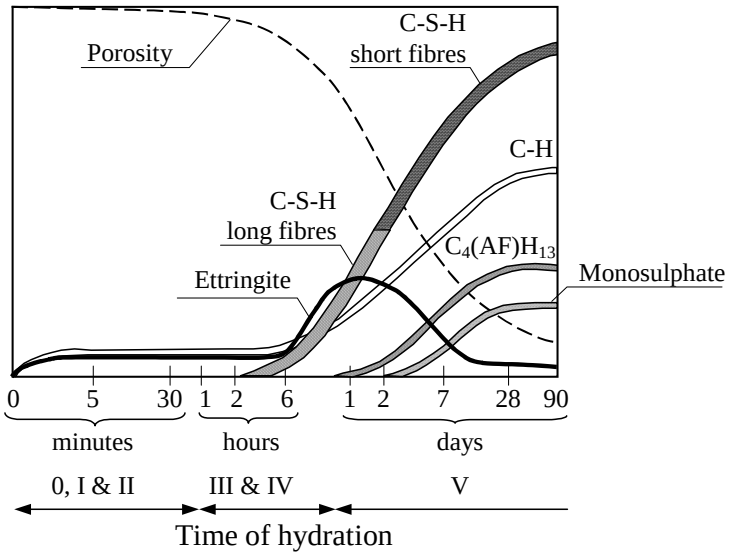

Figure 2. Products associated with the stages of cement hydration (from Locher et al. 1976).

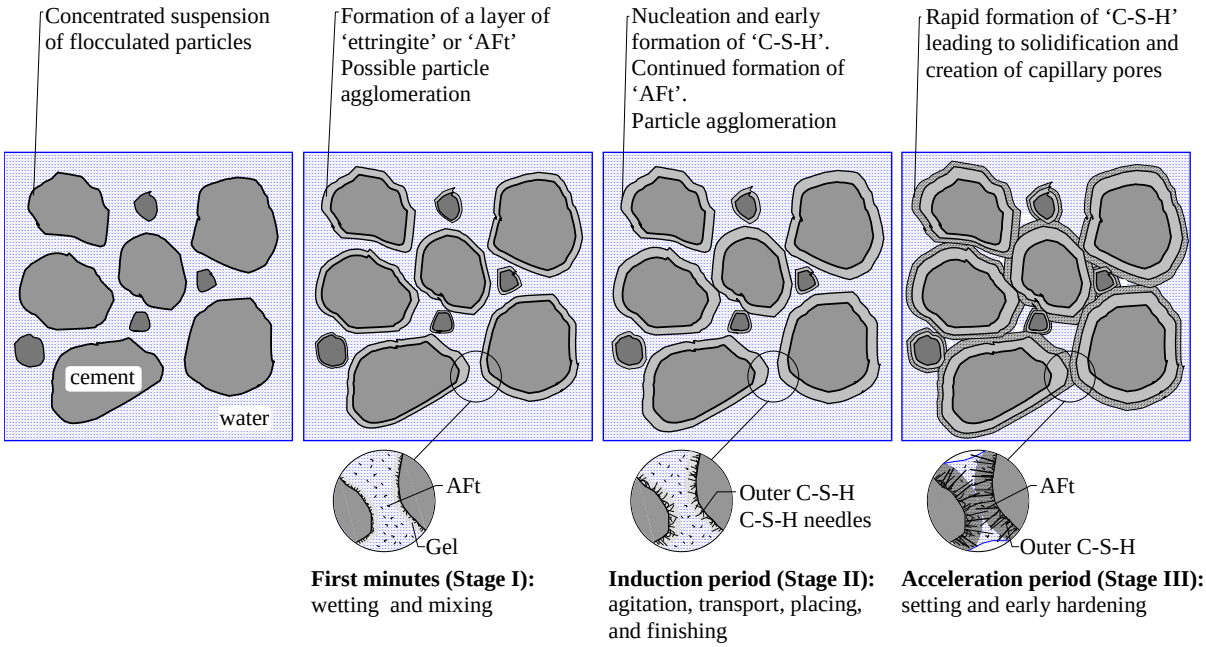

Figure 3. Schematic representation of the early microstructural development.

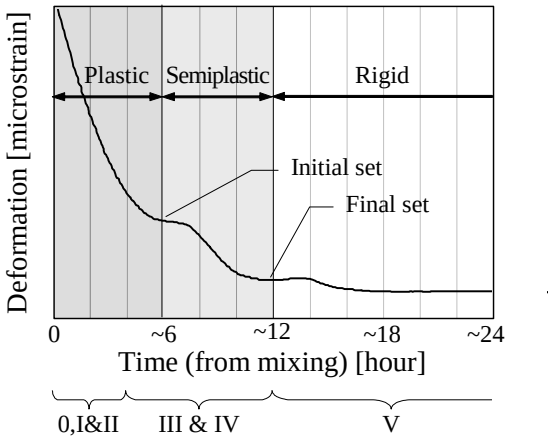

Figure 4. Schematic representation of the early-age linear autogenous defromation.

The setting also results in the creation of the first capillary pores and changes the transport properties, which, for example, has an influence on the early evaporation as this is slowed down (see Figure 5).

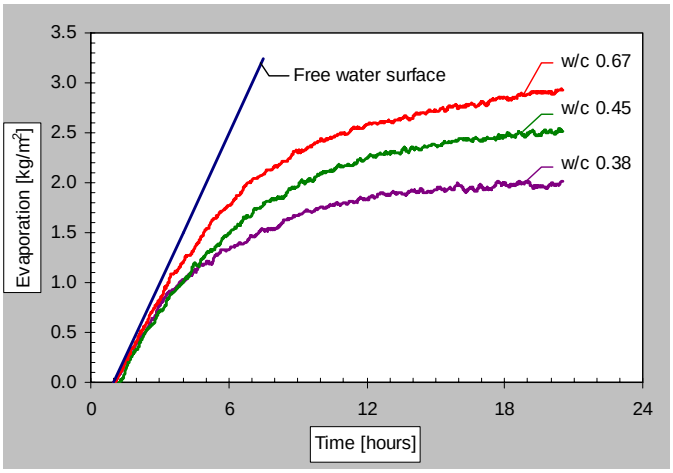

Figure 5. Example of evaporation from self-compacting concrete with w/c from 0.38 to 0.67.

2.2 Plastic shrinkage cracking

Plastic shrinkage is in the literature defined as the shrinkage of fresh concrete, exposed to drying, that takes place during the time when the concrete is 'plastic', see e.g. Neville (2000). The duration is usually short and ends when the concrete has reached its final set. If the shrinkage is non-uniform, or if there is restraint, tensile stresses develops which may result in cracking as the concrete has a low tensile strength and strain capacity at this stage, see Figure 6. These cracks are usually referred to as 'plastic shrinkage cracks'. However, it is difficult to distinguish between plastic shrinkage cracks and cracks caused by thermal dilation (e.g. rapid cooling during night) or early age drying and autogenous shrinkage. The cracks may or may not be detrimental to the structural integrity and durability, but they are unsightly since they are usually wide, long, and visible to the unaided eye. Moreover, it is not uncommon, especially in slabs, that these cracks run through the whole depth of the member.

The environmental factors that promote early age cracks are wind speed, air temperature, and the relative humidity. These factors, together with the temperature of the concrete, govern the rate of evaporation from the concrete. It is suggested that if the evaporation exceeds 1.0 kg/m^2/h there is a significant risk of cracking, but cracks may occur also at evaporation rates lower than 0.5 kg/m^2/h. For example, the experience with the use of low w/b concretes, e.g. in bridge decks, has revealed that severe cracking may occur in spite of proper protection (curing membrane, plastic sheets, water spray, etc), see Bjøntegaard et al. (1998). It has been suggested that if the early age shrinkage magnitude exceeds 1 mm/m (1000 μstrain), there is a high risk of cracking (see Holt 2001). This corresponds well to the American Concrete Institute guidelines (see ACI 209-92) where it is stated that cracks may occur for an shrinkage of about 0.4–1.0 mm/m (400–1000 μstrain). Moreover, this seems to be consistent with the actual tensile strain capacity of the concrete during the early hours, see Figure 6.

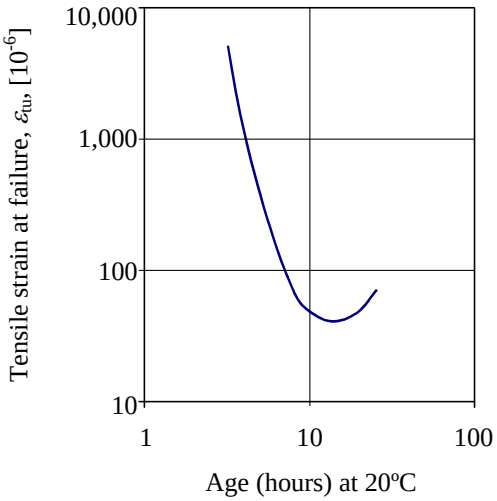

Figure 6. Relationship between tensile strain capacity and age of concrete, based on Kasai et al. (1972).

The prevalent theory is that plastic shrinkage is directly caused by evaporation of water from the concrete surface. If the rate of evaporation exceeds the rate of bleeding, the concrete surface dries out which leads to the formation of water menisci near the concrete surface. The creation of water menisci results in a negative pressure in the pore water and consequently contraction forces between particles. The average distance between the particles then tends to be reduced and the concrete will contract. These capillary forces are in reverse ratio to the meniscus radius. The capillary tension stresses will therefore increase with decreasing interparticle spaces (low w/b, high fineness etc.). Practical observations support the theory of plastic shrinkage, as cracks tend to occur in hot, dry and windy weather conditions leading to extensive drying of the concrete.

For a concrete where evaporation is prevented, the capillary pressure (negative) will also start to develop as the concrete sets. As a solid skeleton starts to form, the chemical shrinkage is not totally transformed into external volume change. If the water supply is restricted, empty pores will be formed inside the paste and an air-water menisci occurs (see Figure 7). The capillary force (P_c) that is generated can be described by the Gauss – Laplace's equation (1), which relates the pressure to the capillary radius, and by the Kelvin's equation (2), which relate the pressure to the relative humidity (RH):

$$P_c - P_v = \gamma\left(\frac{1}{r_1} + \frac{1}{r_2}\right) \quad (1)$$

where P_c is the capillary tensile pressure [MPa]; P_v is the vapour pressure [MPa]; γ is the surface tension of the capillary water [N/m]; and r_1 and r_2 are the principle radii of curvature.

$$P_c - P_v = \frac{R \cdot T}{M \cdot \nu} \cdot \ln(RH) \quad (2)$$

where R is the ideal gas constant [8.314 J/mol K]; T is the absolute temperature [K]; M is the molar mass of water [kg/mol]; ν is the water specific volume; and RH is the relative humidity

If the two equations are combined, and by setting P_v equal to zero and r_1 equal to r_2, the following relationship is obtained:

$$P_c = -\frac{2\gamma}{r} = \frac{R \cdot T}{M \cdot \nu} \cdot \ln(RH) \quad (3)$$

Equation (3) shows that a small reduction in RH leads to very large capillary tensile pressure. The pressure can only develop if there are partly empty pores available in the system. Empty pores will be created during the hydration and the RH will drop because of dissolution of salts into the pore water.

According to Powers (1968) the maximum capillary pressure developed in a cement mixture is indirectly proportional to the *w/c*:

$$P_c = 1 \times 10^{-3} \frac{\gamma \cdot S}{w/c} \quad (4)$$

where P_c is the capillary tensile pressure [MPa]; γ is the surface tension of the capillary water [N/m]; and S is the mass specific surface area of the cement [cm^2/kg].

Assuming that γ = 0.07 N/m, S = 350 m^2/kg, and w/c = 0.55, the capillary pressure calculated by equation (4) is 45 kPa.

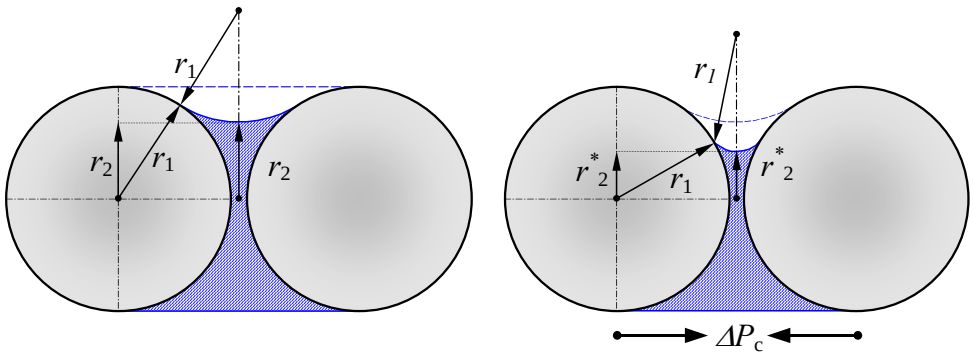

Figure 7. Schematic representation of liquid filled joint between two spherical particles at the surface.

3 Experimental investigation

3.1 Materials and mix design

The mix design and its constituents, used in this study, represent commonly used materials and compositions of self-compacting concrete (SCC) in Sweden.

3.1.1 Materials

Aggregates

Three different aggregates have been used in this study, see Table 1 and Figure 8.

Table 1. Physical properties of aggregates.

ID	Product name	Supplier	Type	Density [kg/dm^3]	Spec surface area by BET(H_2O) [m^2/kg]
A 0-4	Sjögärde	Färdig Betong	Natural	2670	3012
A 0-8	Hol	Färdig Betong	Natural	2650	1755
A 8-16	Kungälv	Färdig Betong	Crushed	2700	93

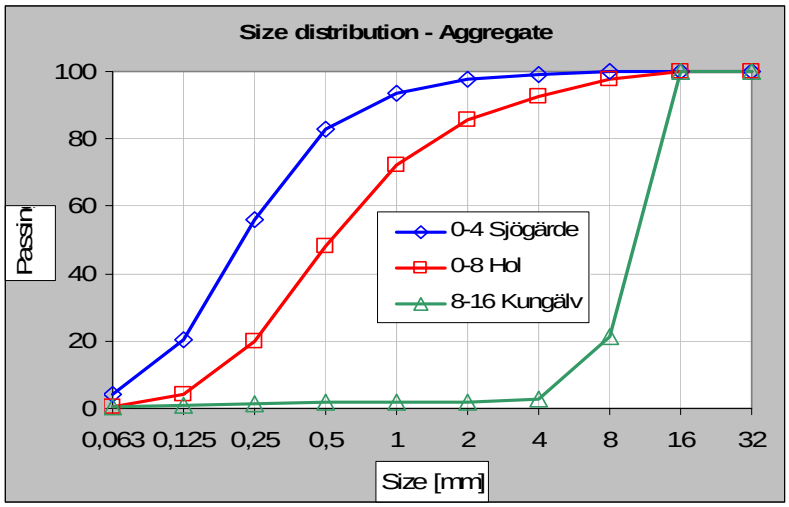

Figure 8. Aggregate size distribution.

Cementitious and pozzolanic materials

Three different cements types and two pozzolans have been used, see Table 2 and Figure 9.

Table 2. Physical properties of cementitious and pozzolanic materials.

ID	Product name	Supplier	Type	Density [kg/dm^3]	k-value [-]	Spec surface area by BET [m^2/kg]
BYGG	Byggcement Std PK Skövde	Cementa	CEM II/A-LL 42.5R	3080	1.0	2000 (N_2)
SH	Portlandcement SH P Skövde	Cementa	CEM I 52.5R	3150	1.0	1900 (N_2)
ANL	Anläggningscement Std P Skövde	Cementa	CEM I 42.5N	3200	1.0	950 (N_2)
SF	Microsilica	ELKEM	Silica fume	2250	2.0	~20 000 (N_2) 21437 (H_2O)
FA	EFA-Füller BF 1	BauMineral	Fly ash - type 2	2270	0.4	~3000 (N_2) 3234 (H_2O)

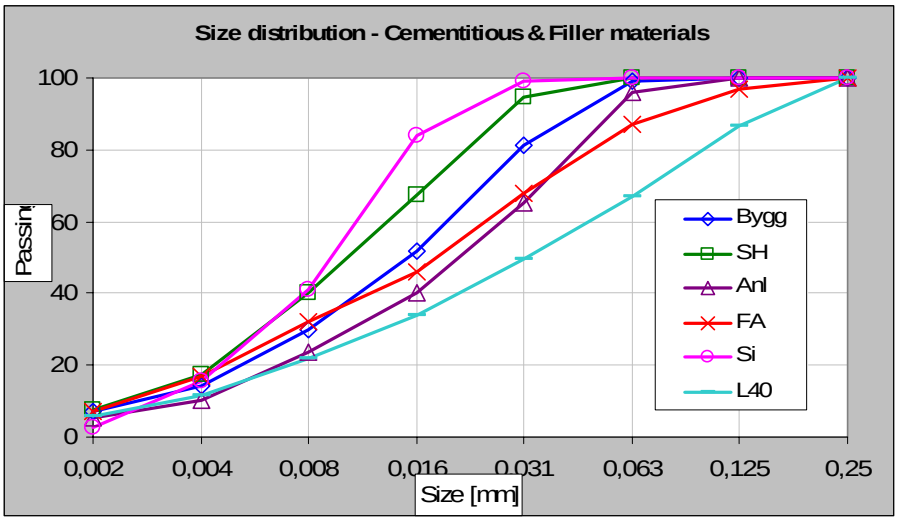

Figure 9. Cementitious and filler materials size distribution.

Filler

One mineral filler have been used, see Table 3 and Figure 9.

Table 3. Physical properties of filler material.

ID	Product name	Supplier	Type	Density [kg/dm^3]	Spec surface area by BET [m^2/kg]
F	Limus 40 (L40)	NordKalk	Ground limestone	2670	1400 (N_2) 1410 (H_2O)

Admixtures

Five different types of admixtures have been tested in this study, see Table 4.

Table 4. Physical properties of admixtures.

ID	Product name	Supplier	Type	Density [kg/dm^3]	Dry content [weight%]
SP	Sikament 56 (S56)	SIKA	Superplastisizer (polycarboxylate ether based)	1100	37%
ACC	SikaRapid-1	SIKA	Accelerator (sodium based)	1200	37%
RE	SikaRetarder	SIKA	Retarder (phosphate based)	1200	27%
SRA	SikaControl-40	SIKA	Shrinkage reducing admixture (polymeric glycol based)	1000	-
AEA	SikaAer-S	SIKA	Air entraining agent (synthetic surfactant based)	1010	4.5%

Fibers

Three different types of fibres have been tested in this study, see Table 5.

Table 5. Physical properties of investigated fibres.

Type	Product name	Supplier	Diameter x Length [mm]	Density [kg/dm^3]	Tensile strength [MPa]	Elasticity modulus [GPa]
Polypropylene Monofilament	Eurofibre 512 PB	BKN Byggkemi	17 – 21 x 12	910	240	5.7
Nylon Monofilement	MultiMesh	NYCON	36 x 19	1160	303	1.57
Alkali Resistance Glass (ARG)	Super-Cracknon ACS 13H-530X	Nippon Electric Glass	13.5 x 13	2700	1 400	74

Curing compounds

Three different curing membranes were investigated, two were acrylic-based while one was based on wax. The membranes were sprayed on the concrete surface approximately 50 minutes after mixing. The amount of membrane sprayed on the surface was according to the manufacturers recommendations.

Acrylic-based membranes:

- SikaTop-71 (from SIKA): 0.2 l/m^2 applied.
- Masterkure 111 CF (from Master Builders): 0.15 l/m^2 applied (diluted 1:6 with water)

Wax-based membrane:

- Antisol-E (from SIKA): 0.2 l/m^2 applied.

3.1.2 Mixture design

All mixes were designed to have a water to filler ratio by volume of one, w/f=1.0 (Okamura 1997). As filler, all solid material smaller then 0.125 mm was included.

The mixes were made in batches of 30 to 60 liters, mixed in a BHS-60 twin-shaft paddle mixer (see Figure 10) for four minutes after water was added to the premixed dry materials.

Figure 10. Photo of BHS mixer used throughout the study.

Four reference mixes with w/c 0.38, 0.45, 0.55 and 0.67 (see Table 6 and Figure 11) were investigated.

Table 6. Recipe of reference mixes.

			SCC 038 REF (w/c 0.38)		**SCC 045 REF** (w/c 0.45)		**SCC 055 REF** (w/c 0.55)		**SCC 067 REF** (w/c 0.67)	
Id	**Material**	**Product name**	**m_{drv} [kg/m^3]**	**V_{drv} [vol%]**	**m_{drv} [kg/m^3]**	**V_{drv} [vol%]**	**m_{drv} [kg/m^3]**	**V_{drv} [vol%]**	**m_{drv} [kg/m^3]**	**V_{drv} [vol%]**
C	Cement	CEM II/A-LL 42.5R (Bygg)	420	13.6	380	11.9	340	10.6	300	9.4
W	Water	-	160	16.0	171	17.1	187	18.7	200	20.0
A 0-4	Aggregate	Sjögärde (0-4)	0	0 *(0%A)*	0	0 *(0%A)*	81	3 *(5%A)*	155	5.8 *(10%A)*
A 0-8		Hol (0-8)	1021	38.5 *(60%A)*	998	37.7 *(60%A)*	879	33.2 *(55%A)*	771	29.1 *(50%A)*
A 8-16		Kungälv (8-16)	694	25.7 *(40%A)*	678	25.1 *(40%A)*	651	24.1 (40%A)	628	23.3 *(40%A)*
F	Filler	Limus 40 (L40)	40	1.5	100	3.7	160	6	220	8.2
SP	Super-plasticizer	Sikament 56 (S56)	7.6 *(1.8%C)*	0.7	5.7 *(1.5%C)*	0.5	4.1 *(1.2%C)*	0.4	2.4 *(0.8%C)*	0.2

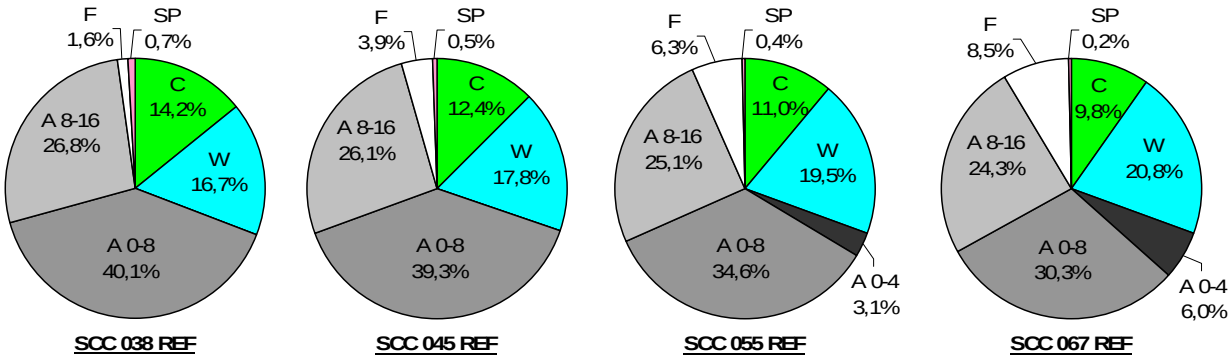

Figure 11. Reference mixes constituents distribution by volume.

To investigate the influence of different constituents the following mixes were studied:

1. Cement type; Reference mix SCC 067 with "BYGG" replaced by "SH" and "ANL" and reference mix SCC 055 with "BYGG" replaced by "ANL".

2. Coarse aggregate content; Reference mix SCC 055 with 20% to 50% "8-16 Kungälv" of total volume of aggregate. The changes were replaced by equal volume of "0-8 Hol".

3. Water content; Reference mix SCC 067 with 6 and 12 liters extra water (W). The extra water corresponds to approximately 0.5% and 1.0% incorrect gravel moisture content. The changes were replaced by equal volume aggregate.

4. Fly ash; Addition of 25% FA by cement weight to the mixes SCC 045 REF, SCC 055 REF and SCC 067 REF. The FA reduced the cement content with an efficiency factor of 0.4, so the water to binder ratio (w/b) was equal to w/c in the reference. The surplus of the FA was adjusted by reduced filler content.

5. Silica fume: Addition of 5% and 10% SF by cement weight to mix 055 REF. The cement was reduced by the corresponding addition of SF volume. No efficiency factor was used (w/b of 0.54 and 0.53 with a factor of 2.0)

6. Superplasticizer dosage; Reference mix SCC 067 with 0.6%, 0.8% (REF) and 1.0% SP dosage of cement weight.

7. Accelerator and retarder; Addition of 1.5% ACC and 0.2% RE by cement weight to mix SCC 067 REF.

8. Shrinkage reducing admixture; Addition of 1.0% and 2.0% SRA by cement weight to mixes SCC 045 REF, SCC 055 REF and SCC 067 REF.

9. Air entraining agent; Addition of 0.005% and 0.01% AEA (concentrate) by cement weight to mix SCC 067 REF.

10. Fibres; Addition of 0.1% Polypropylene, 0.05% Glass or 0.1% Nylon fibres by total volume to mix SCC 067 REF. The addition was replaced by reduced aggregate content.

3.2 Test methods

3.2.1 Concrete Digital Dilatometer (CDD) test

The concrete digital dilatometer is a test method for evaluation of linear autogenous deformation of fresh and hardening concrete at sealed conditions and constant temperature (see Appendix A). With this method is possible to start measure before setting, when concrete is fresh. The method is a modification of the CT1 digital dilatometer for pastes and mortars, see Jensen & Hansen (1995).

The concrete is cast in a vapour proof flexible polyurethane (PE) tube mould with inner diameter 82 mm and specimen length ~400 mm. The mould is placed in a mechanical stable measuring rig in a thermally controlled room (20±1ºC), and the unrestrained, time-depending, linear bulk deformation is recorded by a digital gauge (Mitutoyu 543-450B, resolution 1 μm and accuracy 3 μm) and logged with an interval of 5 minutes for a period of 24 hours or more.

Main equipment and apparatus for a typical test is three complete CDD set-up (mould consisting PE-tube, end-caps, fixture and hose-clamps and measuring rig), as shown in Figure 12. One of the specimens is to be equipped with one set of sensors for recording the concrete cross section temperature. The result from a test is presented graphically as the development of deformation (mean value from two or more tests) is plotted against time.

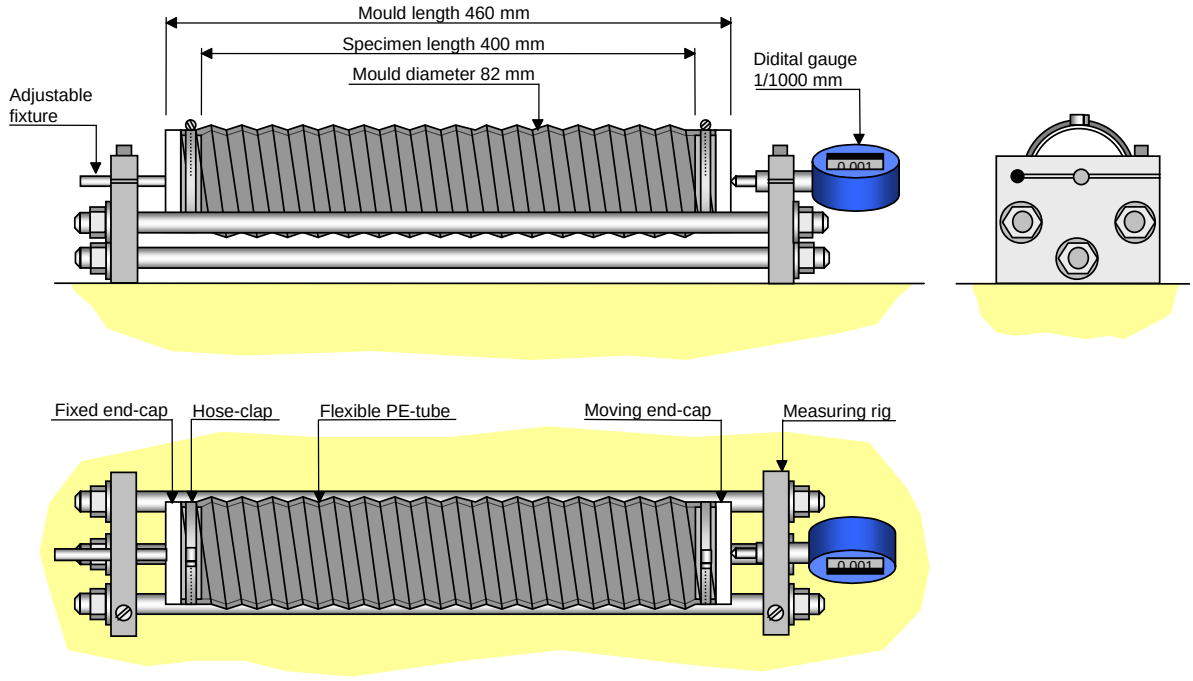

Figure 12. Test arrangement of the Concrete Digital Dilatometer (CDD) for linear autogenous deformation measurement.

3.2.2 Ring Test

The method is intended for the determination of the cracking tendency of concrete at early ages. The method was developed at NTNU/SINTEF by Johansen and Dahl (1993) (NORDTEST-method NT Build 433, see Appendix B) in order to map the influence of

material parameters on the cracking tendency at a “macro-level”. In the test, wind was blown over the fresh concrete surface restrained between two concentric steel rings and the crack sensitivity was expressed as a crack index. The test method evaluates the cracking tendency of concrete exposed to external drying immediately after casting. The method is intended for laboratory use and the test results cannot be directly transferred to predict the extent of cracking which will in practice occur under the prevailing field conditions. A drawback with this test method, as proposed in NORDTEST-method NT Build 433 (see NORDTEST, 1995), is that the test only provides information on the cracking tendency (i.e. if or if not the concrete cracks, the time of cracking, the number of cracks, the total crack length, and the crack width) but the underlying mechanisms are not quantified. As plastic shrinkage are thought to be related to the capillary pressure in fresh concrete, in this investigation the test method was also equipped with a Pore Pressure Transducer so that the development of the pore pressure could be recorded, see e.g. Wittmann (1976), Radocea (1992), and Holt (2001). The magnitude of the pressure drop depends on relative humidity, temperature, wind velocity, spaces between solid particles in the concrete, and permeability.

The specimens are ring-shaped, see Figure 13, and the concrete is cast between two concentric steel rings with diameter 300 and 600 mm with a depth of 80 mm. The steel rings have ribs attached to provide crack initiation and are fixed to a stiff base plate with a smooth surface, coated with a thin layer of oil. The steel rings are not oiled. After casting, the ring specimens are positioned under air funnels. The test conditions used in this investigation were: wind velocity = 4.5 m/s, air temperature = 23±2ºC, relative humidity = 35±5% RH.

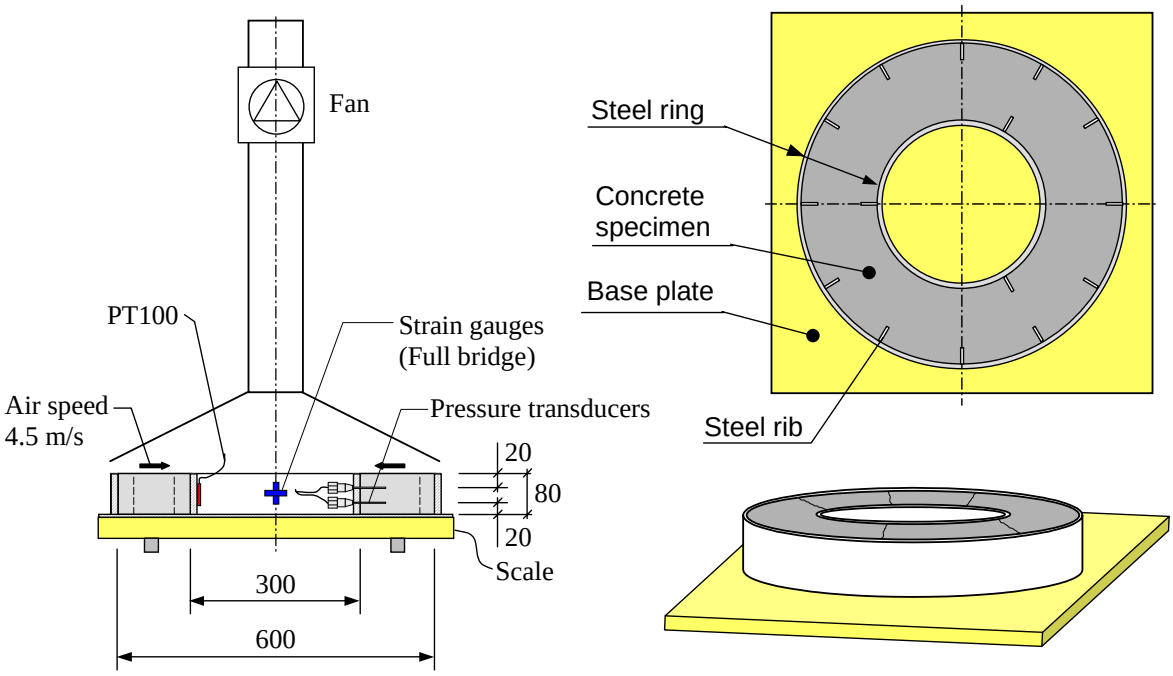

Figure 13. Test arrangement for the determination of the cracking tendency.

The test lasts for about 24 hours and both the temperature, the weight loss of the specimens, and the restraint strain are continuously recorded. The measurements start 60 minutes after mixing. After 20 hours of drying, the rings are taken out of the rig and the cracking tendency

is evaluated as the average total crack area (crack length × crack width) on the concrete surface of each of the three specimens. The crack width was measured with a crack microscope (to an accuracy of 0.05mm) and the crack length was measured with a digital measuring wheel (to an accuracy of ±1mm). The weight change was measured using a scale (load cell based) with an accuracy better than 0.03% for a weight of 100 kg (the minimum detectable weight change was 20 g). The concrete temperature was measured using both a thermo thread and a PT100 sensor. The temperature and relative humidity in the room was measured using a Visala sensor. The capillary pore pressure was measured with two pressure transducers (Model AB from Data Instruments). The pressure transducers were connected to de-aired water filled system with a needle with an internal diameter of 0.4 mm (Sterican® 0.70×50 mm BL/LB, from B. Braun Melsungen AG) at the end, see Figure 14. The data was logged every minute using a data logger from INTAB (PC-logger3100i, with 16 channels).

Figure 14. Picture of pressure gauge and the needle used to measure the capillary pore pressure.

4 Results and discussion

4.1 Autogenous deformation (CDD)

The results from the measures of linear autogenous deformation by the CDD is presented both graphically and as a number of deformation factors, evaluated by a model presented in Figure 15. The pattern of deformation comprises three distinct stages which can be rheologicaly defined as: *1. Plastic, 2. Semiplastic* and *3. Rigid* period. In the *plastic* (1) and *semiplastic* (2) period the rate of deformation ($d\varepsilon/dt_1$ and $d\varepsilon/dt_2$), period time (t_1 and t_2) and deformation (ε_1 and ε_2) is evaluated from the deformation/time graph. In the *rigid* period (3) the rate of deformation ($d\varepsilon/dt_3$) is evaluated between 48 to 72 hours from water addition.

The transition from *plastic* to *semiplastic* (t_1) takes place ~6 hours after water addition, and the transition to *rigid* period ($t_1 + t_2$) at ~12 hours. Compared to traditional vibrated concrete without addition of superplasticizer, the self-compacting concrete (SCC) tends to be retarded for about one hour.

The time (t) is relating to the point where the mixing water was added to the premixed solid material (including the cement). As the measures starts after 30 minutes, the curve has been extrapolated to the time zero.

It should to be pointed out that linear measurements of autogenous deformation on a concrete mix before setting are very sensitive and associated with a large scatter. It is not fully correct to define the fresh concrete deformation as linear, since the length cannot be defined for a fluid system. Start of the linear measurement should coincide with setting, but exact determination of the plastic to rigid transition is difficult and subjective.

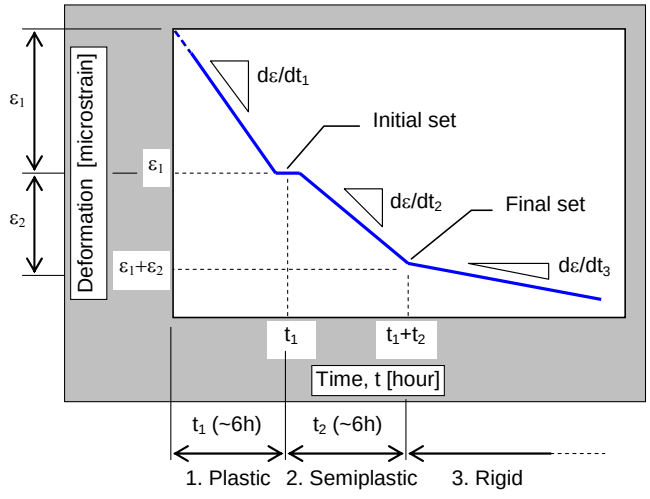

(a)

ε_1:	Plastic deformation (to initial set) [µstrain]
ε_2:	Semiplastic deformation (from initial to final set) [µstrain]
t_1:	Plastic time (to initial set) [h]
t_2:	Semiplastic time (from initial to final set) [h]
$d\varepsilon/dt_1$:	Plastic rate of deformation (to initial set) [µstrain /h]
$d\varepsilon/dt_2$:	Semiplastic rate of deformation (between initial and final set) [µstrain /h]
$d\varepsilon/dt_3$:	Rigid rate of deformation (after final set, <72h) [µstrain /h]

(b)

Figure 15. Model of how the deformation parameters are evaluated from the linear autogenous deformation measurements, where the deformation is divided into plastic/semiplastic/rigid period, illustrated in (a) and symbols explained in (b).

4.1.1 Reference concretes influence of w/c

The investigated reference concretes were four traditional SCC mixes with water cement ratio *w/c*: 0.38, 0.45, 0.55 and 0.67. The type of cement was the CEM II/A-LL 42.5 R (BYGG). When w/c was changed, the composition of constituents also changed, e.g. increased cement and superplasticizer content at lower w/c.

The results of the autogenous deformation from the reference concretes are presented in Figure 16 and Figure 17. The evaluated deformation factors (ε, $d\varepsilon/dt$ and t), for each period (1 to 3), are presented in Figure 18.

The results tendency is significant, and showed that:

- as the *w/c* decreased, the rate and magnitude of the autogenously deformation ($d\varepsilon/dt_1$, $d\varepsilon/dt_2$, $d\varepsilon/dt_3$, ε_1, ε_2) increased, Figure 18(a) & (b); and
- as the *w/c* decreased, the length of the plastic and semiplastic periods (t_1 and t_2) increased, see Figure 18(c).

The result are expected as an increased cement content (lower *w/c*) increases the total chemical shrinkage and the effect on length of the plastic and semiplastic periods can be explained by the retarding effect of the super plasticizer and the increased dosage at low *w/c*.

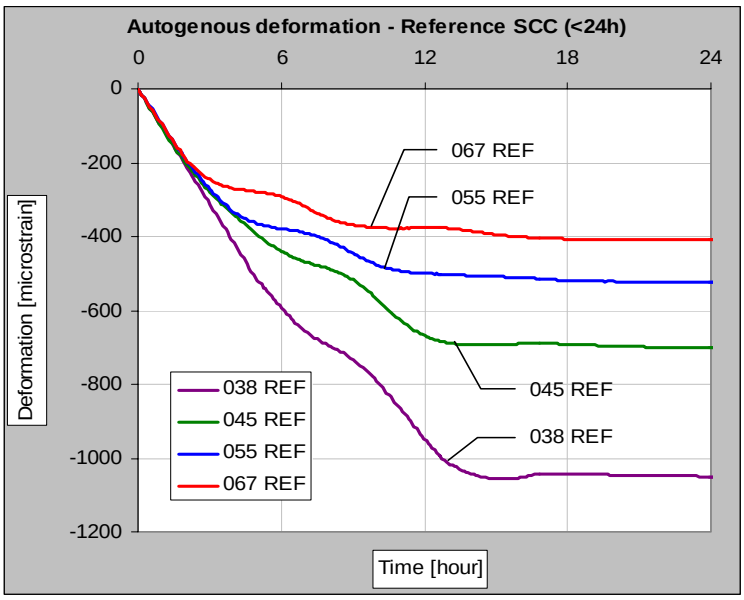

Figure 16. Autogenous deformation for the reference mixes with w/c: 0.38, 0.45, 0.55 and 0.67

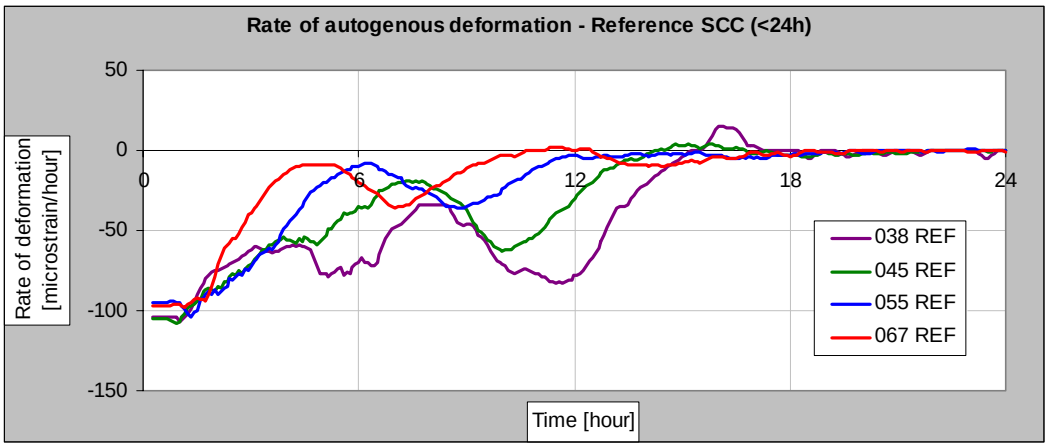

Figure 17. The rate of autogenous deformation by time for the reference mixes with w/c: 0.38, 0.45, 0.55 and 0.67

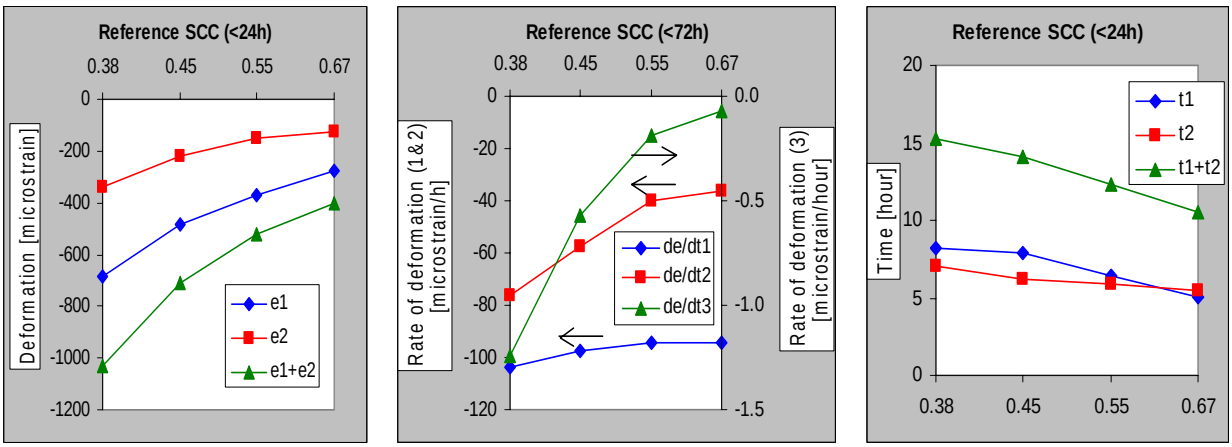

(a) *(b)* *(c)*

Figure 18. Autogenous deformation factors by w/c at the plastic (1), Semiplastic (2) and rigid (3) period. In (a) the total deformation for each period is presented, in (b) the rate of deformation is presented, and in (c) the period times.

4.1.2 Cement type

The cements investigated were: CEM I 52.5R (a fine ground, rapid hardening portland cement); CEM II/A-LL 42.5R (used in the reference concretes); and CEM I 42.5N (a coarse ground, slow hardening, low alkali cement). The results are shown in Figure 19, (a) for *w/c* 0.67 and (b) for *w/c* 0.55.

The “CEM I 52.5R” (SH) had initially a slower shrinkage development then the CEM II/A-LL 42.5R (BYGG). However, after initial setting the “CEM I 52.5R” had a higher rate of deformation and also the total magnitude of deformation was larger, see Figure 19(a). The delayed initial response could perhaps be explained by the fact that the SH-cement used in these experiments was not fresh (~ one year old). The “CEM I 42.5N” had a decreased rate of deformation and the total deformation was much smaller than for the CEM II/A-LL 42.5R (BYGG).

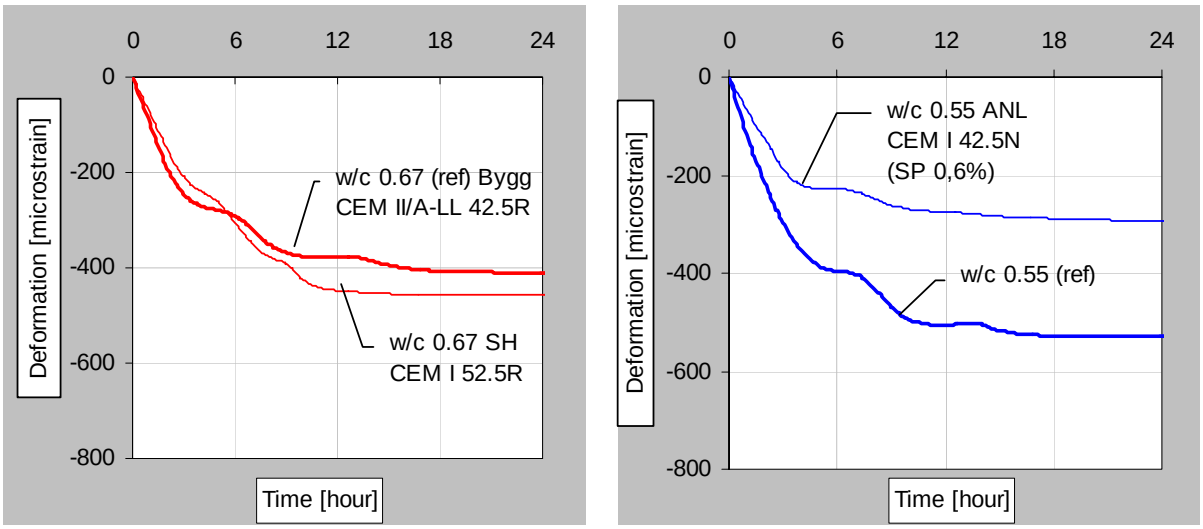

(a) *(b)*

Figure 19. Autogenous deformation for (a) the SCC 067 with cement types: BYGG (CEM II/A-LL 42.5R) and SH (CEM I 52.5R) and (b) for the SCC 055 with cement types: BYGG (CEM II/A-LL 42.5R) and ANL (CEM I 42.5N)

4.1.3 Coarse aggregate content

The investigated concretes were composed with 5/75/20%, 5/65/30%, 5/55/40% and 5/45/50% aggregate ("0-4mm"/"0-8mm"/"8-16mm"). The total volume of aggregate was kept constant. The results of the autogenous deformation are presented in Figure 20 and Figure 21. The evaluated deformation factors (ε, $d\varepsilon/dt$ and t), for each period (1 to 3), are presented in Figure 22.

The results indicate that:

- Increased coarse aggregate content decreased the magnitude and rate of autogenous deformation (ε_1, ε_2, $d\varepsilon/dt_1$, $d\varepsilon/dt_2$ and $d\varepsilon/dt_3$). The effect was more apparent at higher content of coarse aggregate, which might be explained by the coarser particles ability to create a restraining matrix.

- No significant changes in times (t_1 and t_2) could be observed, but an increased content of coarse aggregate tended to delay the rigid (3) period.

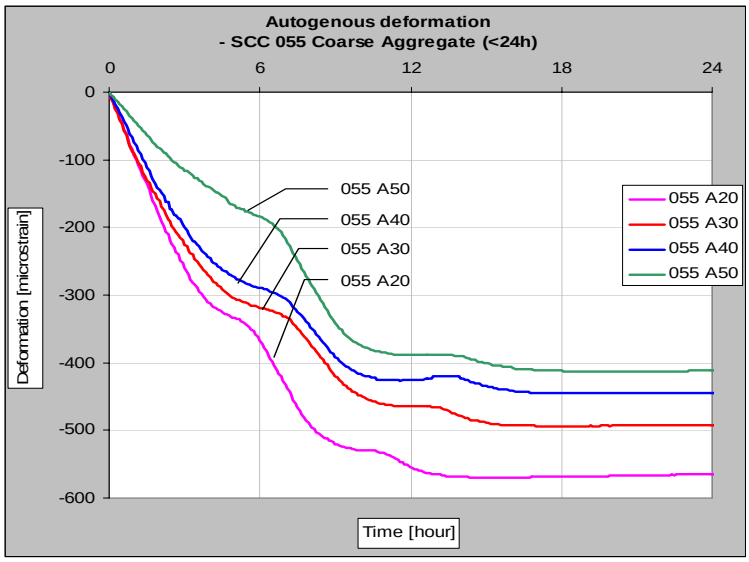

Figure 20. *Autogenous deformation for the mixes with 20%, 30%, 40% and 50% coarse of total aggregate content.*

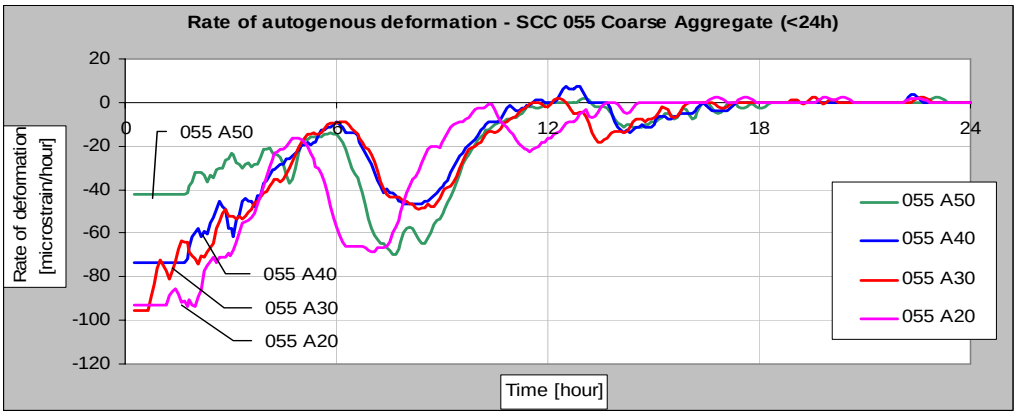

Figure 21. *The rate of autogenous deformation by time for the mixes with 20%, 30%, 40% and 50% coarse of total aggregate content.*

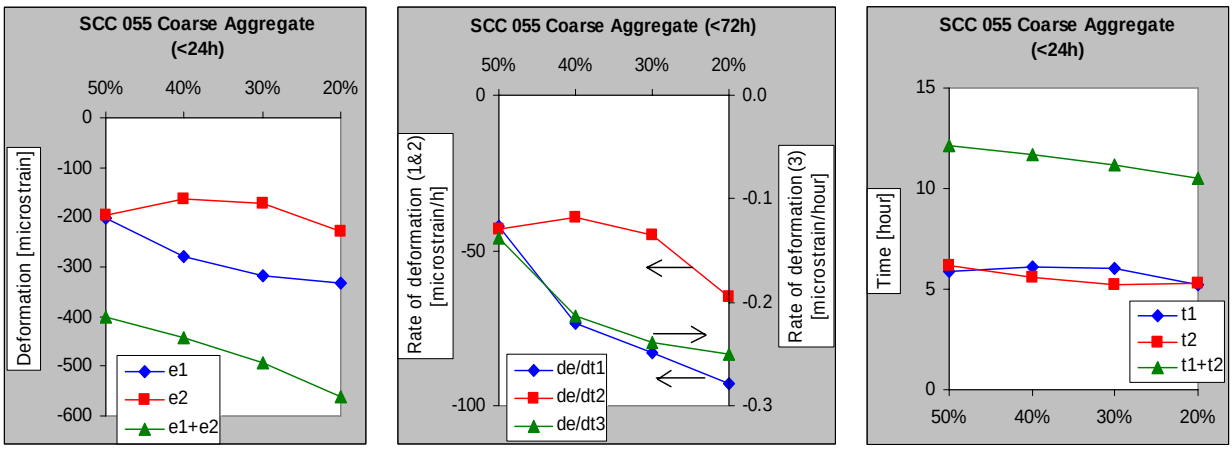

(a) *(b)* *(c)*

Figure 22. *Autogenous deformation factors by coarse aggregate content at the plastic (1), semiplastic (2) and rigid (3) period. In (a) the total deformation for each period is presented, in (b) the rate of deformation is presented, and in (c) the period times.*

It can be noted that the content of coarse aggregate had a large impact on the rheology, which can be deduced from the aggregate packing. An improved packing governs the flowability as more water is freed for dispersing the particles. The results from rheological measurements are presented in Figure 23 and the aggregate packing in Figure 24. As the packing improves, water is "released" to the mix and parallels can be made to increased water content, in chapter 4.1.4, where more water decreases the magnitude and rate of autogenous deformation.

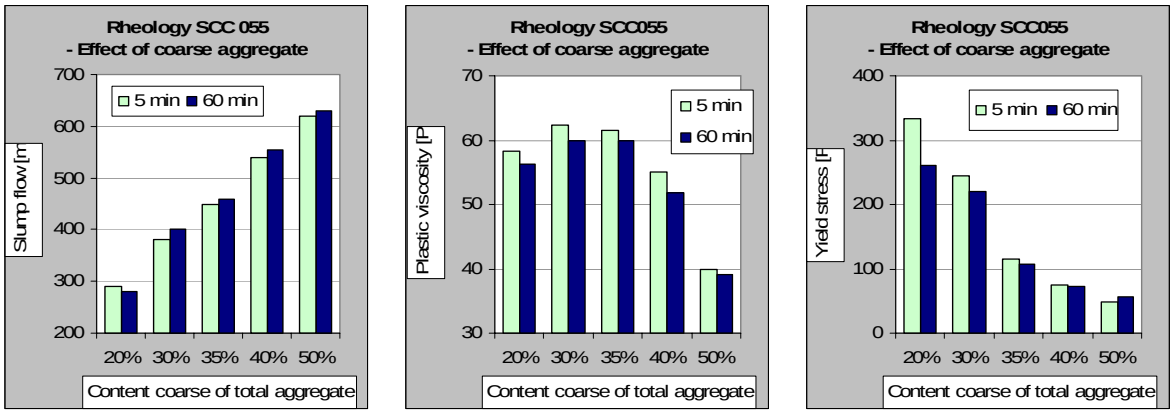

(a) *(b)* *(c)*

Figure 23. The rheological parameters (a) slump flow, (b) plastic viscosity and (c) yield stress for the SCC 055 with 20%, 30%, 35%, 40% (REF) and 50% coarse (8-16 mm) aggregate of total aggregate content.

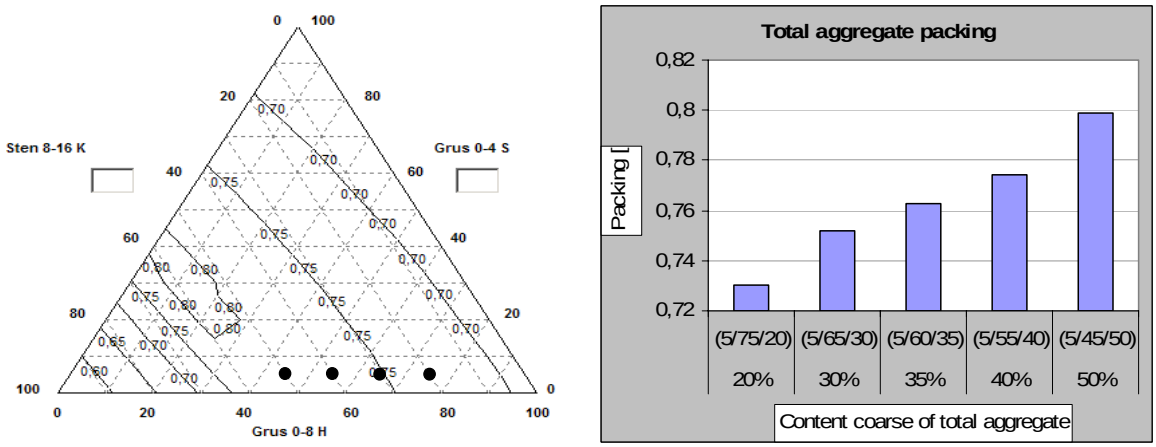

(a) *(b)*

Figure 24. The total aggregate packing; in (a) as a 3-D graph and in (b) for 20%, 30%, 35%, 40% (REF) and 50% coarse (8-16 mm) aggregate content. According to (a) is maximum packing at 60% 8-16.

4.1.4 Water content

To investigate the effect of changes in water content, 6 and 12 liter extra water was added to the reference mix with w/c 0.67. The extra water can be viewed as a simulation of incorrect gravel moisture content by 0.5% respective 1.0%.

The results of the autogenous deformation are presented in Figure 25 and Figure 26. The evaluated deformation factors (ε, $d\varepsilon/dt$ and t), for each period (1 to 3), are presented in Figure 27.

The tendency is significant and indicates that:

- Increased water content decreased the magnitude and rate of autogenous deformation (ε_1, ε_2, $d\varepsilon/dt_1$ and $d\varepsilon/dt_2$), which can be explained by increased interparticle distances (decreases the interparticle forces). At w/c 0.67 the larger surplus of water will probably have small or no effect on the cement hydratation.

- No significant changes in times (t_1 and t_2) could be observed.

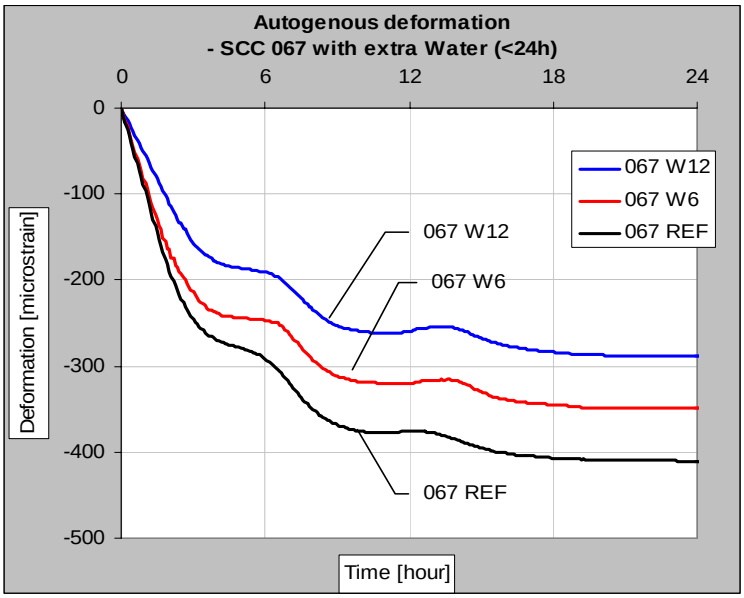

Figure 25. Autogenous deformation for the reference mix (w/c 0.67) with 6 and 12 liter extra water.

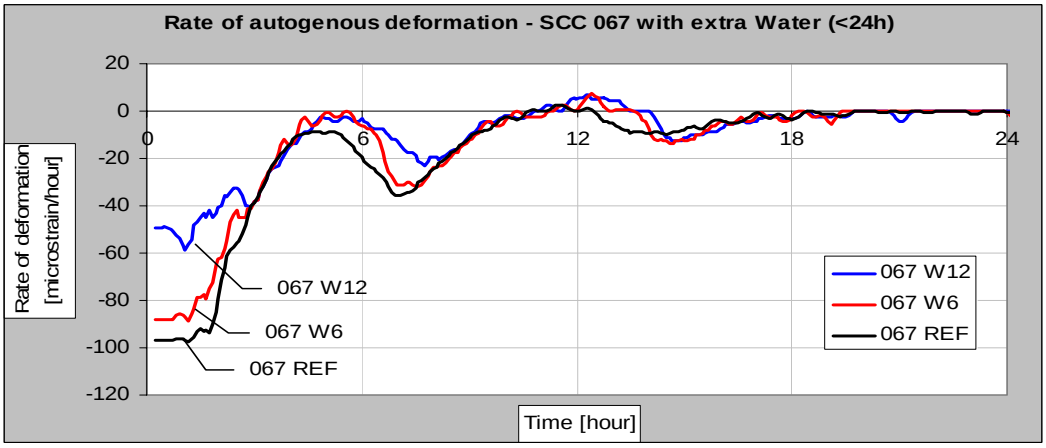

Figure 26. The rate of autogenous deformation by time for the reference mix (w/c 0.67) with 6 and 12 liter extra water.

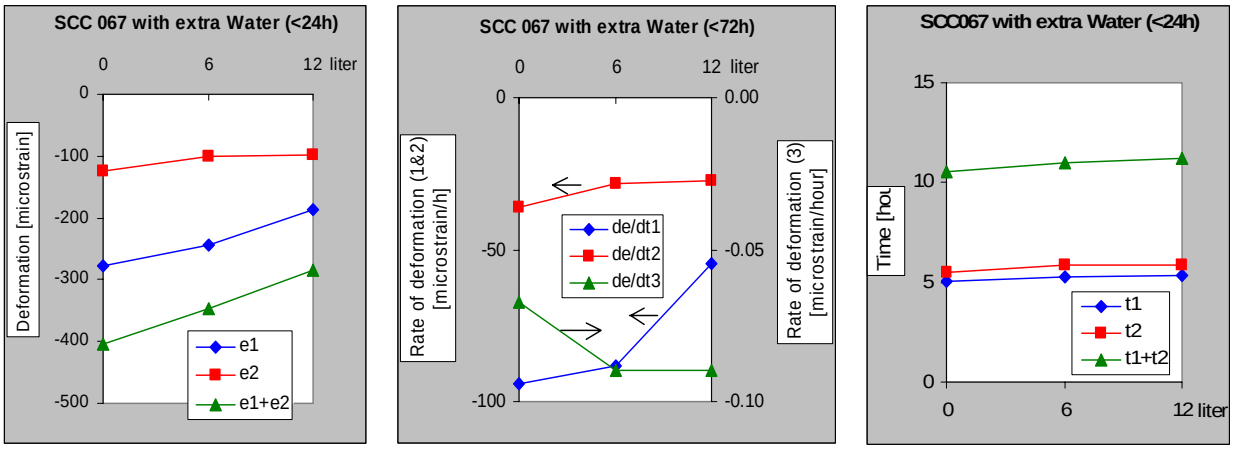

(a) *(b)* *(c)*

Figure 27. Autogenous deformation factors by 6 and 12 liter extra water for reference mix w/c 0.67 at the plastic (1), semiplastic (2) and rigid (3) period. In (a) the total deformation for each period is presented, in (b) the rate of deformation is presented, and in (c) the period times.

4.1.5 Fly ash

To investigate the effect of fly ash, 25% FA by cement weight was added to SCC 045 REF, SCC 055 REF and SCC 067 REF. The results of the autogenous deformation are presented in Figure 28. The evaluated deformation factors (ε, $d\varepsilon/dt$ and t), for each period (1 to 3), are presented in Figure 29, Figure 30 and Figure 31.

With this type of specific chemical composition and physical properties of the cement and FA, the results show the common tendency:

- The addition of FA caused the concrete to swell drastically in the *plastic* period. In the *semiplastic* period the deformation (ε_2 and $d\varepsilon/dt_2$) were similar to those without FA. The effect of FA at the *rigid* period is not clear, but at high w/c the FA seemed to have a reducing effect of the rate of deformation ($d\varepsilon/dt_3$), and at low w/c the opposite was observed.

- The early swelling increased with lower w/c. This can be explained by that the dosage of FA is based on the cement content, the FA addition increases with decreased w/c (86, 77 and 68 kg FA for w/c 0.45, 0.55 and 067).

- A small incensement of times (t_1 and t_2), when FA addition, could be observed. The lower w/c the higher effect was observed.

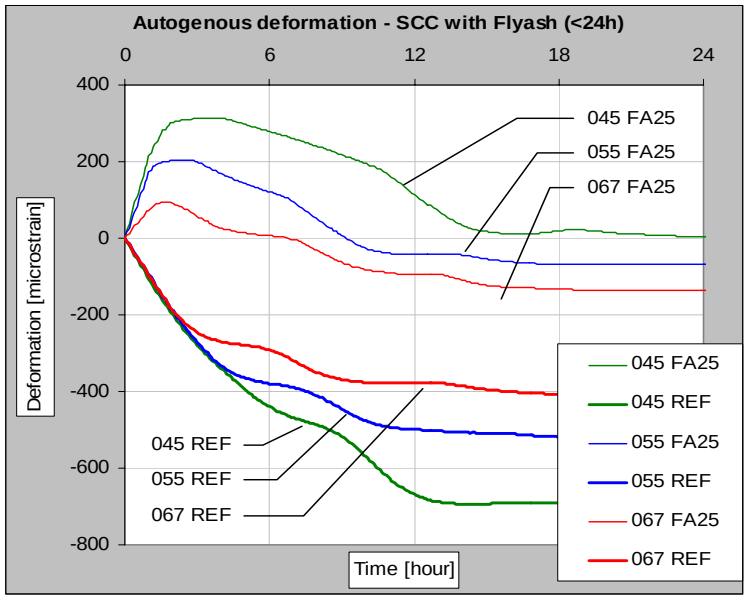

Figure 28. Autogenous deformation for the reference mixes (w/c 0.45, 0.55 and 0.67) with 25% addition of fly ash (by cement weight).

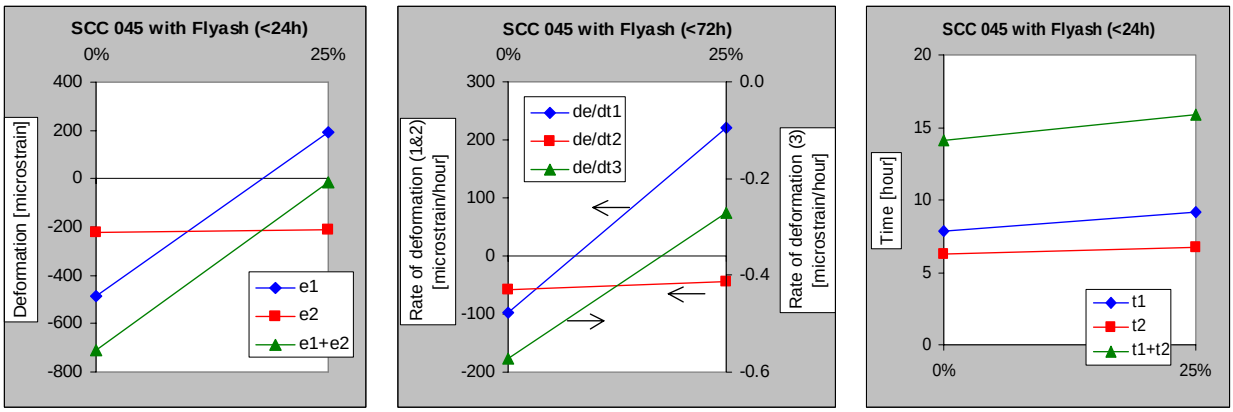

(a) *(b)* *(c)*

Figure 29. Autogenous deformation factors for reference concrete w/c 0.45 with 25% (by C) fly ash. In (a) the total deformation for each period is presented, in (b) the rate of deformation is presented, and in (c) the period times.

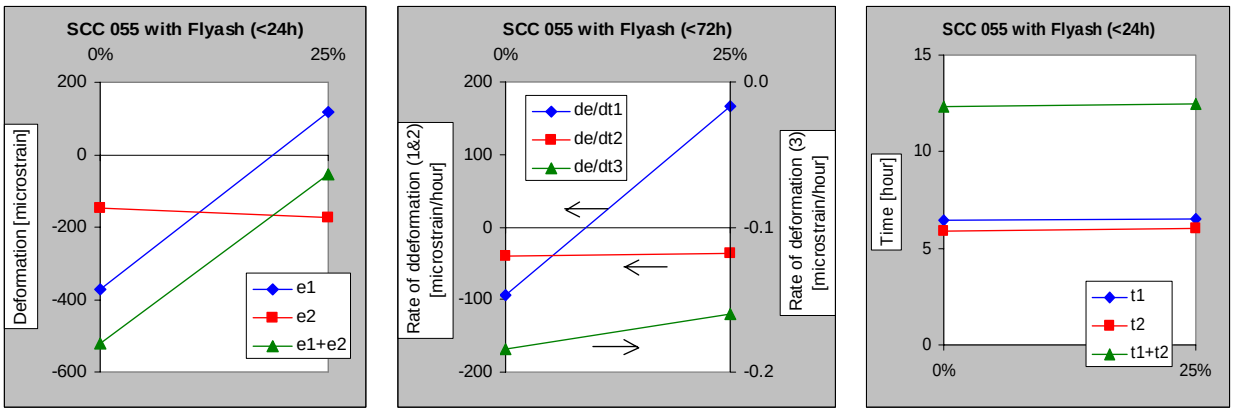

(a) *(b)* *(c)*

Figure 30. Autogenous deformation factors for reference concrete w/c 0.55 with 25% (by C) fly ash. In (a) the total deformation for each period is presented, in (b) the rate of deformation is presented, and in (c) the period times.

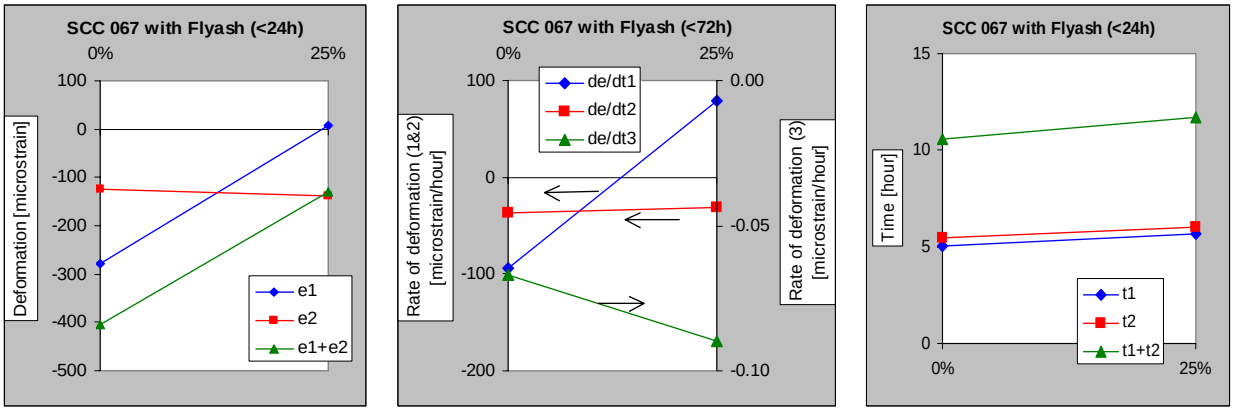

(a) *(b)* *(c)*

Figure 31. Autogenous deformation factors for reference concrete w/c 0.45 with 25% (by C) fly ash. In (a) the total deformation for each period is presented, in (b) the rate of deformation is presented, and in (c) the period times.

It is has been observed that a concrete with FA addition tends to be retarded at early stages ("dormant" period), especially at low w/c (see e.g. Langana et al., 2002). Furthermore, the behavior with expansion (swelling) at early ages has been proposed to be caused by a larger and faster rate of ettringite formation, see Ravina (1986). In addition to those from the cement, sulfates may also originate from the fly ash; where sulfates (alkali, and perhaps also calcium) have been found to be deposited on the surface of the fly ash particles and on those of unburned carbon (which have a high internal surface), from the vapor phase in the boiler, as the particles cool. The sulfates are fully soluble and, being freely available to the mix water in their deposited state, augment both the alkalies and sulfate brought into solution from the cement. Moreover, the hydration is affected by the concentration of Ca^{2+}, OH^- and SO_4^{2+} in the pore water. It has been observed that when the ion concentration is high, small crystals of ettringite are formed while, on the contrary, in low ion concentration conditions large amounts of ettringite are produced in the shape of large needles. In this case, the hydration of the interstitial phase continues to produce large amounts of ettringite, which causes the stiffness and pseudo-setting, see Hanehara and Yamada (1999). Hanehara and Yamada (1999) observed that fly ash fixed Ca^{2+}, which lowered the concentration and resulted in slump loss and stiffness. This was thought to be caused by the production of large amounts of ettringite.

4.1.6 Silica fume

5% and 10% silica fume by cement weight was added to reference mix with w/c 0.55. The cement was reduced by the corresponding addition of SF volume (w/b of 0.58 and 0.61 with an efficient factor of 2.0).

Silica fume is a very fine powder mainly consisting spherical SiO_2 particles. The principal effects of silica fume on microstructure of concrete are due to the pozzolanic reaction and to the filler effect as a result of particle dimension (Neville 2000), where the small silica particles fills the gap between the coarser cement grain and reacts with the calcium hydroxide, generating a more dense and fine porous structure with high chemical shrinkage.

The results of the autogenous deformation are presented in Figure 32 and Figure 33. The evaluated deformation factors (ε, $d\varepsilon/dt$ and t), for each period (1 to 3), are presented in Figure 34.

The tendency is significant and indicates that:

- Addition of silica fume increased the magnitude and rate of autogenous shrinkage in all periods (ε_1, ε_2, $d\varepsilon/dt_1$, $d\varepsilon/dt_2$ and $d\varepsilon/dt_3$), and the effect increased with increased silica dosage.

- Silica fume decreased the *plastic* time period (t_1), and the effect increased with increased silica dosage. No changes in *semiplastic* time (t_2) could be observed.

It is well known that silica fume increases the autogenous shrinkage, as well as it accelerate the early hydratation and initiate the stiffness at earlier age. The results clearly verify these phenomena.

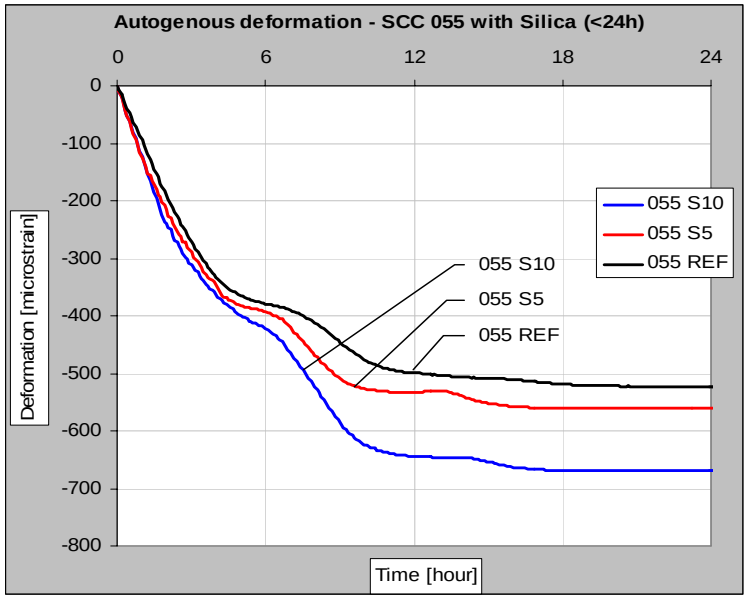

Figure 32. Autogenous deformation for the reference mix w/c 0.55 with 5% and 10% addition of silica fume (by cement weight).

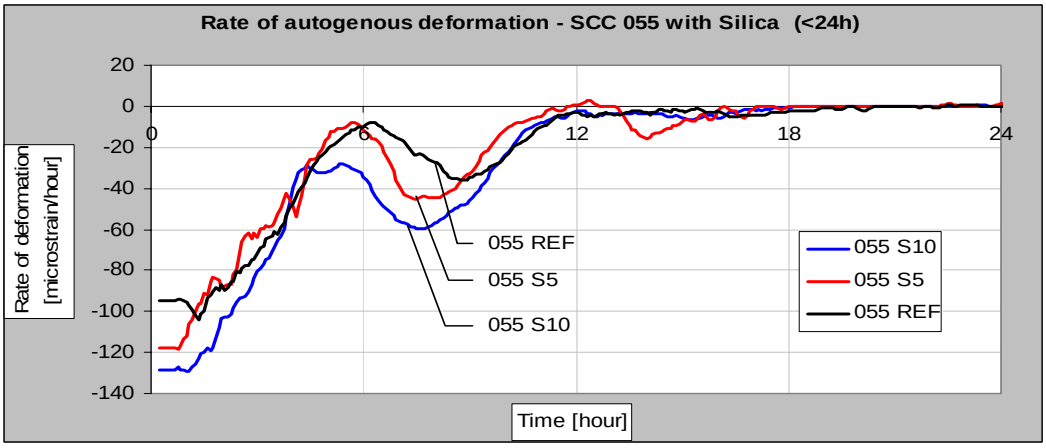

Figure 33. The rate of autogenous deformation by time for the reference mix w/c 0.55 with 5% and 10% addition of silica fume (by cement weight).

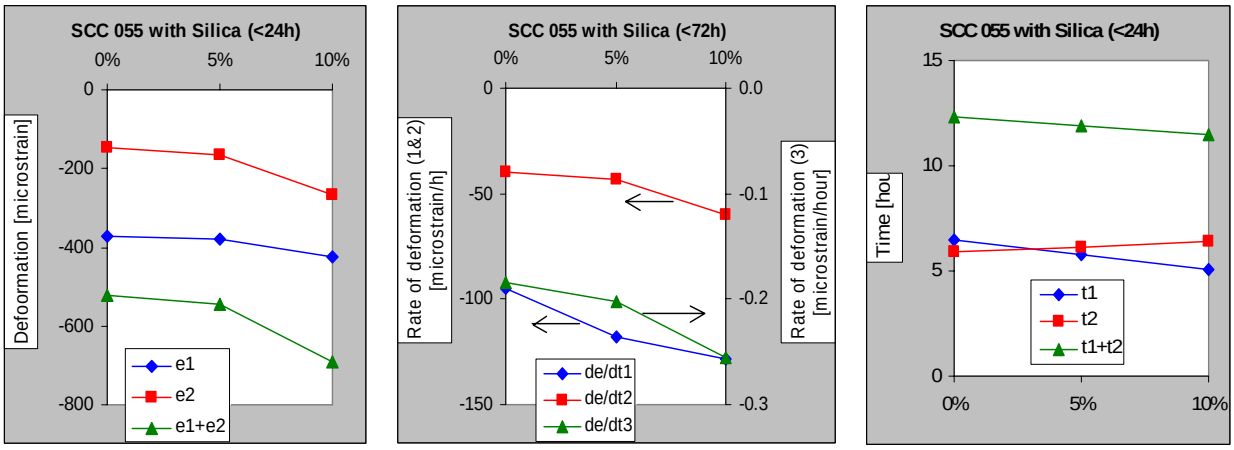

(a) *(b)* *(c)*

Figure 34. Autogenous deformation factors by silica fume addition (5% and 10% by cement weight) at the plastic (1), semiplastic (2) and rigid (3) period. In (a) the total deformation for each period is presented, in (b) the rate of deformation is presented, and in (c) the period times

4.1.7 Superplasticizer dosage

Low and high dosage of superplasticizer (SP) was applied to the reference mix w/c 0.67. At low, reference, and high the SP dosage was 0.6%, 0,8% and 1.0% of the cement weight.

The results of the autogenous deformation are presented in Figure 35 and Figure 36. The evaluated deformation factors (ε, $d\varepsilon/dt$ and t), for each period (1 to 3), are presented in Figure 37.

The results tendency is significant and indicates that:

- SP dosage increased the magnitude of autogenous shrinkage (ε_1 and ε_2), which can be explained by the better cement dispersion (Holt 2001)
- SP dosage increased the rate of shrinkage at the *plastic* and *semiplastic* period ($d\varepsilon/dt_1$ and $d\varepsilon/dt_2$). After setting, the effect was the opposite, where the rate of shrinkage ($d\varepsilon/dt_3$) decreased with SP dosage.
- SP dosage increased the *plastic* time period (t_1). No changes in *semiplastic* time (t_2) could be observed.

It is well known that SP retards the concrete, as it delays the early hydratation and setting is initiated at a later age. The results clearly verify these phenomena.

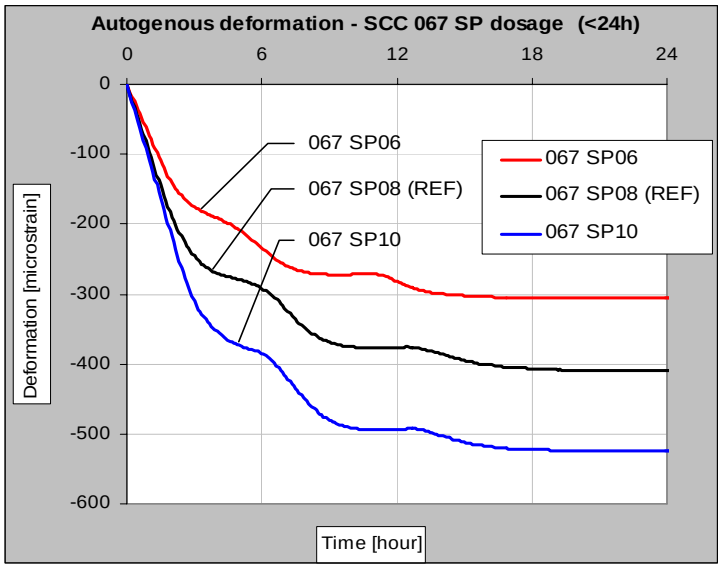

Figure 35. Autogenous deformation for the reference mix w/c 0.67 with 0.6%, 0.8% and 1.0% dosage pf superplasticizer (by cement weight).

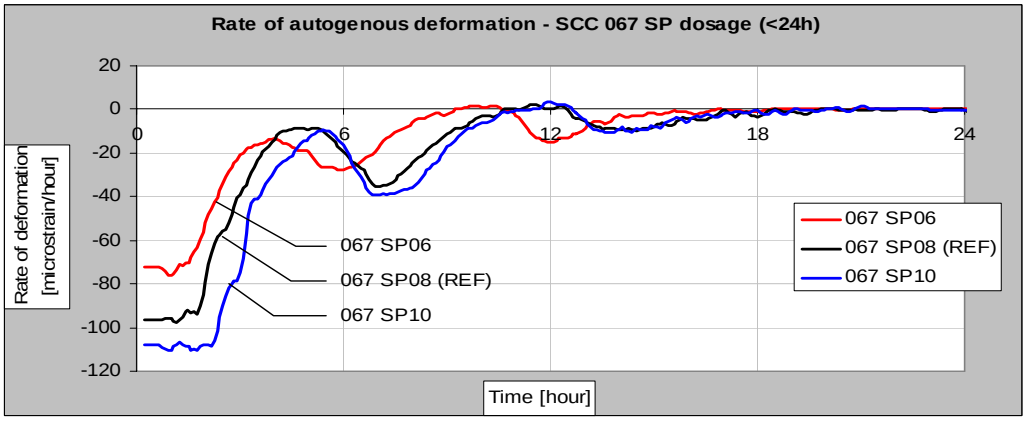

Figure 36. The rate of autogenous deformation by time for the reference mix w/c 0.67 with 0.6%, 0.8% and 1.0% dosage pf superplasticizer (by cement weight).

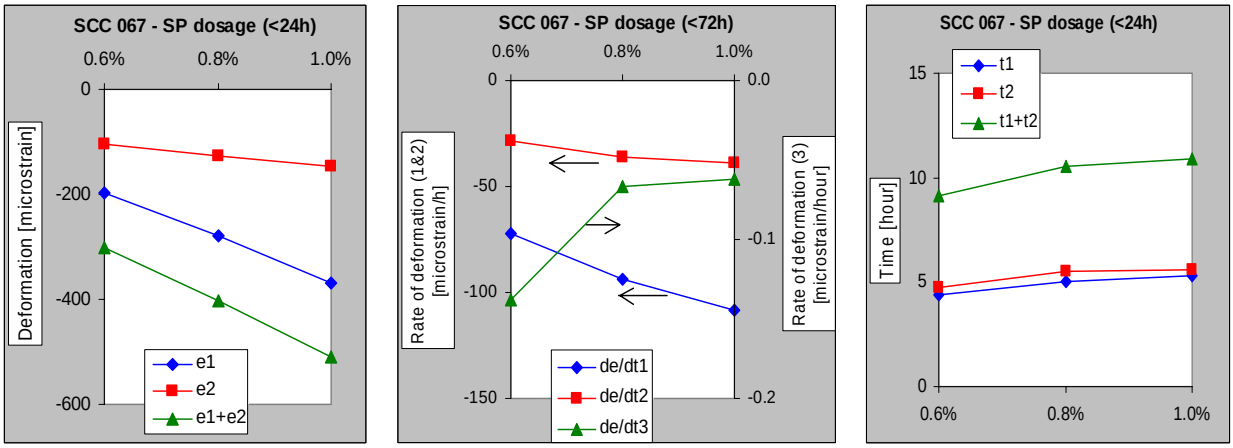

(a) *(b)* *(c)*

Figure 37. Autogenous deformation factors by SP dosage (0.6%, 0.8% and 1.0% by cement weight) at the plastic (1), semiplastic (2) and rigid (3) period. In (a) the total deformation for each period is presented, in (b) the rate of deformation is presented, and in (c) the period times

4.1.8 Accelerator and retarder

Accelerator (ACC) and retarder (RE) was added to the reference mix w/c 0.67. The dosage was made according to the supplier recommendation.

The results of the autogenous deformation are presented in Figure 38 and Figure 39. The evaluated deformation factors (ε, $d\varepsilon/dt$ and t), for each period (1 to 3), are presented in Figure 40.

The results tendency is significant and indicates that:

- In the *plastic* period (before initial setting), ACC increased the magnitude and rate of shrinkage (ε_1 and $d\varepsilon/dt_1$) while the RE hade the opposite effect, which could be expected.
- In the *semiplastic* period, ACC and RE showed no significant effect of magnitude and rate of shrinkage (ε_2 and $d\varepsilon/dt_2$).
- In the rigid period, both ACC and RE increased the rate of shrinkage ($d\varepsilon/dt_3$).
- ACC and RE showed no significant effect on the time of the periods (t_1 and t_2), but RE tended to delay the time to initial setting (t_1)

According to the supplier (SIKA) will RE have a small delaying effect at early hydration (to initial setting), and ACC will have no effect in the same time of period. The results in this study showed the same tendency.

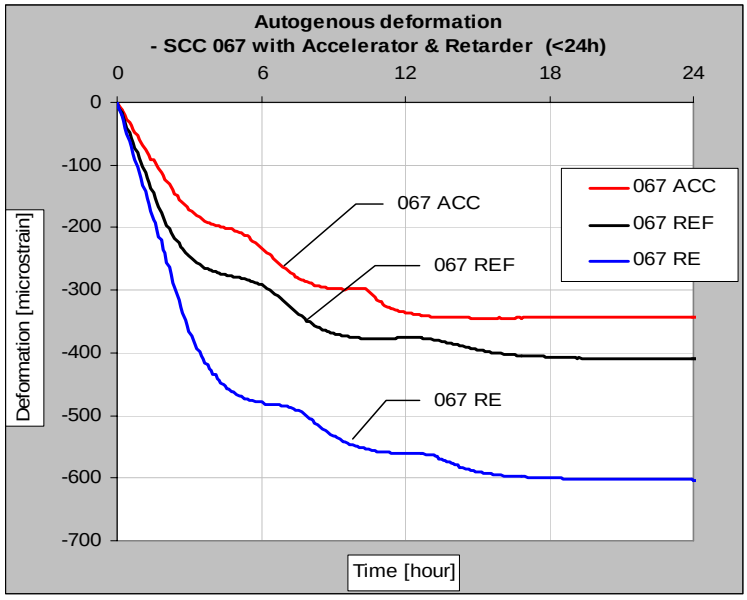

Figure 38. Autogenous deformation for the reference mix w/c 0.67 with addition of accelerator and retarder.

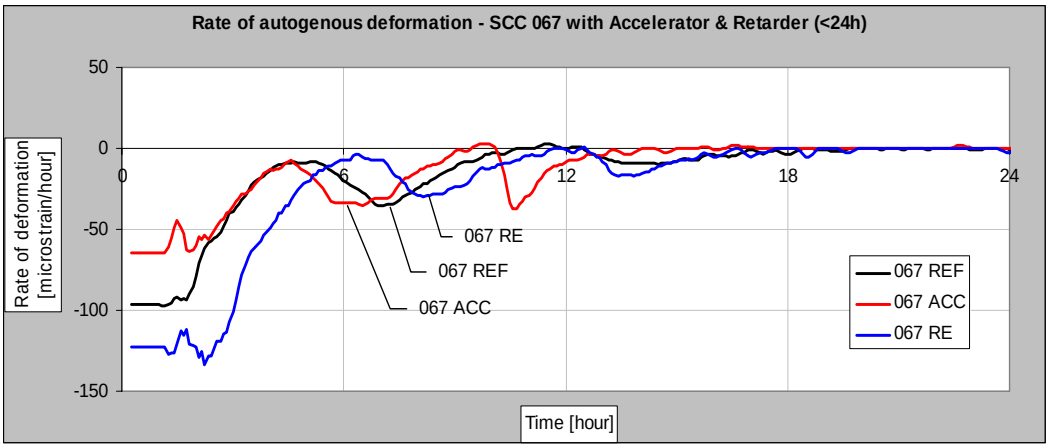

Figure 39. The rate of autogenous deformation by time for the reference mix w/c 0.67 with addition of accelerator and retarder.

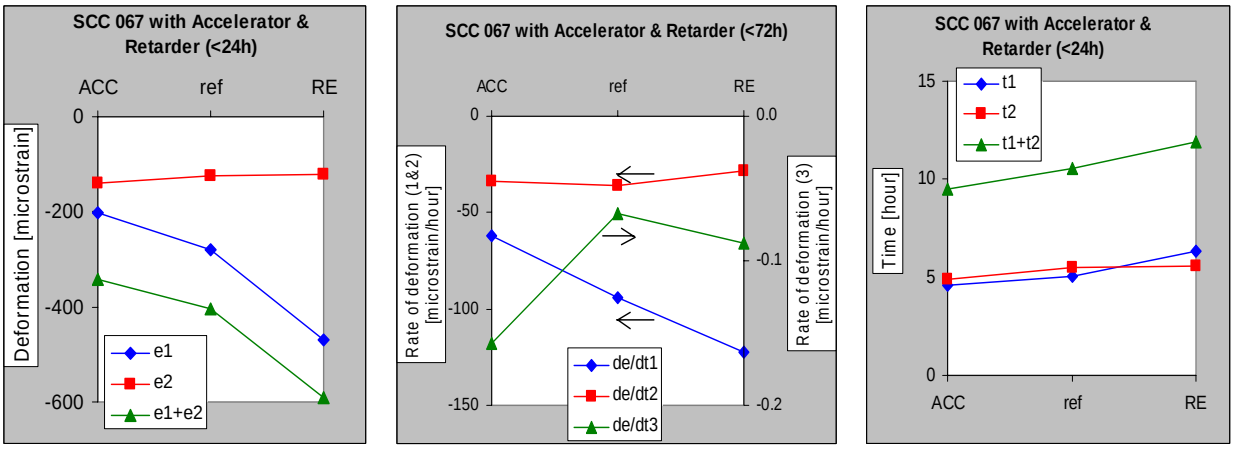

(a) *(b)* *(c)*

Figure 40. Autogenous deformation factors for the reference concrete w/c 0.67 with addition of accelerator and retarder. In (a) the total deformation for each period is presented, in (b) the rate of deformation is presented, and in (c) the period times

4.1.9 Shrinkage reducing admixture

Shrinkage reducing admixture (SRA) was added to the reference mix w/c 0.45, w/c 0.55, and w/c 0.67. The dosage was according to the supplier recommendation; 1.0% and 2.0% SRA by cement weight. The SRA, used in this study, was an alcohol (polymeric glycol based) that reduces the surface tension of water (capillary), which will decrease the internal contraction forces and thereby the autogenous shrinkage.

The results of the autogenous deformation are presented in Figure 41 and Figure 42. The evaluated deformation factors (ε, $d\varepsilon/dt$ and t), for each period (1 to 3), are presented in Figure 43, Figure 44 and Figure 45.

The results tendency is significant and indicates that:

- Addition of SRA decreased the magnitude and rate of autogenous shrinkage for all concretes (ε_1, ε_2, $d\varepsilon/dt_1$, $d\varepsilon/dt_2$ and $d\varepsilon/dt_3$), and the effect increased with increased SRA dosage.

- In the *semiplastic* period the effect of SRA was not as pronounced as in the *plastic* and *rigid* period.

- SRA showed no effect on the times of the periods (t_1 and t_2).

According to the supplier (SIKA), SRA reduce surface tension of the capillary water and thereby the drying shrinkage, which is caused by loss of water from the concrete, is reduced. Furthermore, the SRA is not to have any effect on hydration and setting of the concrete. The results of this investigation showed the same tendency regarding the cement hydration. However, it was also found that the SRA significantly reduced the rate of and the total evaporation during the first 24 hours and that it reduced the magnitude and rate of autogenous deformation.

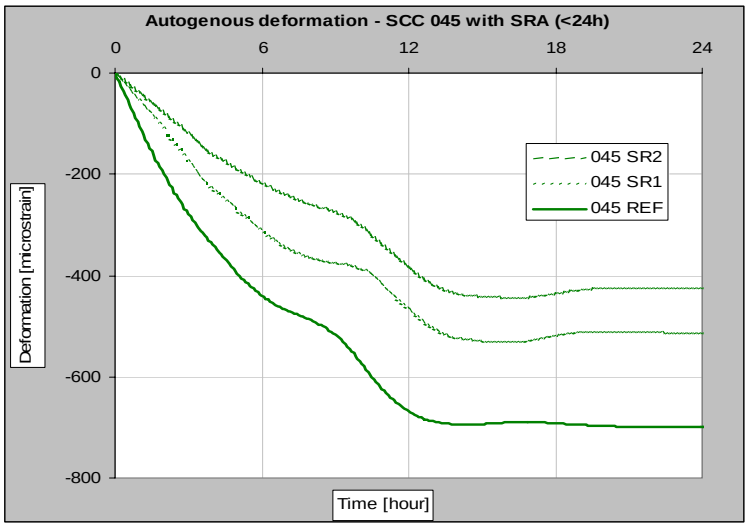

(a)

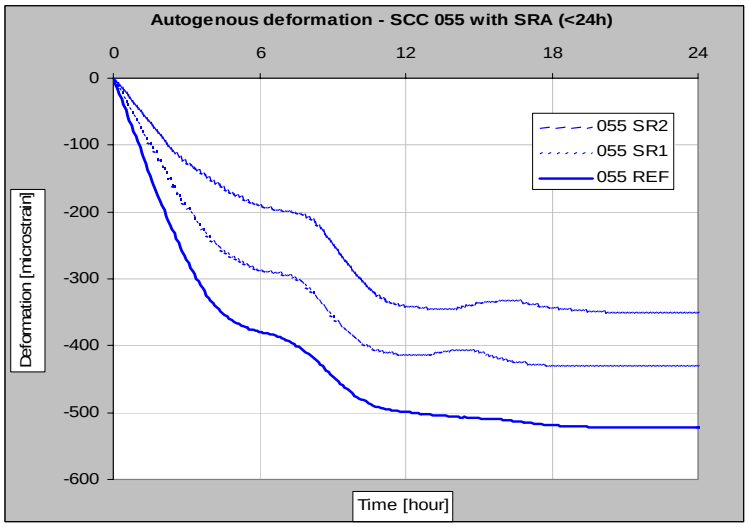

(b)

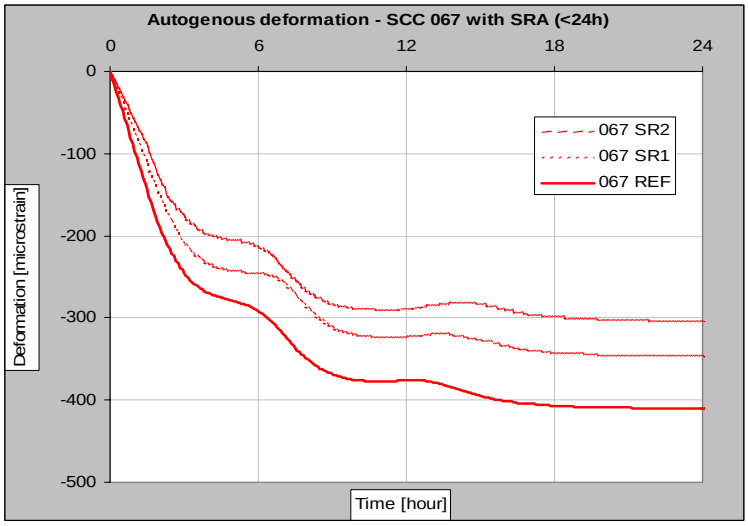

(c)

Figure 41. Autogenous deformation for the reference mixes (a) w/c 0.45, (b) w/c 0.55 and (c) w/c 0.67, with addition of 1.0% and 2.0% SRA by cement weight.

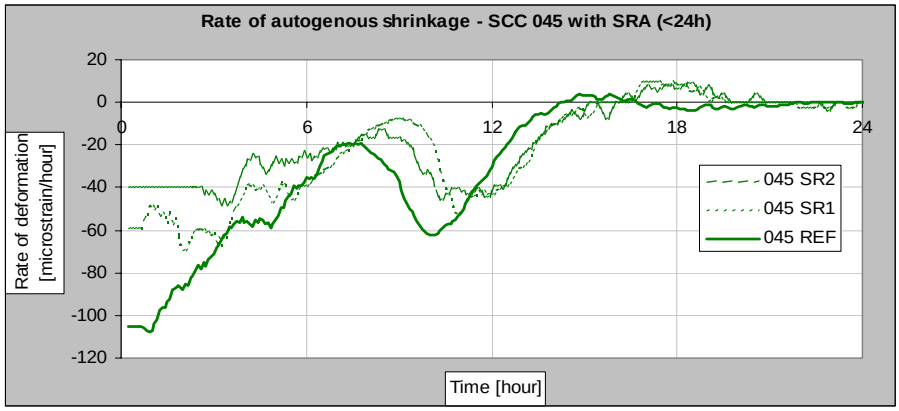

(a)

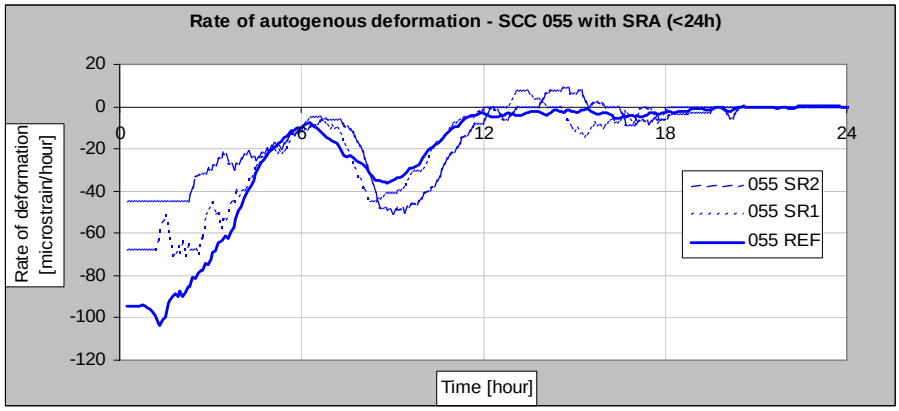

(b)

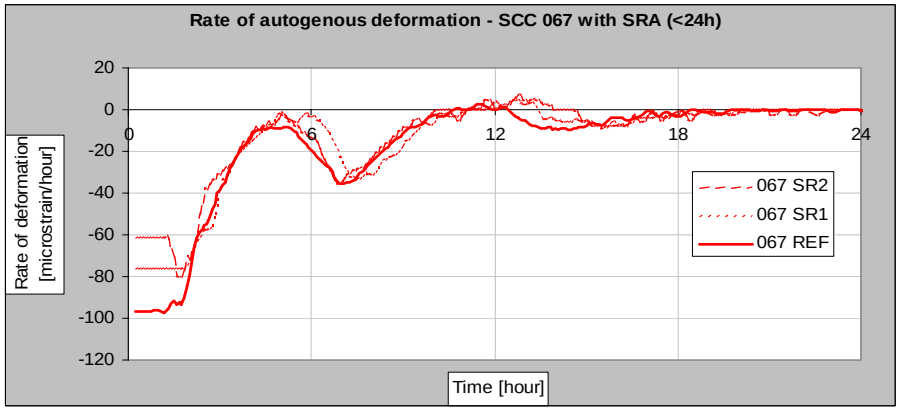

(c)

Figure 42. The rate of autogenous deformation by time for the reference mixes (a) w/c 0.45, (b) w/c 0.55 and (c) w/c 0.67, with addition of 1.0% and 2.0% SRA by cement weight.

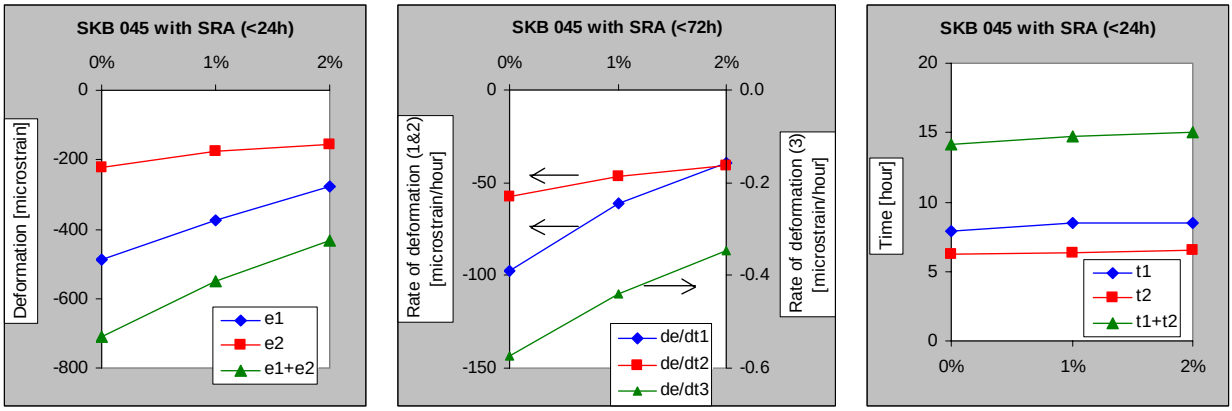

(a) *(b)* *(c)*

Figure 43. Autogenous deformation factors for the ref concrete w/c 0.45 with addition of 1% and 2% SRA. In (a) the total deformation for each period is presented, in (b) the rate of deformation is presented, and in (c) the period times

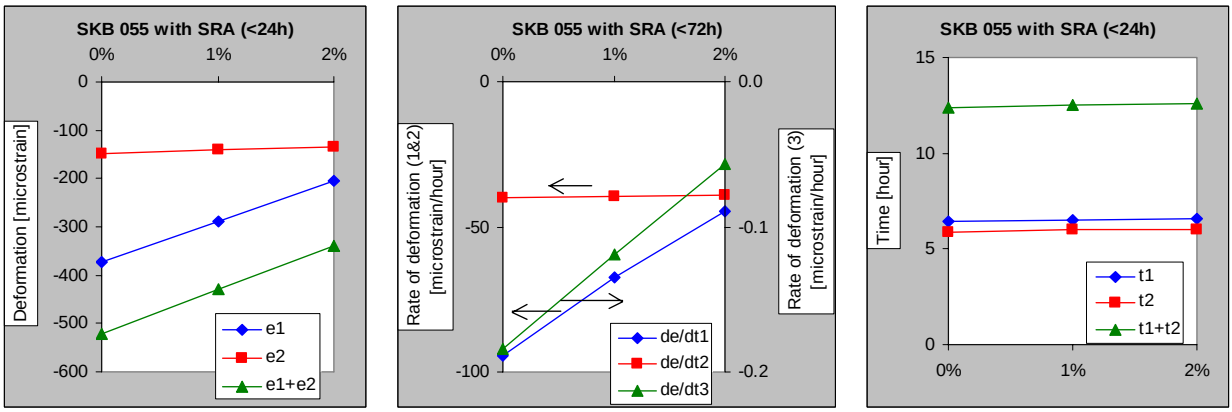

(a) *(b)* *(c)*

Figure 44. Autogenous deformation factors for the ref concrete w/c 0.55 with addition of 1% and 2% SRA. In (a) the total deformation for each period is presented, in (b) the rate of deformation is presented, and in (c) the period times

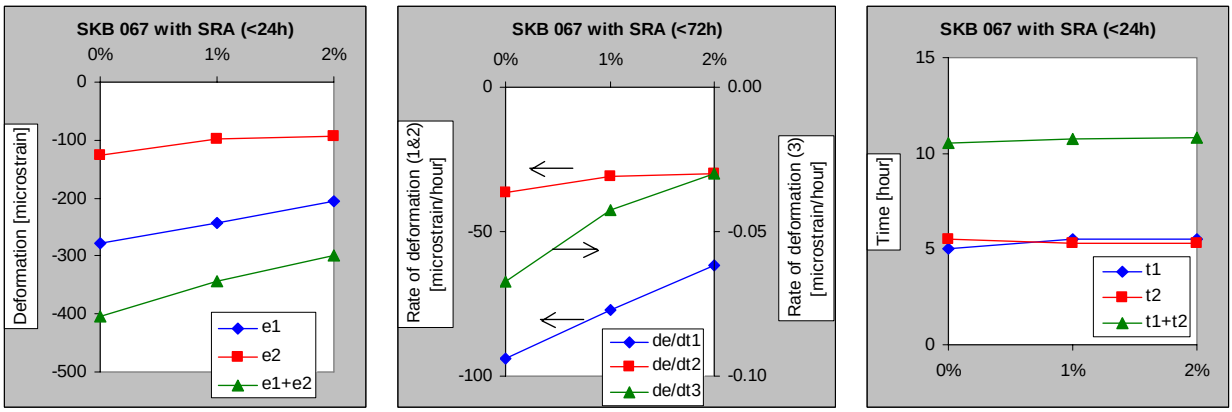

(a) *(b)* *(c)*

Figure 45. Autogenous deformation factors for the ref concrete w/c 0.67 with addition of 1% and 2% SRA. In (a) the total deformation for each period is presented, in (b) the rate of deformation is presented, and in (c) the period times

4.1.10 Air entraining agent

Air entraining agent (AEA) was added to the reference mix w/c 0.67. The dosage was made according to the supplier recommendation; 0.005% and 0.01% AEA (concentrate) by cement weight. The AEA, used in this study, is a synthetic surfactant that generates a fine distributed air void system with tiny bubbles. The addition of AEA is usually intended to increase the concretes frost resistance.

The results of the autogenous deformation are presented in Figure 46 and Figure 47. The evaluated deformation factors (ε, $d\varepsilon/dt$ and t), for each period (1 to 3), are presented in Figure 48.

The results indicate that:

- Addition of AEA caused the concrete to swell (expand) in the *plastic* period. In the *semiplastic* period the AEA tended to decrease the magnitude and rate of deformation (ε_2 and $d\varepsilon/dt_2$). The effect of AEA at the *rigid* period was not clear.

- The magnitude and rate of autogenous shrinkage increased with increasing AEA dosage.

- In the *semiplastic* period the effect of AEA was not as pronounced as in the *plastic* and *rigid* period.

- AEA showed no effect on the times of periods (t_1 and t_2), which agrees with the supplier (SIKA) information.

The behavior of expansion (swelling) at early ages is not clear. One explanation could be that when the concrete is highly flowable the air system is unstable, where the small bubbles with relatively high surface tension can be joined creating few large bubbles with smaller surface tension which increases the volume.

It can be noted that the addition of AEA had a large impact on the rheology and primarily the viscosity, which can be explained by the “ball-bearing” effect. The air also tends to decrease the constancy loss. The results from rheological measurements are presented in Figure 23. For a stable air system the concrete can not have to low viscosity, which might the case here causing the early swelling.

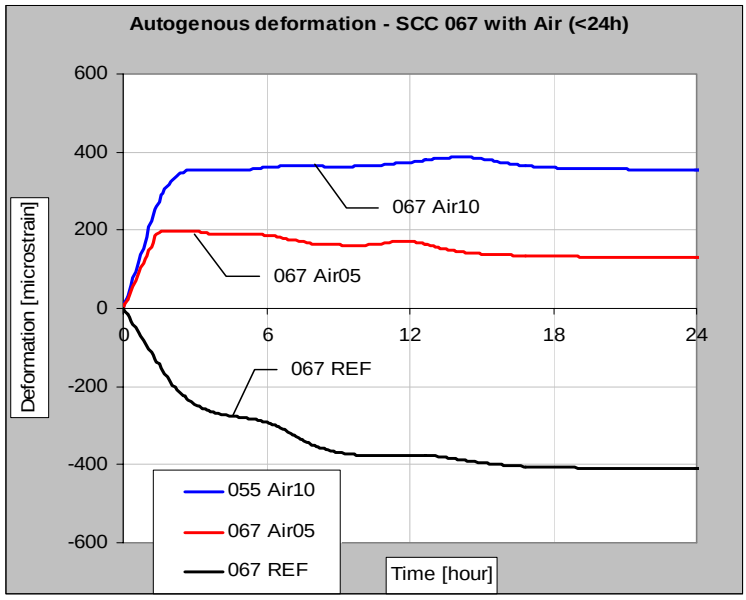

Figure 46. Autogenous deformation for the reference mix w/c 0.67 with addition of 0.05% and 0.1% air entraining agent (by cement weight).

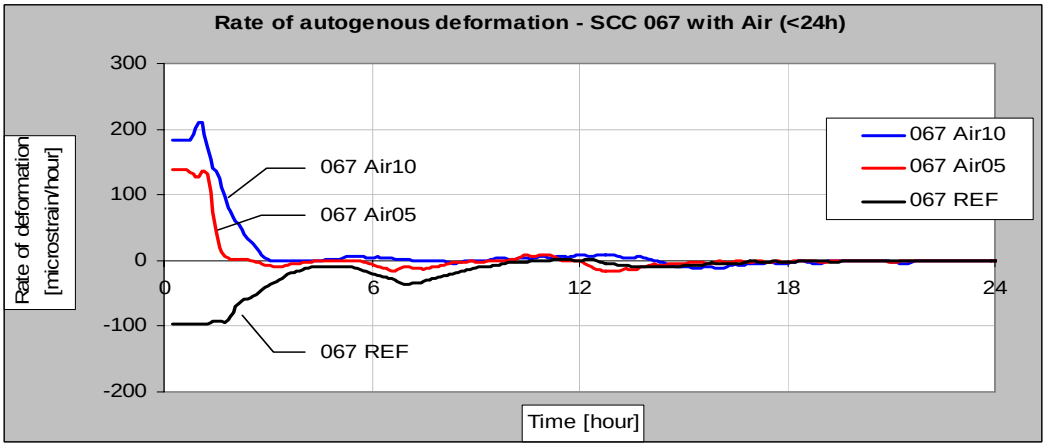

Figure 47. The rate of autogenous deformation by time for the reference mix w/c 0.67 with addition of 0.05% and 0.1% air entraining agent (by cement weight).

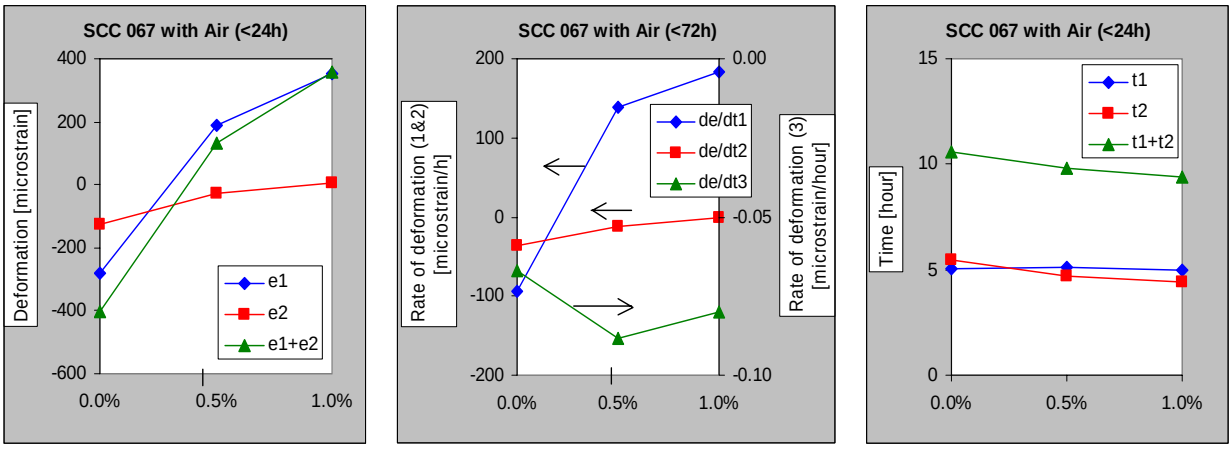

(a) *(b)* *(c)*

Figure 48. *Autogenous deformation factors for the reference concrete w/c 0.67 with addition of air entraining agent. In (a) the total deformation for each period is presented, in (b) the rate of deformation is presented, and in (c) the period times*

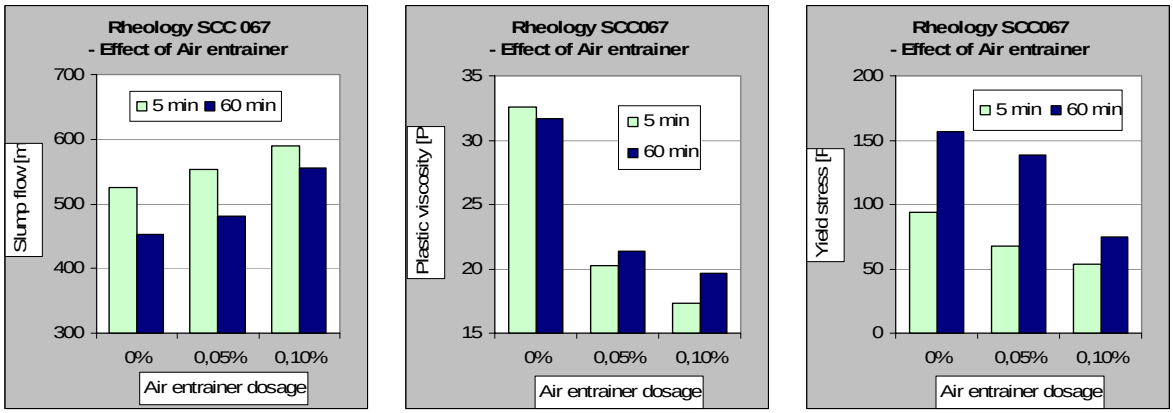

(a) *(b)* *(c)*

Figure 49. *The rheological parameters (a) slump flow, (b) plastic viscosity and (c) yield stress for the reference mix w/c 0.67 and with addition of 0.05% and 0.1% air entraining agent (by cement weight).*

4.2 Ring test

From the recorded weight loss the evaporation, E, was calculated (loss of water per square meter) and the rate of evaporation, E_r, have been determined. The evaporation parameters evaluated from the measurements are defined in Figure 50, these are: the initial rate of evaporation, E_{ri}, which is determined as the average slope of the first part of the evaporation curve when there is an almost linear relationship; the final rate of evaporation, E_{rf}, which is determined as the average slope of the last part of the evaporation curve with, again, an almost linear relationship. Furthermore, the evaporation (E_1, E_2, and E_3) at the start and end points of the two linear parts are to be determined.

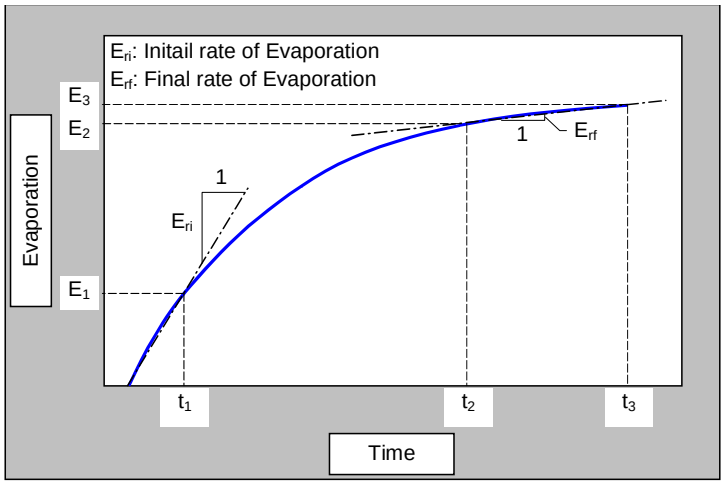

Figure 50. Evaporation parameters evaluated from the weight loss measurements.

From the temperature measurements the following "hydration" parameters were determined, see Figure 51: the time when the dormant period, $t_{dormant}$, ends, which was defined as the point when the rate of temperature change accelerates, after a plateau with, and exceeds 0.5°C/h; the maximum rate of temperature change $(\Delta T/\Delta t)_{max}$ and the time $t(\Delta T/\Delta t)_{max}$ when this occurs; and the maximum temperature change ΔT_{max} and the time when this occurs $t(\Delta T_{max})$.

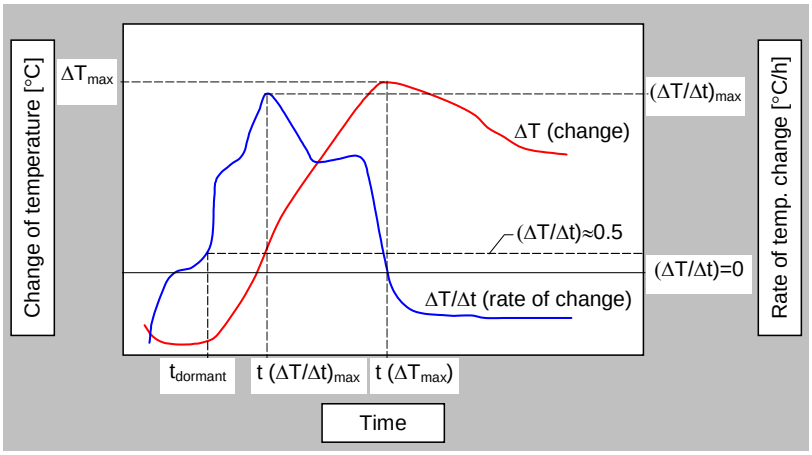

Figure 51. Hydration parameters evaluated from the temperature measurements.

From the measurements of the capillary pore pressure the following parameters have been determined, see Figure 52: the time to reach –5 and –20 kPa; the rate of the pore pressure change at pressures of –5 and –20 kPa; and the final rate of the pore pressure change. It should, however, be pointed out that this test technique is highly sensitive to local conditions at the needle tip. This sensitivity manifests itself in, for example, a loss of pressure at a random point in time. This point was named by Wittman (1976) as the breakthrough pressure. The breakthrough pressure probably occurs by local disturbances at the needle tip, such as destruction of the water menisci by air pores, which relieves the pressure. As a result, the maximum recorded pressure may not be representative for the concrete.

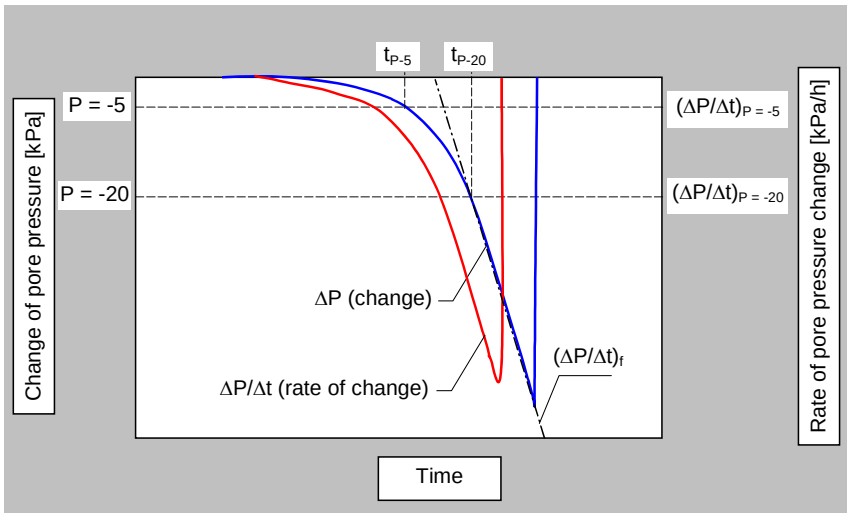

Figure 52. Capillary pore pressure parameters evaluated from the measurements.

4.2.1 Reference concretes – influence of *w/c*

Evaporation

In Figure 53(a) the evaporation curves of the reference concretes can be seen and in Figure 53(b) the effect of the w/c ratio on the evaporation can be seen. Furthermore, Figure 54 shows the effect of the w/c ratio on rate of evaporation. As can be seen, there was an effect of the w/c ratio on the amount of evaporated water and the lower the w/c ratio was the less water evaporated. However, in this study, the exception was that the evaporation for the concrete with w/c 0.55 were greater than for the one with w/c 0.67. The reasons for this may be due to that the environmental conditions (temperature and relative humidity) were not entirely the same and that the concrete with w/c 0.55 had a higher dosage of superplasticizer which delayed the hydration which may lead to a higher evaporation. However, as can be seen in Figure 54, the rate of evaporation, which is an important factor for plastic shrinkage cracking, increased with the w/c ratio. This is valid both for the initial and final rate of evaporation.

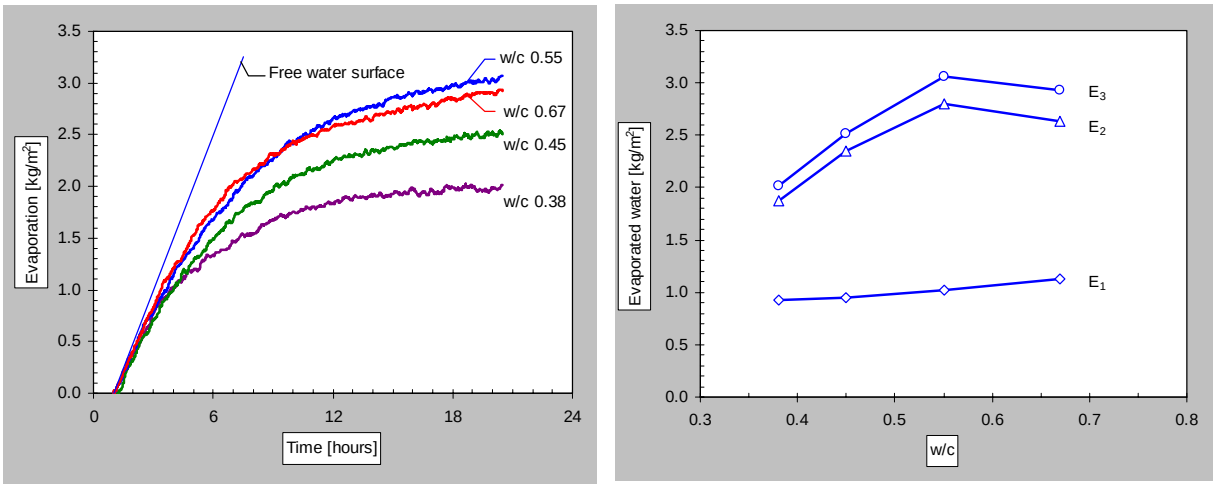

(a) *(b)*

Figure 53. (a) Evaporation curves for the reference concretes. (b) Effect of w/c ratio on the evaporation at time t_1, t_2, and t_3.

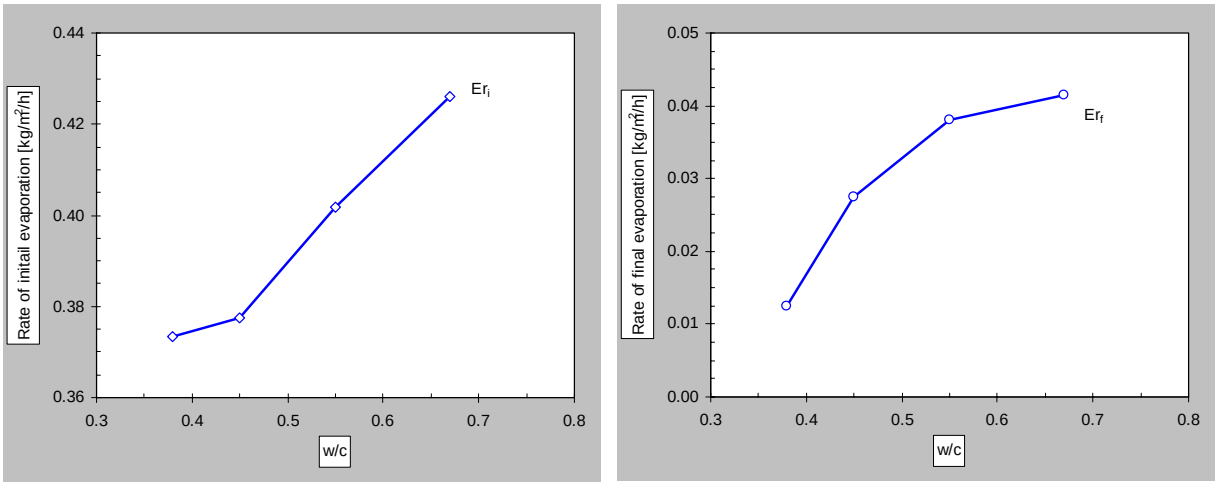

(a) *(b)*

Figure 54. Rate of evaporation of the reference concretes, effect of w/c ratio on: (a) the initial rate of evaporation and (b) the final rate of evaporation.

Temperature development

The change of temperature in the reference concretes can be seen in Figure 55(a) and the rate of temperature change can be seen in Figure 55(b). In Figure 56(a) the effect of the w/c-ratio on the maximum temperature change and the time when this occurs is presented, while Figure 56(b) shows the maximum rate of temperature change and the time when this occurs. Finally, in Figure 57 the effect of the w/c-ratio on the length of the dormant period is presented. As can be seen in these figures, as the w/c-ratio decreases the hydration was delayed (both the length of the dormant period and the time at max temperature change and max rate of temperature change), with the exception of the concrete with w/c 0.38. Furthermore, the maximum temperature change and the maximum rate of temperature change decreased with the w/c-ratio, again with the exception for the 0.38 concrete. One possible explanation for this behaviour may be the effect of the increased SP-dosage, which has a retarding effect. However, the temperature change in these experiments was also influenced by the rate of evaporation and the cooling effect this has, which affect the results.

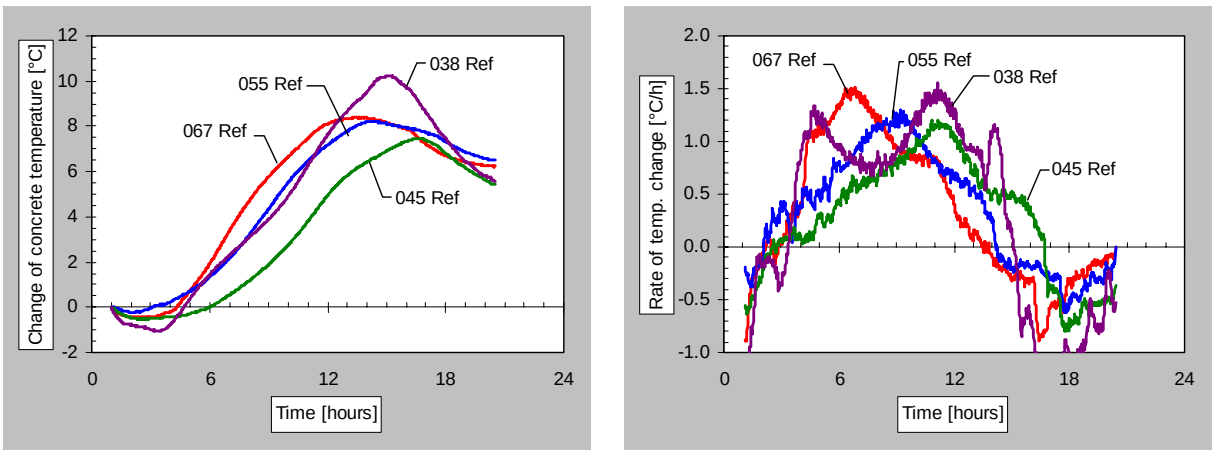

(a) *(b)*

Figure 55. Comparison of temperature development in reference concretes: (a) comparison of change of temperature; and (b) comparison of the rate of temperature change.

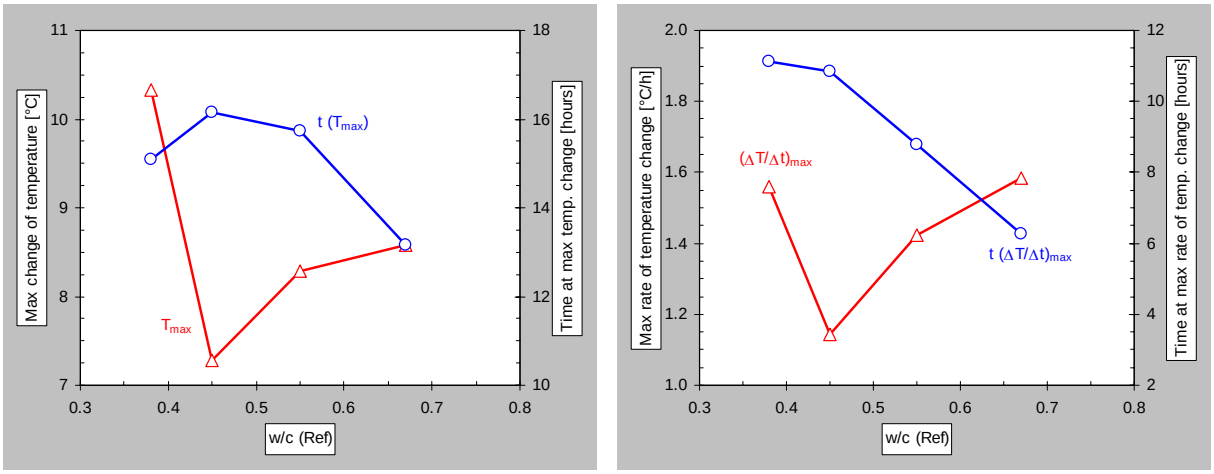

(a) *(b)*

Figure 56. Effect of w/c on hydration of reference concrete: (a) comparison of max temperature change and point of time; and (b) comparison of max rate of temperature change and point of time.

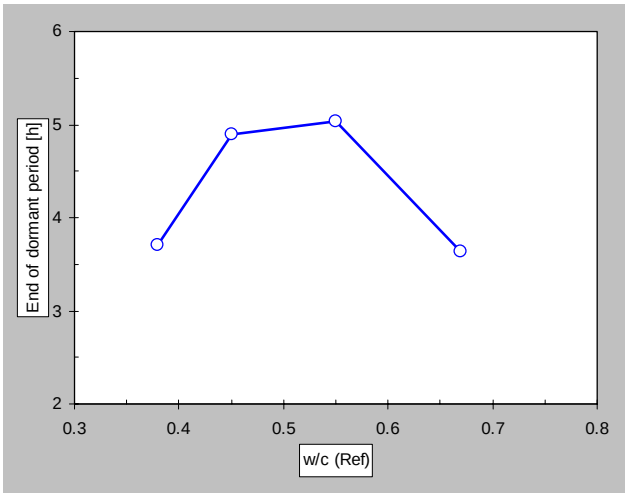

Figure 57. Effect of w/c on hydration of reference concrete, comparison of the end of the dormant period.

Pore pressure change

In Figure 58 the development of the negative pore pressure for the reference concretes can be seen. In Figure 59 the time to reach –5 kPa respectively –20 kPa and rate of pressure change at this point is presented. The rate of the pore pressure change is related to both the rate of evaporation and the cement hydration, and as can be seen the pore pressure developed faster and earlier for the concretes with a high w/c-ratio (0.67 and 0.55), see Figure 68. The result from the evaporation (see Figure 54) and the temperature measurements (see Figure 55 to Figure 57) confirms that both the evaporation and the hydration were more rapid for the concrete with w/c 0.67.

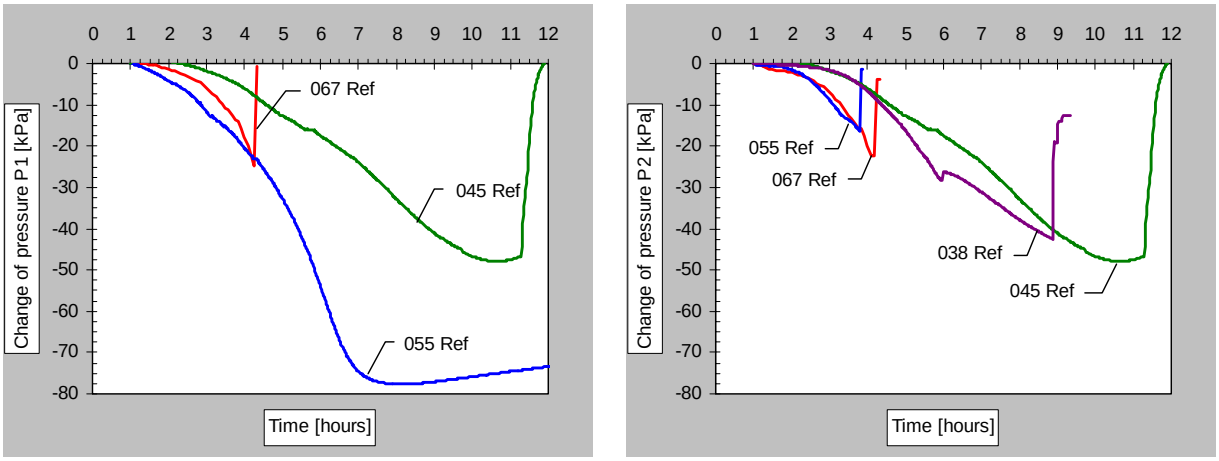

(a) *(b)*

Figure 58. Effect of w/c on pore pressure change for the reference concretes: (a) pressure P1 at a depth of 60 mm; and (b) pressure P2 at a depth of 20 mm.

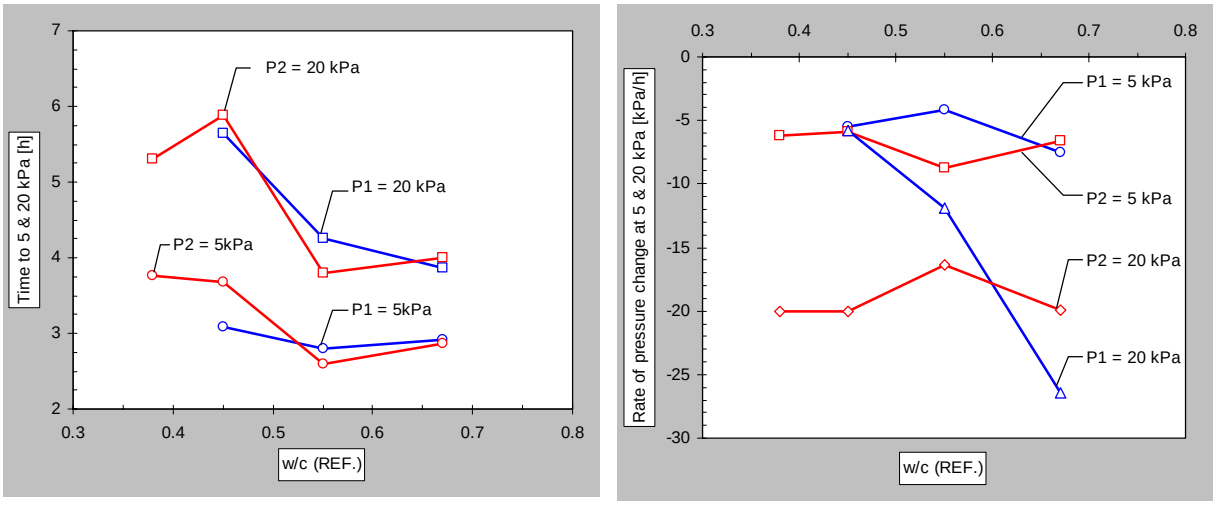

(a) *(b)*

Figure 59. Effect of w/c on pore pressure change for the reference concretes: (a) Time to 5 and 20 kPa; and (b) the rate of pressure change at 5 and 20 kPa.

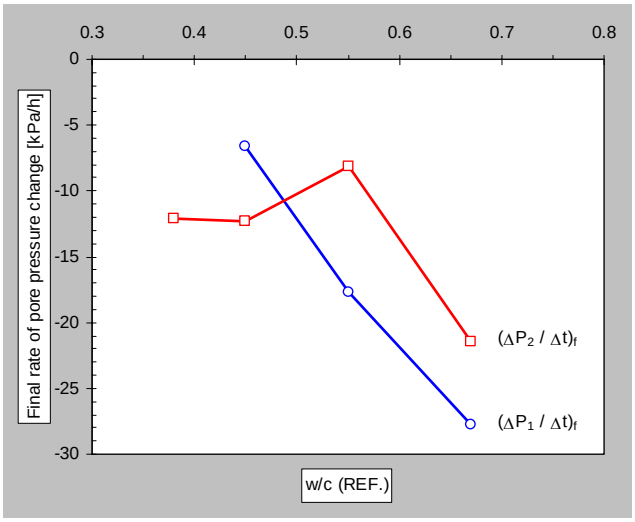

Figure 60. Effect of w/c on the final rate of pore pressure change for the reference concretes (pressure P1 at a depth of 60 mm and P2 at a depth of 20 mm).

Cracking tendency

The results for the average crack area for the reference concretes are presented in Figure 61. To complement the reference mixes an additional mix with *w/c* 0.61 was also investigated. As can be seen, it is evident that the concrete with the high w/c-ratio (0.67) had the highest crack area and that the concrete with w/c 0.55 had the smallest crack area (the ratio between the two crack areas are 0.22). Furthermore, there seems to exist an optimum w/c-ratio for the investigated reference mixes, which indicates that the w/c-ratio should be in the region of 0.55. In Figure 62 the measured restraint strain in the steel ring is presented, the strain has been normalized to its maximum value for easier comparison. A sudden drop in the stain indicates the occurrence of cracks. As can be seen, the first cracks seems to appear for the concrete with w/c 0.67 at five hours after mixing – this was also confirmed by visual inspection. For the concrete with w/c 0.55 a sudden drop in the strain curve is observed at eight hours and for the concrete with w/c 0.38 at nine to ten hours. For the concrete with w/c 0.45 no sudden drops can be seen in the strain curve.

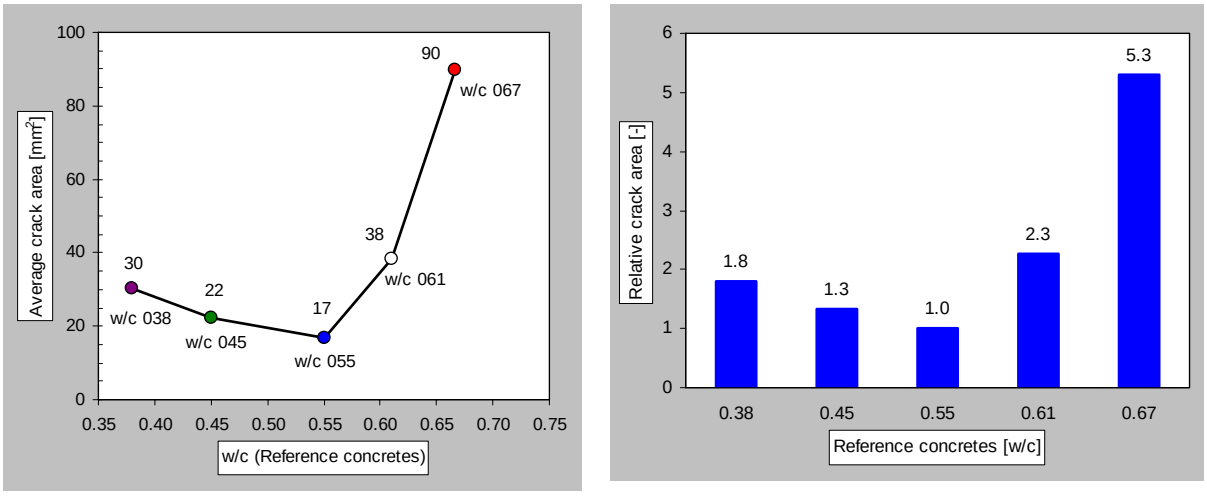

(a) *(b)*

Figure 61. *(a) Comparison of the average crack area for the reference concretes, influence of w/c ratio. (b) Comparison of the relative crack area using concrete with w/c 0.55 as reference.*

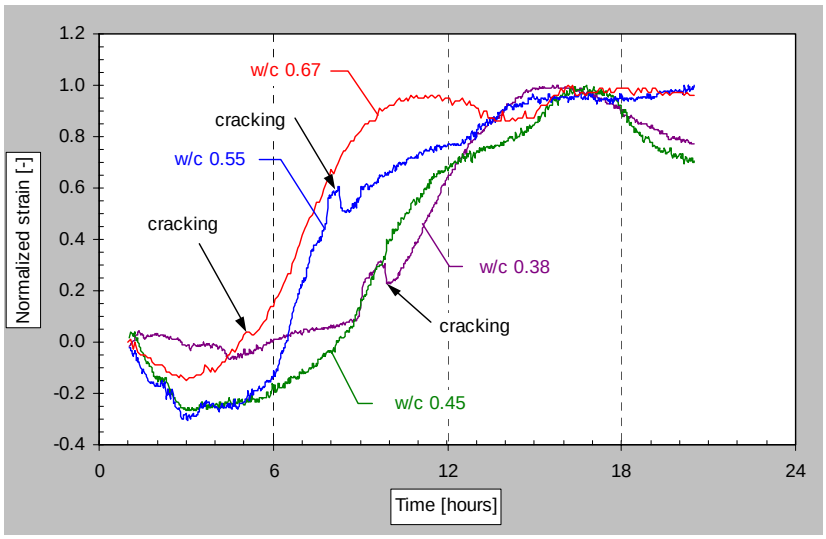

Figure 62. *Comparison of the normalized restraint strain in the steel ring for the reference concretes indicating the time of cracking.*

4.2.2 Type of cement

Evaporation

In Figure 63 a comparison of the evaporation for three types of cement is made. As can be seen, the evaporation were significantly larger for the slow hardening, low alkali, cement (CEM I 42,5 N) than for the other types of cement. The reasons for this are thought to be that: the water requirement is less (leads to higher workability and more pore water is available); the setting is delayed in comparison to the other cements; the cement is more coarsely grounded and water can more easily be transported to the surface. The rate of evaporation, which can be seen in Figure 63 (b), were lower for the rapid hardening cement (CEM I 52,5 R) while the slow hardening, low alkali, cement (CEM I 42,5 N) had the highest evaporation rate.

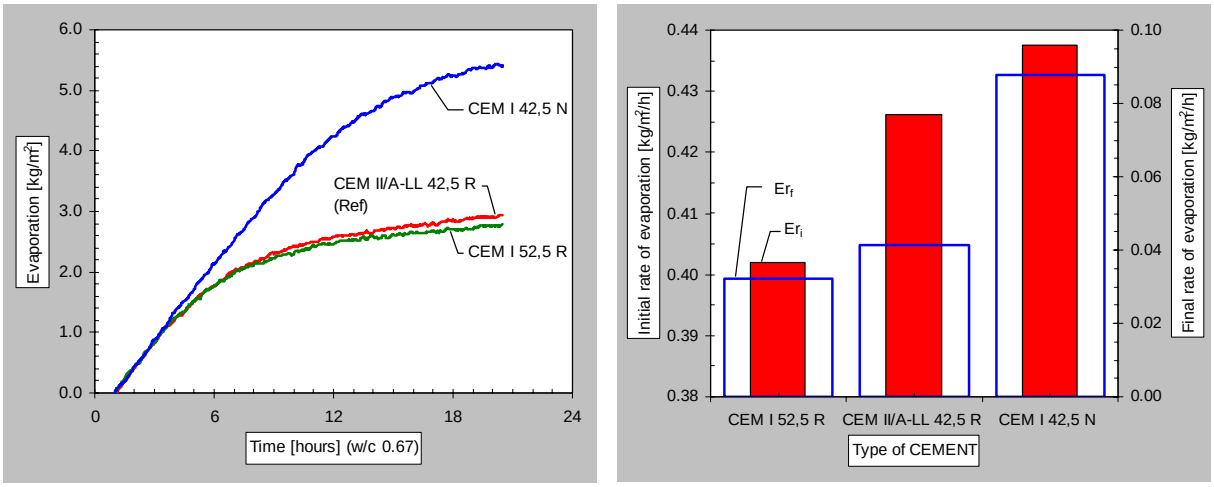

(a) *(b)*

Figure 63. Effect of cement type on evaporation for concrete with w/c 0.67: (a) evaporation curves; and (b) comparison of the rate of evaporation.

Temperature development

The temperature development for the three types of cement can be seen in Figure 64 The interpretation of the temperature curves is presented in Figure 65 and Figure 66. The different cements had about the same length of the dormant period (see Figure 66), but as soon as the hydration started there was a notable difference. As expected, the rapid hardening cement (CEM I 52,5 R) had a higher and faster temperature development while the slow hardening cement (CEM I 42,5 N) had a much lower temperature development and a late temperature peak.

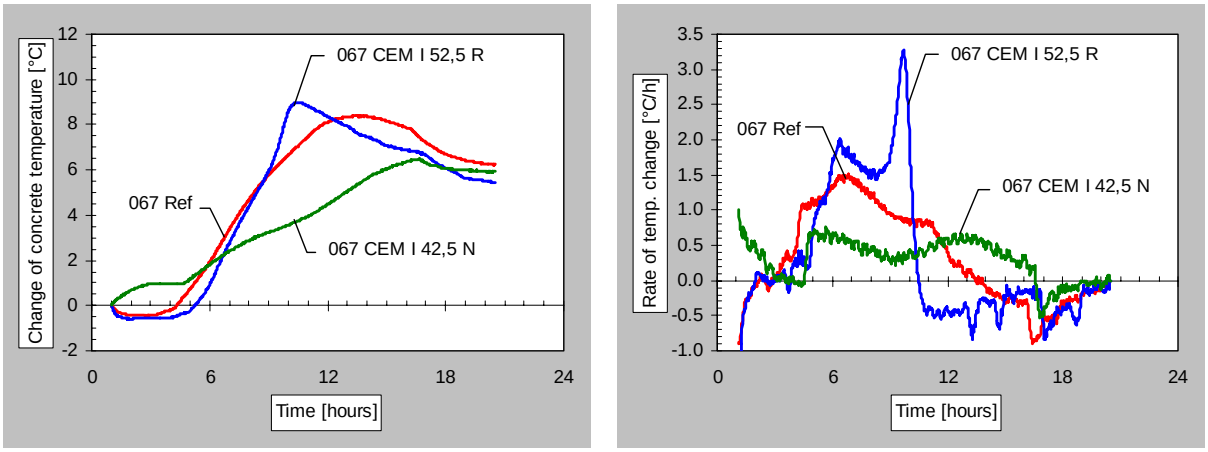

(a) *(b)*

Figure 64. Effect of cement type on temperature development in reference concretes with w/c 0.67: (a) comparison of change of temperature; and (b) comparison of the rate of temperature change.

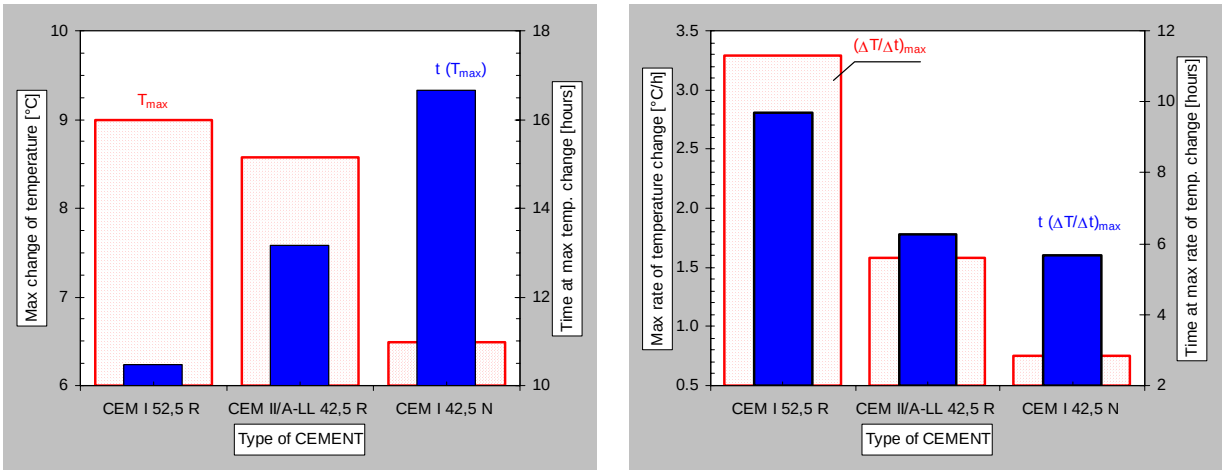

(a) *(b)*

Figure 65. Effect of cement type on hydration of reference concrete with w/c 0.67: (a) comparison of max temperature change and point of time; and (b) comparison of max rate of temperature change and point of time.

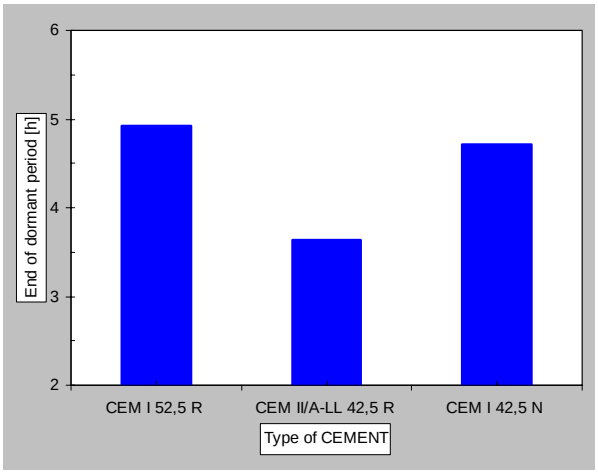

Figure 66. Effect of cement type on the end of the dormant period.

Pore pressure change

The development of the negative pore pressure can be seen in Figure 67. The only significant difference that could be observed when comparing the different types of cement was that: the pressure developed slightly faster for the rapid hardening cement (CEM I 52,5 R); and that the pressure development was slightly delayed for the slow hardening cement (CEM I 42,5 N).

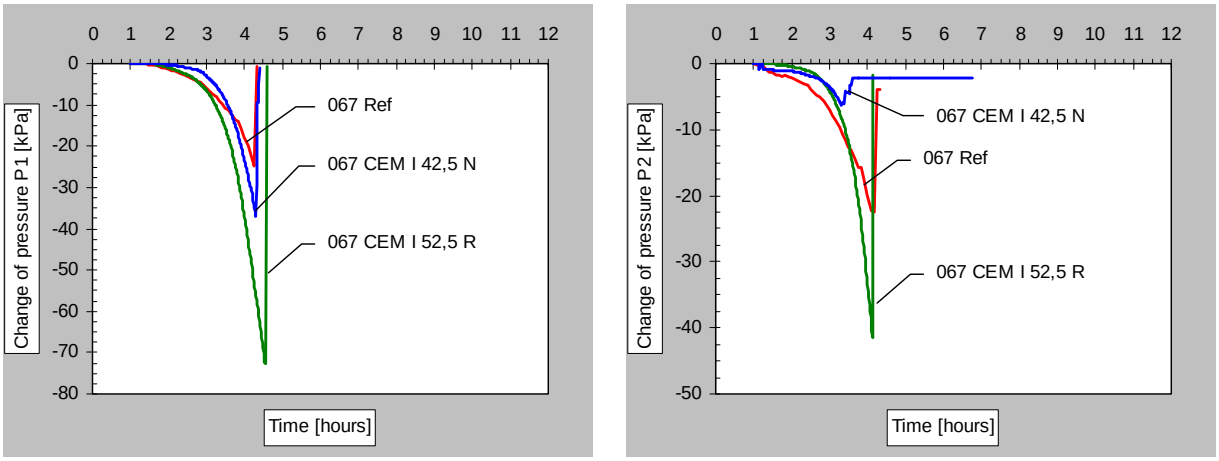

(a) *(b)*

Figure 67. Effect of cement type on pore pressure change for the reference concrete with w/c 0.67: (a) pressure P1 at a depth of 60 mm; and (b) pressure P2 at a depth of 20 mm.

Cracking tendency

In addition to the normal cement used in the reference mixes (CEM II/A-LL 42,5 R), two other types of cements were investigated. Namely, a rapid hardening portland cement (CEM I 52,5 R) and a slow hardening, low alkali, portland cement (CEM I 42,5 N). The relative crack area, which can be seen in Figure 68, has been normalized against the reference concrete (CEM II/A-LL 42,5 R). For the rapid hardening cement (CEM I 52,5 R) the crack area was 1.5 times that of the reference; and for the slow hardening, low alkali, cement (CEM I 42,5 N) the crack area was 2.4 times that of the reference. The increased crack area for the slow hardening, low alkali, cement (CEM I 42,5 N) was probably caused by larger evaporation, as a result of the delayed hydration, and also by some aggregate segregation.

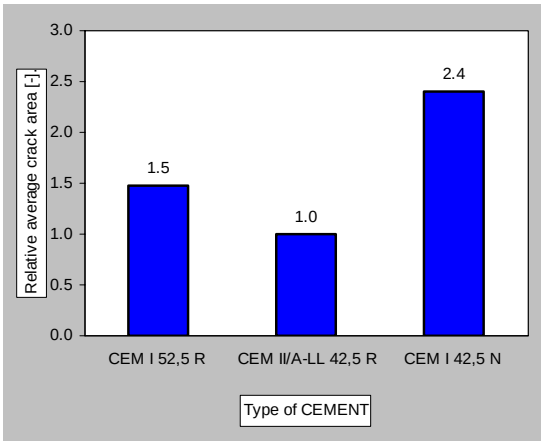

Figure 68. Effect of the cement type on the average crack area for the reference concrete with w/c 0.67 (the crack area has been normalised against the reference concrete).

4.2.3 Coarse aggregate content

Evaporation

The evaporation curves for the concrete with varying coarse aggregate content can be seen in Figure 70. A reduction of the coarse aggregate content, which lead to an increased crack area, resulted in a significantly lower evaporation (Figure 69(a)) and also a lower rate of evaporation (Figure 69(a)). The reasons for this, explained in section 4.1.3, is that for the concrete with a higher coarse aggregate content the packing is better and water is "released" to the mix.

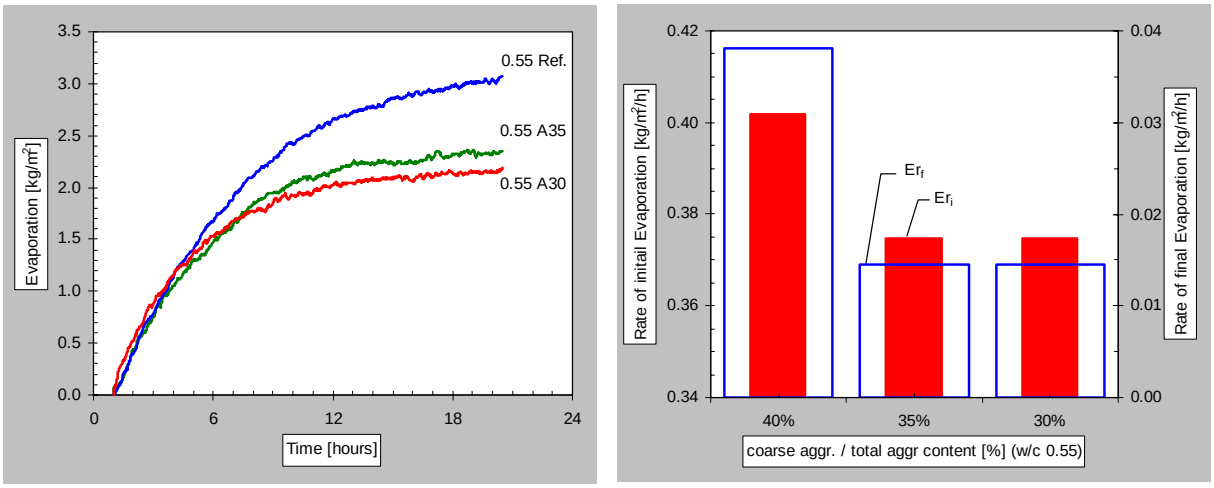

(a) *(b)*

Figure 69. Effect of coarse aggregate content on evaporation for concrete with w/c 0.55: (a) evaporation curves; and (b) comparison of the rate of evaporation.

Temperature development

In Figure 70 and Figure 71 the effect the coarse aggregate content had on the temperature development is presented. From the temperature development there was a trend that as the hydration started earlier as the coarse aggregate content was reduced, see Figure 71. A possible explanation for the observed behaviour (that the aggregate content affected the temperature development and the hydration) could be that the reduced coarse aggregate content lead to less evaporation that meant a reduced cooling effect.

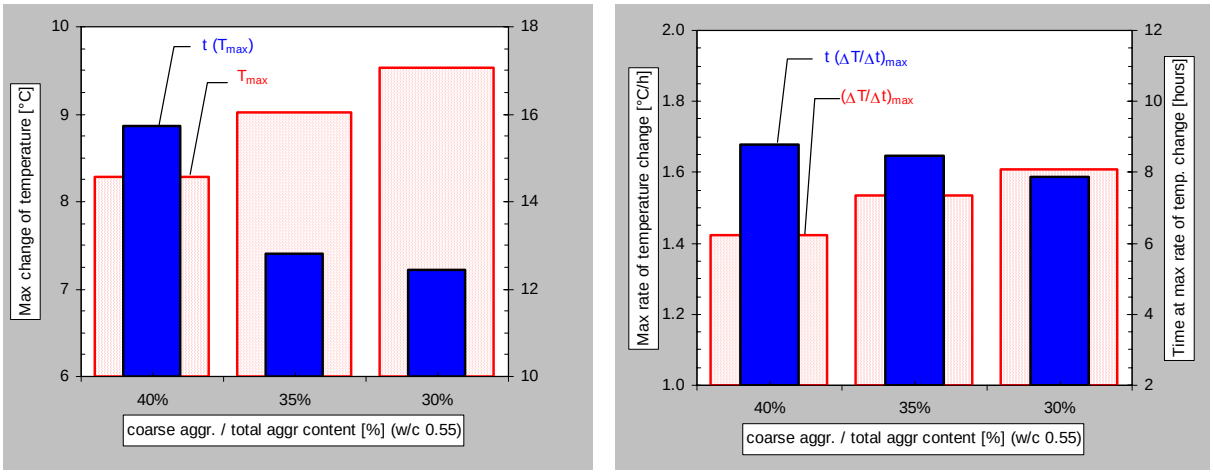

(a) *(b)*

Figure 70. Effect of coarse aggregate content on hydration of reference concrete with w/c 0.55: (a) comparison of max temperature change and point of time; and (b) comparison of max rate of temperature change and point of time.

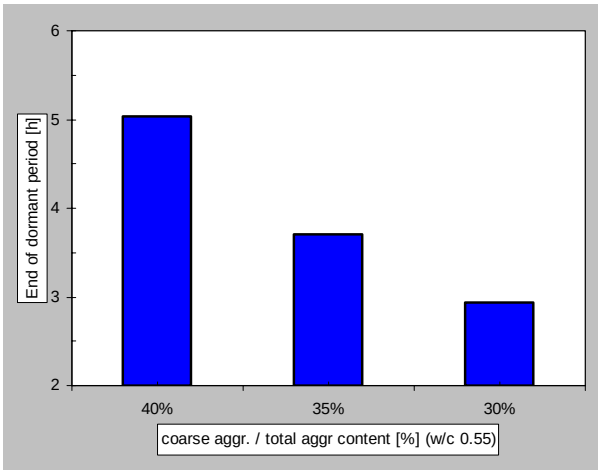

Figure 71. Effect of coarse aggregate content on hydration of reference concrete with w/c 0.55, comparison of the end of the dormant period.

Pore pressure change

Figure 72 shows the development of the pore pressure and the effect the coarse aggregate content had. As can be seen, the development of pore pressure was slightly delayed for the concretes with a reduced coarse aggregate content but at higher pressures the rate of the pore pressure development was increased (see Figure 73). It is thought that initially delayed pressure development was a result of the reduced evaporation whereas the higher final rate of pore pressure development was a result of a finer pore structure.

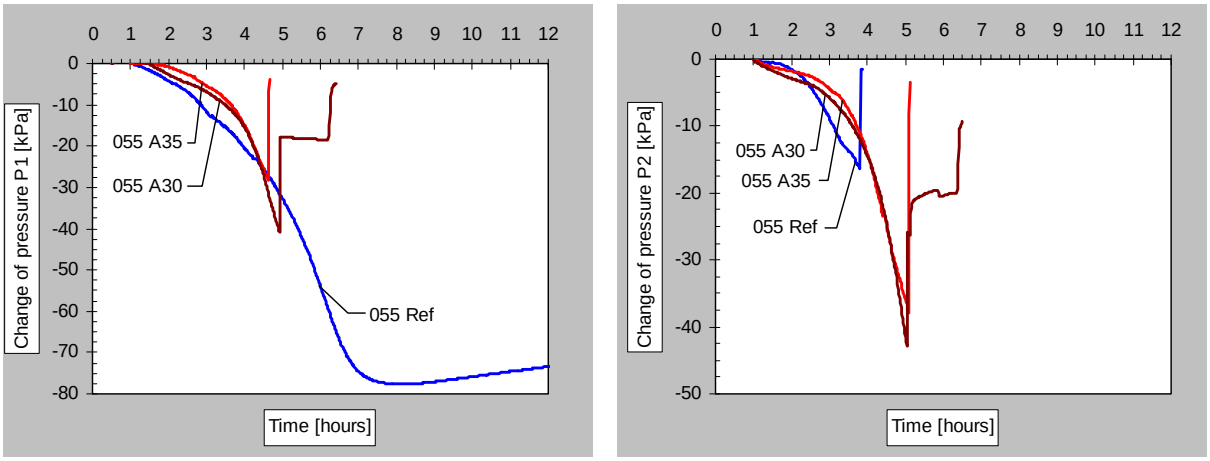

(a) *(b)*

Figure 72. Effect of coarse aggregate content on pore pressure change for the reference concrete with w/c 0.55: (a) pressure P1 at a depth of 60 mm; and (b) pressure P2 at a depth of 20 mm.

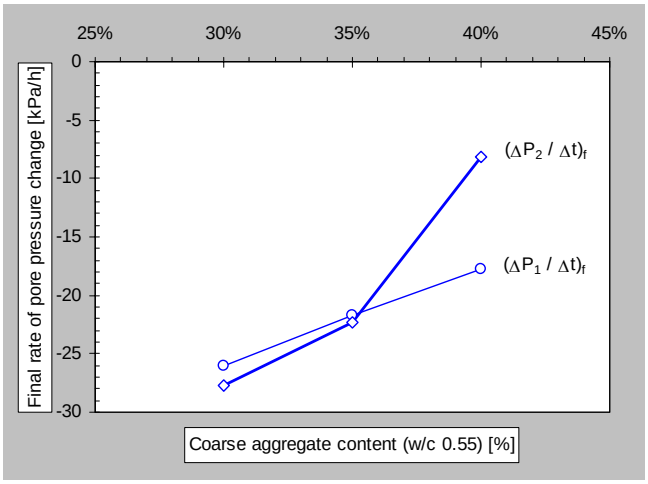

Figure 73. Effect of coarse aggregate content on the final rate of pore pressure change for the reference concrete with w/c 0.55 (pressure P1 at a depth of 60 mm and P2 at a depth of 20 mm).

Cracking tendency

That the aggregates are important is well known and it is beneficial to have large aggregates and a high aggregate content. The effect of the coarse aggregate content (8-16 in relation to total aggregate content) on crack area can be seen in Figure 74. As the coarse aggregate was reduced the crack area increased by a factor of about 2.1 to 2.2. However, interestingly the aggregate content had also an effect on the evaporation (which can be seen in Figure 70) and will be presented in the following section. This indicates that it is not only the rate of evaporation that determines the cracking behaviour, also the autogenous deformation plays an important role.

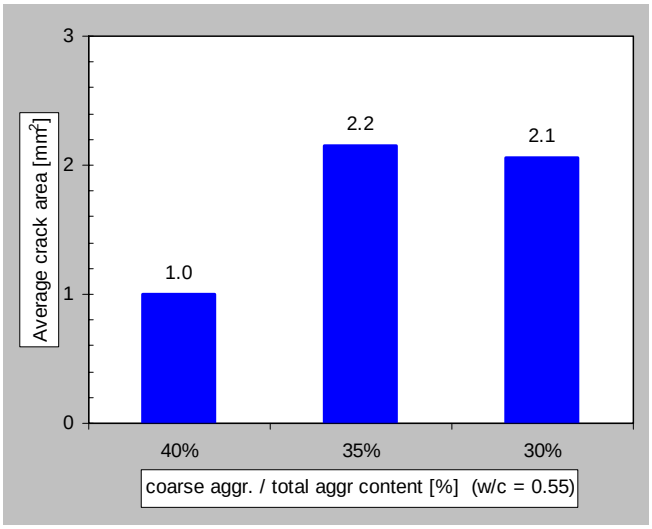

Figure 74. Effect on the coarse aggregate content on the average crack area for the reference concrete with w/c 0.55 (the crack area has been normalised against the reference concrete with 40% coarse aggregate).

4.2.4 Water content

Evaporation

When extra water was added to the reference concrete with w/c 0.67 the total evaporation was slightly increased while it had no significant effect on the initial rate of evaporation, see Figure 75. The increased evaporation was mostly an effect of the prolonged setting time (the length of the dormant period), see Figure 77 in the next section.

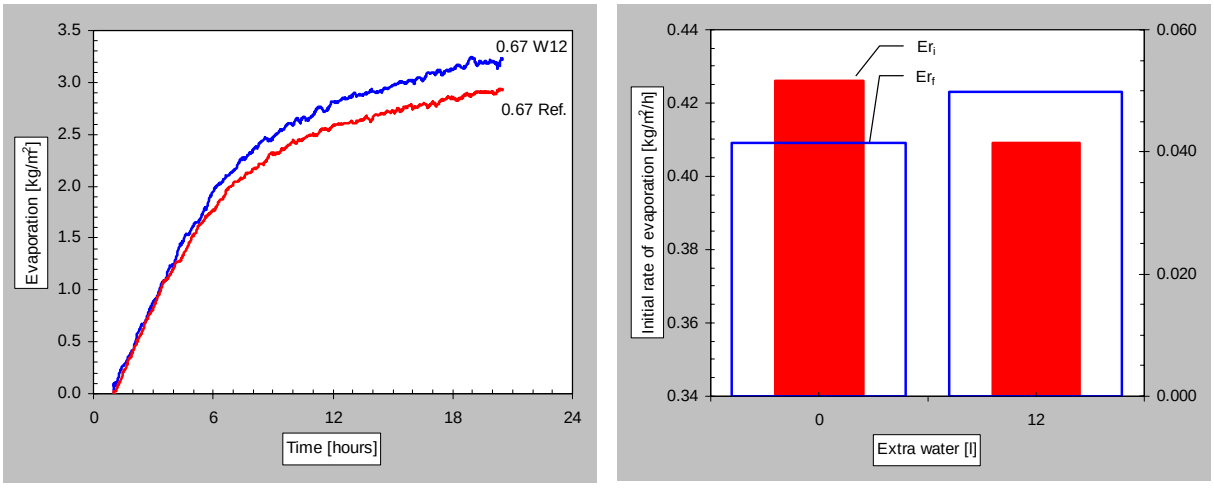

(a) *(b)*

Figure 75. Effect of adding extra water on evaporation for concrete with w/c 0.67: (a) evaporation curves; and (b) comparison of the rate of evaporation.

Temperature development

Figure 76 and Figure 77 presents the hydration parameters for the concrete with additional water (w/c 0.67 with 12 litres extra water, which resulted in w/c = 0.71). As can be seen, there was no significant difference neither in the maximum temperature change nor in the maximum rate of temperature change, and the time at which these occurred. However, as can be seen in Figure 77 the length of the dormant period was prolonged one hour, which could explain the increased evaporation.

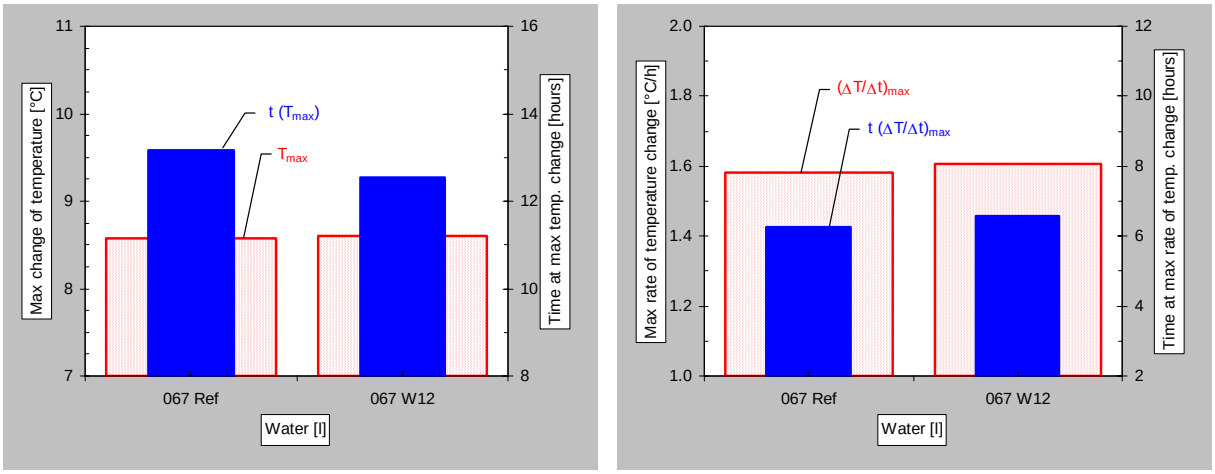

(a) *(b)*

Figure 76. Effect of adding extra water on hydration of reference concrete with w/c 0.67: (a) comparison of max temperature change and point of time; and (b) comparison of max rate of temperature change and point of time.

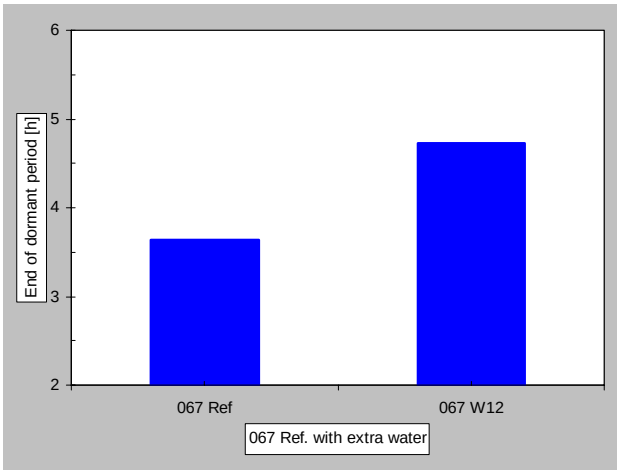

Figure 77. Effect of adding extra water on hydration of reference concrete with w/c 0.67, comparison of the end of the dormant period.

Cracking tendency

The effect of adding extra water had a dramatic effect on crack area, as can be seen in Figure 78. The average crack area was increased by a factor of 2.7 when 12 liters extra water was added to the reference concrete with w/c 0.67. The influence of the w/c-ratio can be seen in Figure 78 where the concrete with extra water (w/c = 0.71) have been inserted into the diagram to indicate the trend of high w/c-ratio.

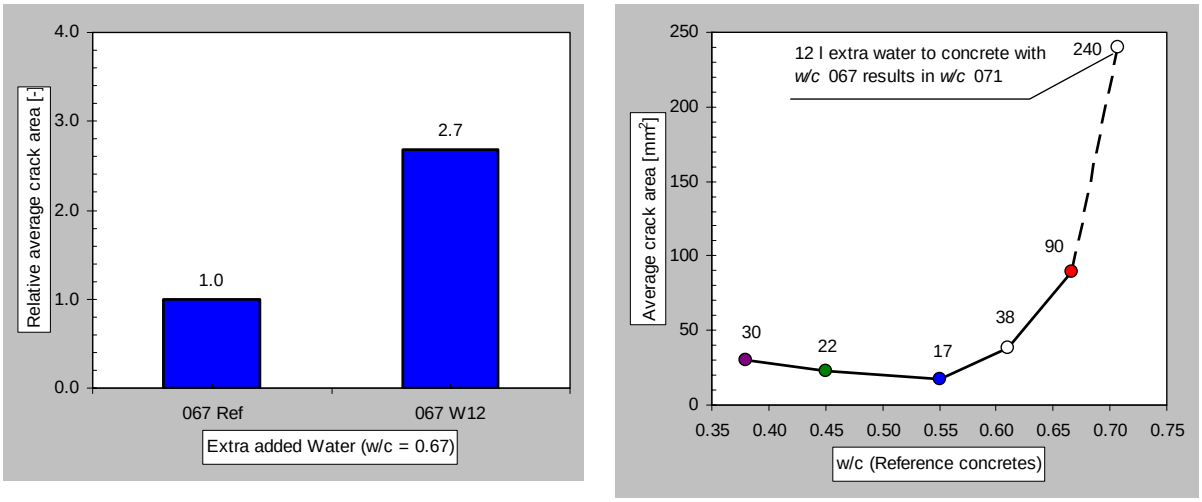

(a) *(b)*

Figure 78. Effect of adding extra water on the average crack area for the reference concrete with w/c 0.67 (the crack area has been normalised against the reference concrete): (a) comparison of the average crack area; and (b) influence of w/c-ratio on the crack area.

4.2.5 Fly Ash

Evaporation

Regarding the evaporation for the two concretes containing fly ash two different behaviours were observed, as can be seen in Figure 79. For the concrete with w/b 0.55 the total evaporation was decreased with 11% while the evaporation for the concrete with w/b 0.67 increased with 12%. For the concrete with w/b 0.55, the fly ash had no effect on the initial rate of evaporation but the final rate of evaporation was reduced by a factor of 0.63. For the concrete with w/b 0.67, on the other hand, the initial rate of evaporation was reduce by a factor of 0.95 while the final rate of evaporation was reduced by a factor of 0.96. The reasons for the observed behaviour (increased evaporation for the concrete with w/b 0.67 and decreased for the 0.55 concrete) are not entirely clear. However, a possible mechanism that might explain this could be that the retarding effect the fly ash has on the hydration is more pronounced for higher w/b-ratios. Furthermore, it was also noticed in rheological measurements that the fly ash improved the rheology of the concrete with w/b 0.55 and while it had the opposite effect on the concrete with w/b 0.67.

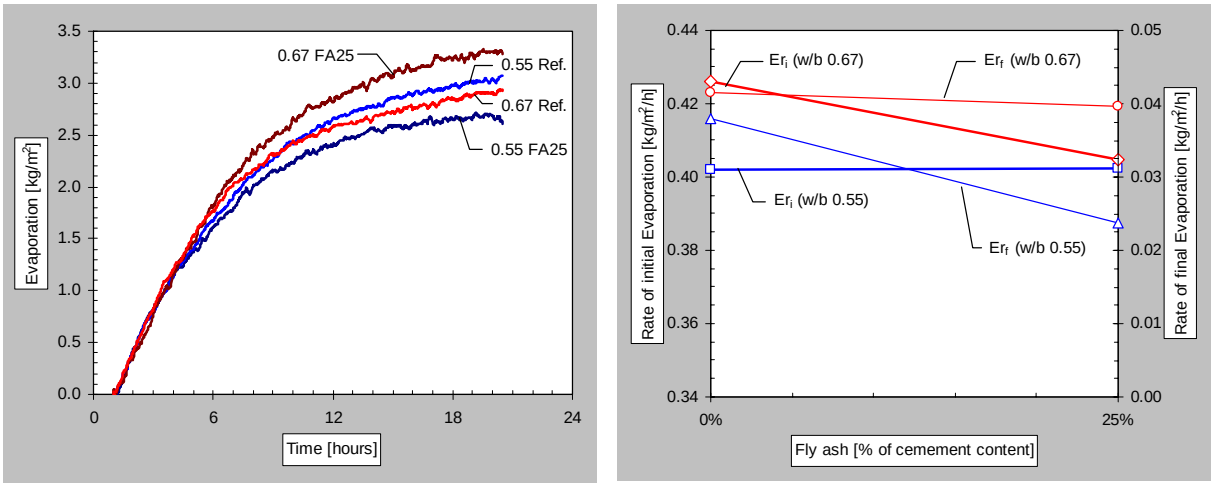

(a) *(b)*

Figure 79. Effect of fly ash on evaporation for concrete with w/b 0.55 and 0.67: (a) evaporation curves; and (b) comparison of the rate of evaporation.

Temperature development

The effect the fly ash had on the temperature development can be seen in Figure 80 and Figure 81 where the hydration parameters are presented. As can be seen, the fly ash reduced the maximum temperature change and the maximum rate of temperature change for both the investigated concretes, slightly more for the concrete with w/b 055. However, regarding the length of the dormant period (see Figure 81), the time at the maximum temperature change, and the time at the maximum rate of temperature change the two concretes behaved different. Similar as to the evaporation the fly ash seemed to have had an retarding effect on the concrete with the higher w/b-ratio (0.67) and almost no effect on the concrete with w/b 0.55. That the fly ash had almost no effect on the concrete with w/b 0.55 was a bit surprising but that it had an retarding effect on the other concrete corresponds well with other studies. For example, Langana et al. (2002) found that fly ash retards hydration in the dormant and acceleration periods, and that it also accelerates hydration after the acceleration period. Furthermore, Langana et al. also noticed that the retarding effect of fly ash was greater the higher the w/c-ratio.

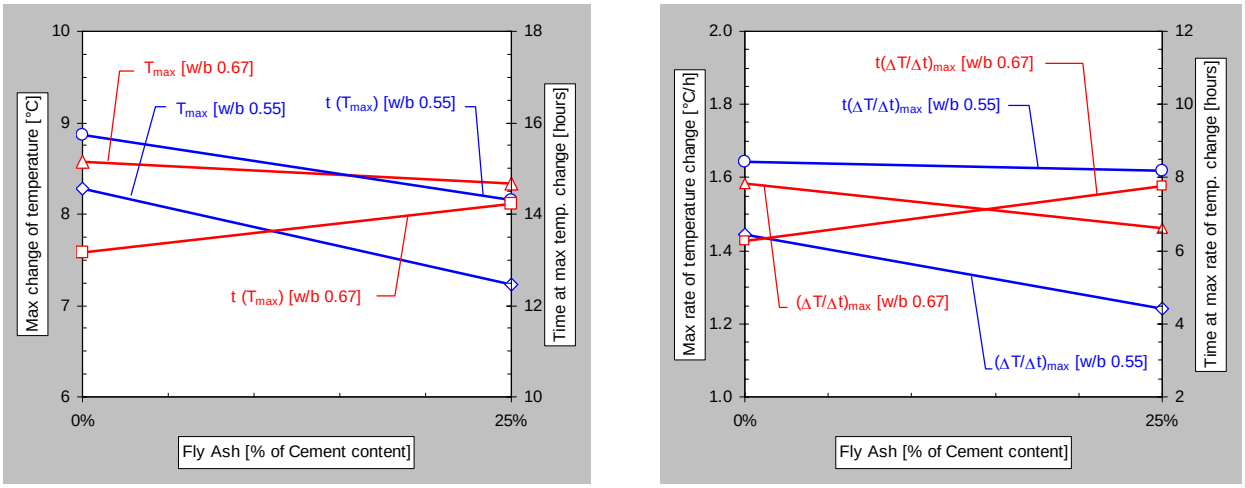

(a) *(b)*

Figure 80. Effect of fly ash on hydration of reference concrete with w/b 0.55 and 0.67: (a) comparison of max temperature change and point of time; and (b) comparison of max rate of temperature change and point of time.

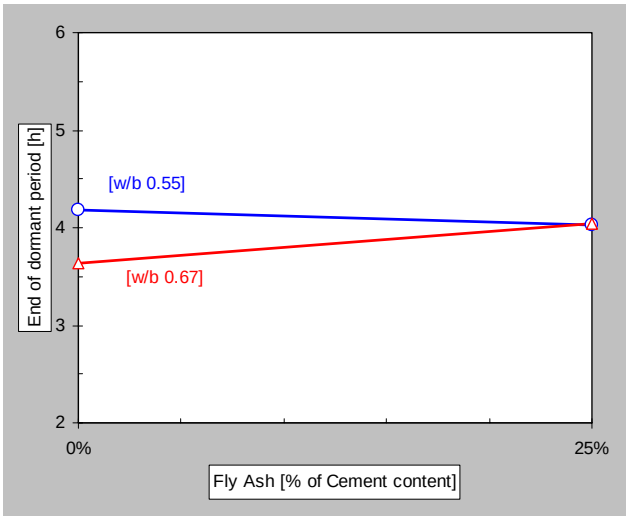

Figure 81. Effect of fly ash on hydration of reference concrete with w/b 0.55 and 0.67, comparison of the end of the dormant period.

Pore pressure change

The development of the pore pressure change for the concretes containing fly ash is presented in Figure 82 for the concrete with w/b 0.55 and in Figure 83 for the concrete with w/b 0.67. In Figure 84 and Figure 85 shows the evaluated pore pressure parameters for the two concretes. The main effect the fly ash seemed to have on the pore pressure development was that it delayed this a little, but it had almost no effect on the rate of the pressure change. This is a bit surprising as the concrete with fly ash cracked earlier and more compared to the reference concrete.

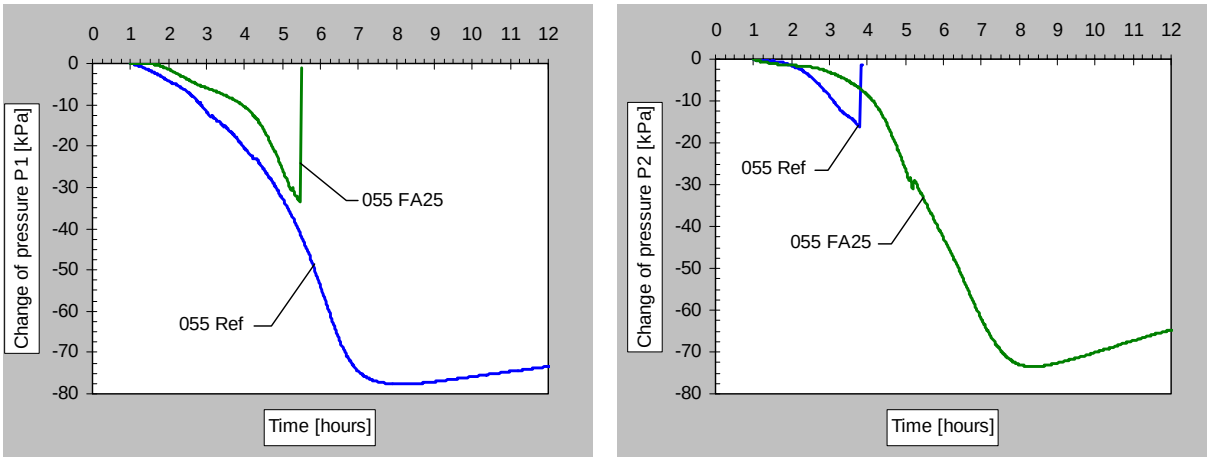

(a) *(b)*

Figure 82. Effect of fly ash on pore pressure change for the reference concrete with w/b 0.55: (a) pressure P1 at a depth of 60 mm; and (b) pressure P2 at a depth of 20 mm.

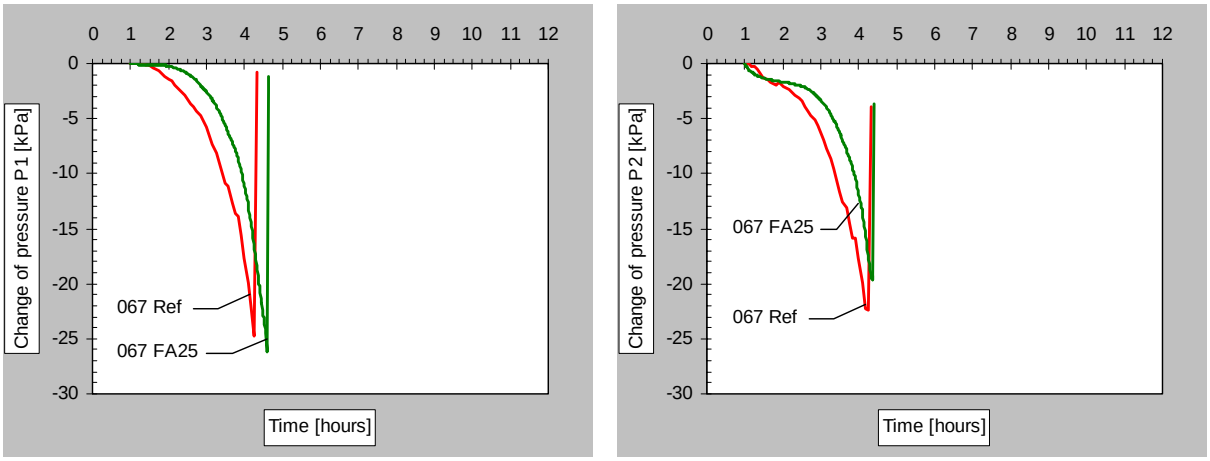

(a) *(b)*

Figure 83. Effect of fly ash on pore pressure change for the reference concrete with w/b 0.67: (a) P1 at a depth of 60 mm; and (b) P2 at a depth of 20 mm.

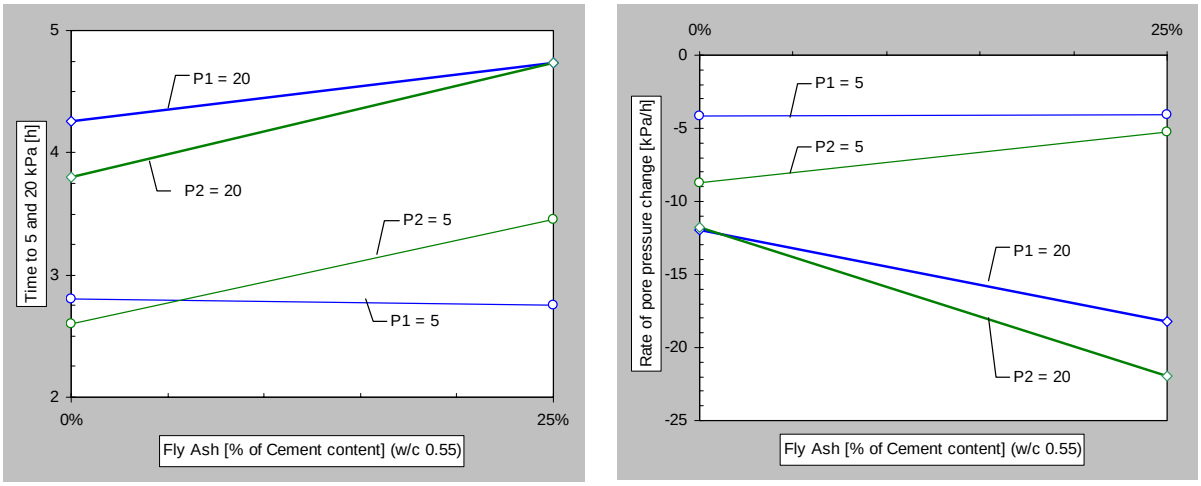

(a) *(b)*

Figure 84. Effect of fly ash on pore pressure change for the reference concrete with w/b 0.55: (a) time to 5 and 20 kPa; and (b) rate of pressure change at 5 and 20 kPa.

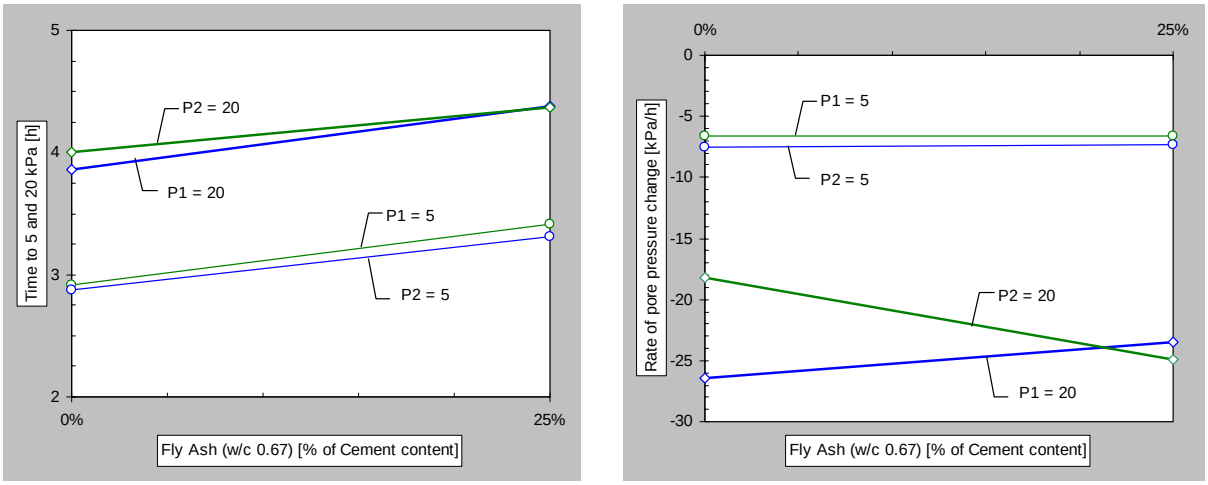

(a) *(b)*

Figure 85. Effect of fly ash on pore pressure change for the reference concrete with w/b 0.67: (a) time to 5 and 20 kPa; and (b) rate of pressure change at 5 and 20 kPa.

Cracking tendency

The cracking tendency for the concrete with fly ash is presented in Figure 86 and in Figure 87 the development of the restraint strain has been plotted. As can be seen in Figure 86, the average crack area was significantly increased for both concretes: with a factor of 1.7 for the concrete with w/b 0.55; and with a factor of 1.6 for the concrete with w/b 0.67. Cracks started to appear four hours after mixing for the concrete with w/b 0.67 and at seven hours for the concrete with w/b 0.55, see Figure 87. This meant that the cracks appeared roughly one hour earlier for the concrete containing fly ash than for the reference concretes (compare with Figure 62). Possible explanations for the increased crack area are: increased amount of fine material, which should results in a higher pore pressure; the fly ash improved the rheology of the fresh concrete; some aggregate segregation as a result of the improved the rheology.

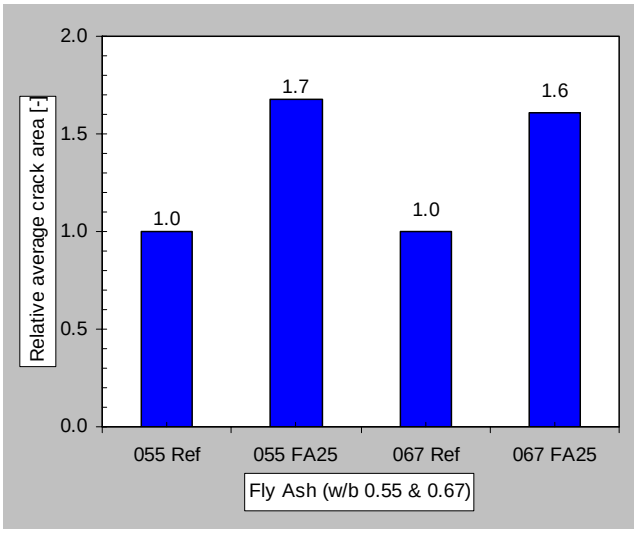

Figure 86. Effect of fly ash (replaced by volume against cement) on the average crack area for the reference concrete with w/b 0.55 and for the reference concrete with w/b 0.67 (the crack area has been normalised against the reference concretes).

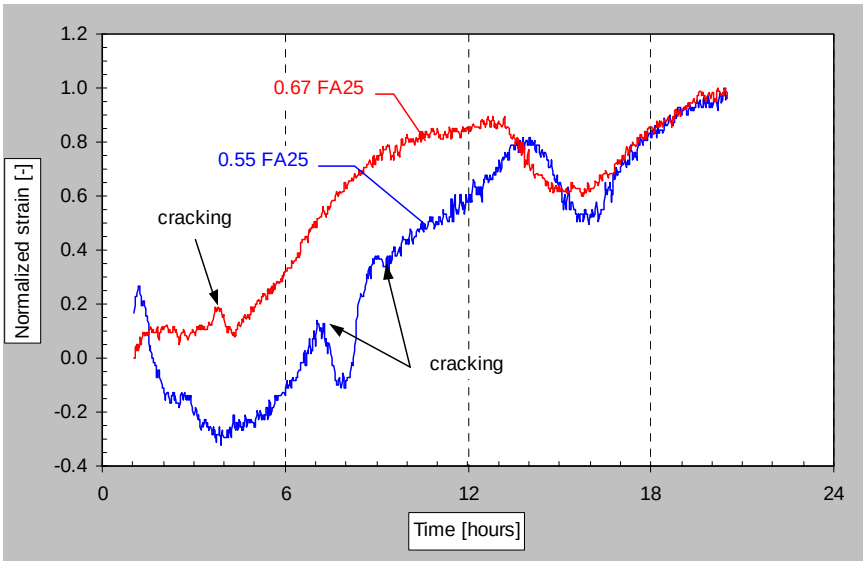

Figure 87. Comparison of the normalized restraint strain in the steel ring for the concrete containing fly ash (055 FA25 & 067 FA25) indicating the time of cracking.

4.2.6 Silica fume

Evaporation

The effect silica fume had on the evaporation can be seen in Figure 88. Silica reduced the total evaporation, by 18% with 5% silica and by 23% with 10 % silica, and the final rate of evaporation (by a factor 2 with 5% silica and by a factor of 2.3 with 10% silica). The initial rate of evaporation was not affected.

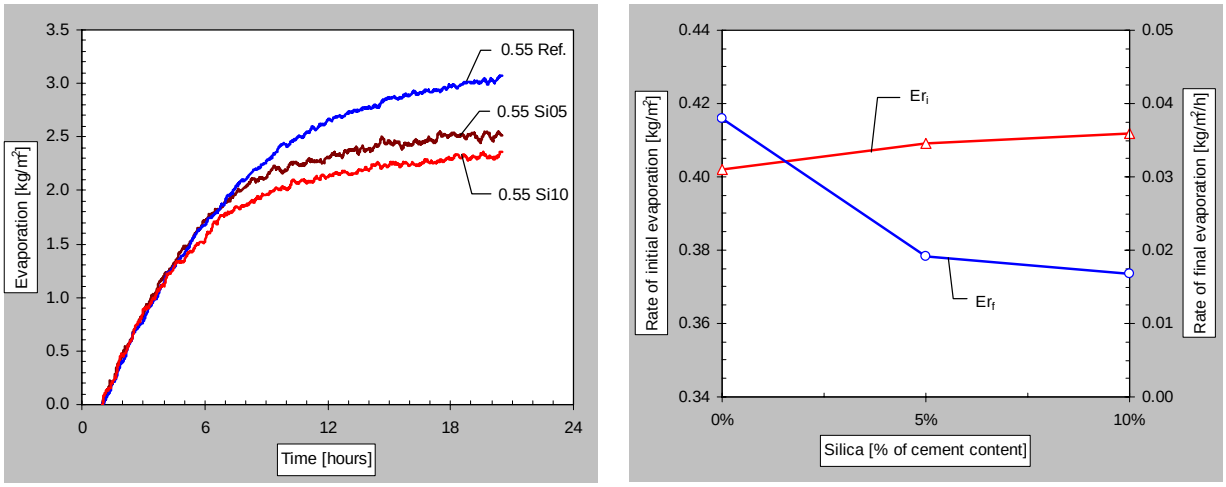

(a) *(b)*

Figure 88. Effect of silica fume on evaporation for concrete with w/c 0.55: (a) evaporation curves; and (b) comparison of the rate of evaporation.

Temperature development

The effect silica had on the temperature development can be seen in Figure 89 and the evaluated hydration parameters are presented in Figure 90 and Figure 91. As can be seen, silica accelerated the early hydration primarily by shortening the dormant period (with 5% silica by one hour and with 10% silica with one and a half hour). The silica had no effect on the maximum temperature change or the rate, but the temperature peak occurred two to three hours earlier. That silica accelerates the early hydration for concrete with w/c higher than 0.5 was also found by Langana et al. (2002), see also Neville (2000) pp. 669.

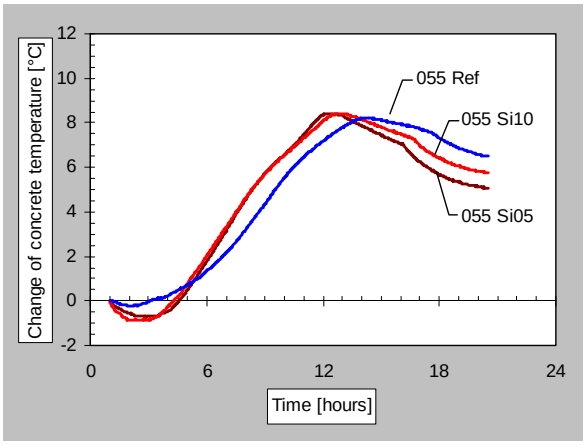

Figure 89. Effect of silica fume on temperature development in reference concrete with w/c 0.55.

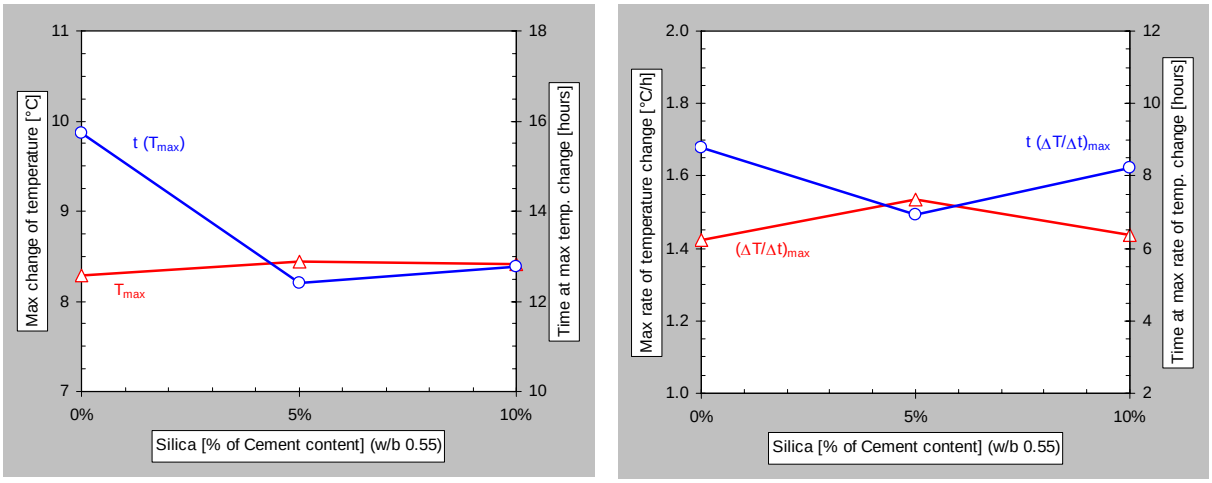

(a) *(b)*

Figure 90. Effect of silica fume on hydration of reference concrete with w/c 0.55: (a) comparison of max temperature change and point of time; and (b) comparison of max rate of temperature change and point of time.

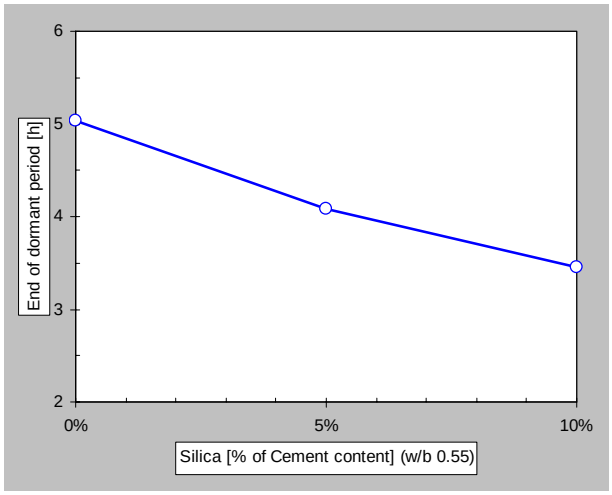

Figure 91. Effect of silica fume on hydration of reference concrete with w/c 0.55, comparison of the end of the dormant period.

Pore pressure change

The effect the silica had on the pore pressure development can be found in Figure 92 to Figure 94. From the results it looks as if the silica primarily increases the rate of the pressure change at higher pressures (see Figure 93 and Figure 94). The increased rate of pore pressure change is believed to be caused by the small particle size of the silica fume and the accelerated early hydration.

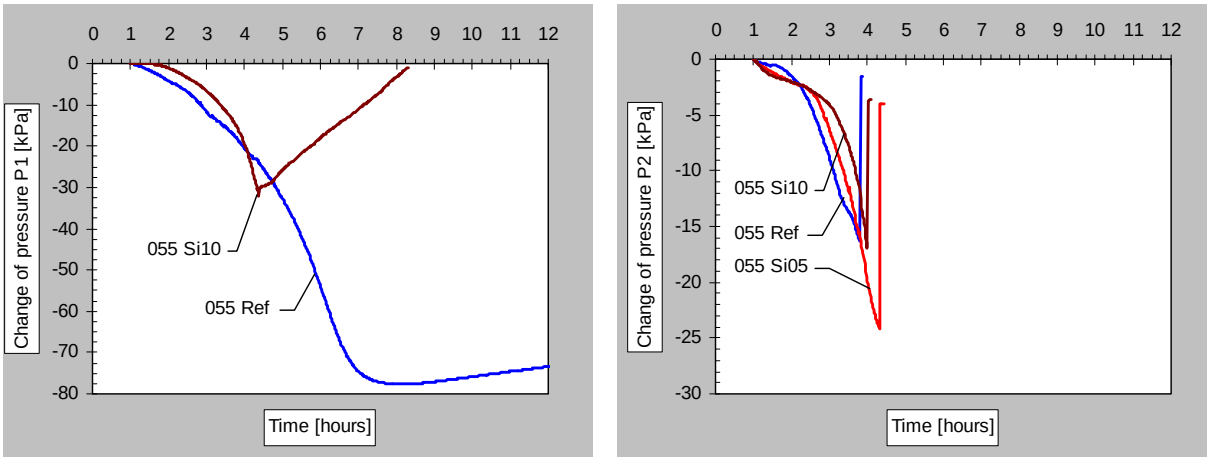

(a) *(b)*

Figure 92. Effect of silica on pore pressure change for the reference concrete with w/c 0.55: (a) P1 at a depth of 60 mm; and (b) P2 at a depth of 20 mm.

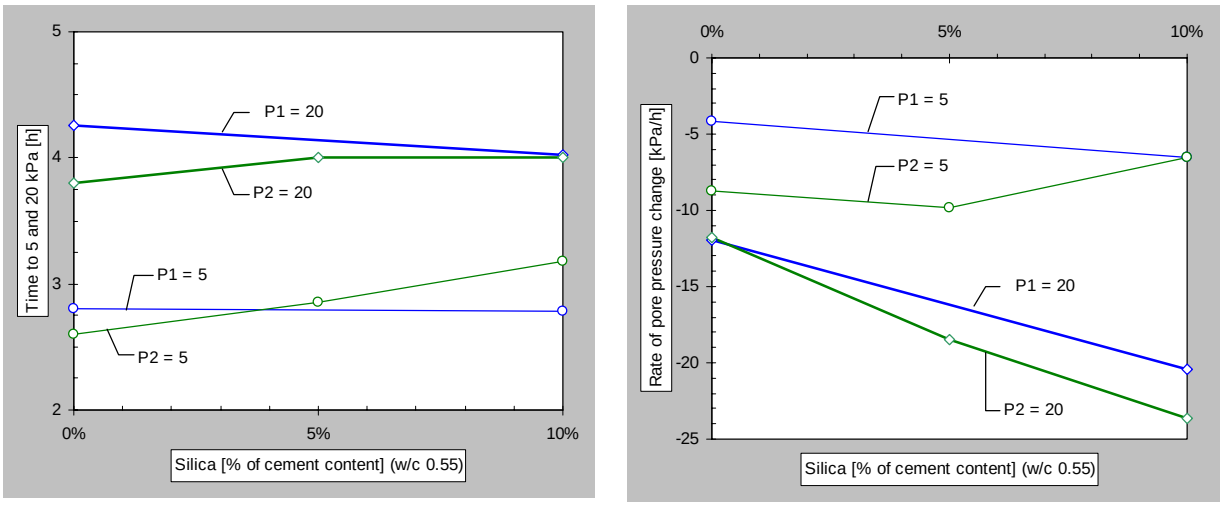

(a) *(b)*

Figure 93. Effect of silica on pore pressure change for the reference concrete with w/c 0.55: (a) time to 5 and 20 kPa; and (b) rate of pressure change at 5 and 20 kPa.

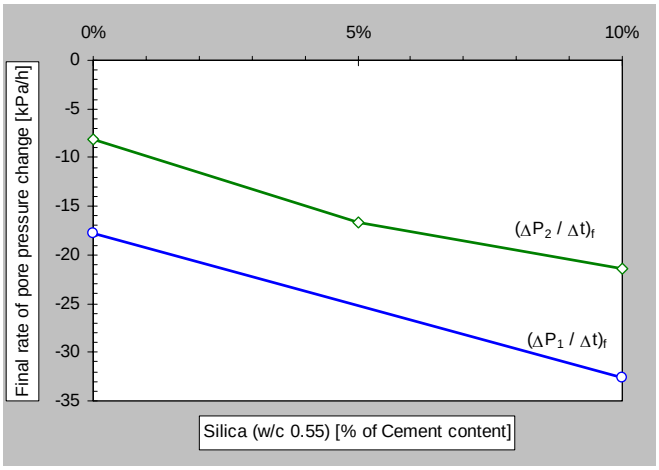

Figure 94. Effect of silica on the final rate of pore pressure change for the reference concrete with w/c 0.55 (pressure P1 at a depth of 60 mm and P2 at a depth of 20 mm).

Cracking tendency

When silica fume replaced 5% and 10% of the cement in the concrete with w/c 0.55 (this gave w/b = 0.54 respectively 0.53) the relative average crack area, which can be seen in Figure 95, increased dramatically. With 5% silica the crack area increased with a factor of 4.0 and with 10% by a factor of 5.1. Figure 96 shows the measured restraint strain and, as can be seen, the first cracks appeared at three and half to four hours after mixing and there was also a large drop in the strain at five and a half hours for the concrete with 10% silica and one hour later for the concrete with 5% silica. Moreover, the drop of the restraint strain was significantly larger for the concrete with 10% silica indicating that this concrete had undergone a larger shrinkage and that it was more brittle. The cracking occurred earlier than for the reference without silica (and also earlier than for the concrete with fly ash). Possible explanations for the increased crack area are: increased amount of small particles, which results in a higher pore pressure; silica accelerates the early hydration; the autogenous shrinkage increases with silica, as could be seen in the CDD-experiments.

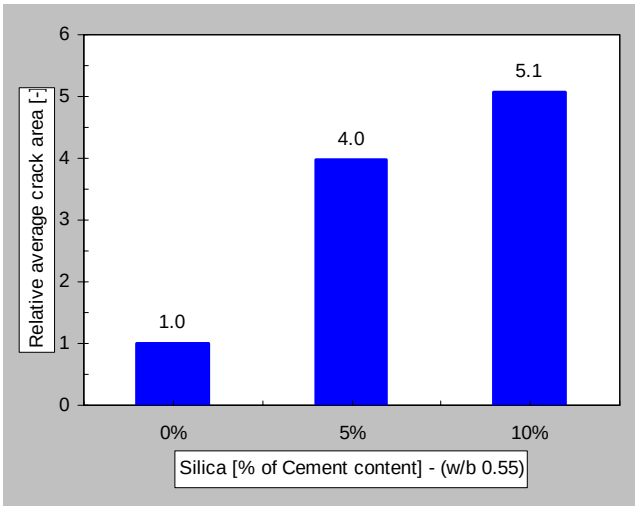

Figure 95. *Effect of silica (replaced by volume against cement) on the average crack area for the reference concrete with w/c 0.55 (the crack area has been normalised against the reference concrete).*

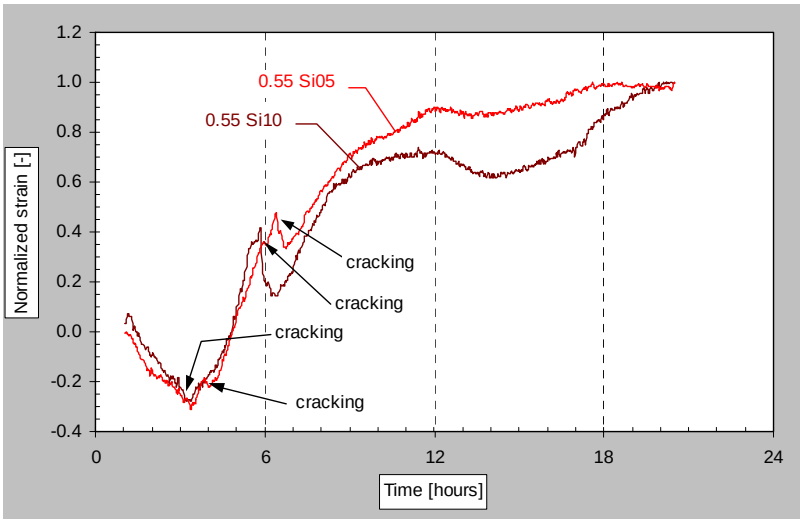

Figure 96. *Comparison of the normalized restraint strain in the steel ring for the concrete with silica (055 Si05 & 055 Si10) indicating the time of cracking.*

4.2.7 Superplasticizer dosage

Evaporation

The effect the superplasticizer (SP) dosage had on the evaporation is presented in Figure 97. The curve for 067 SP10 in Figure 97 have been modified to account for the higher relative humidity during the test, the modified curve is denoted 067 SP10#. An increased dosage, as in the case with 1.0% (067 SP10#) and with a delayed dosage of 0.2% (067 SP08+02), resulted in an increased total evaporation with 4% for SP10 and 6% for SP08+02. With a reduced SP-dosage, 0.6% (067 SP06), the total evaporation was reduced with 16%. The initial rate of evaporation was slightly increased for the low SP-dosage and reduced for the high SP-dosage, the main cause of this is believed to be related to the prolonged setting time which the superplasticizer results in. That the evaporation increases is also likely a result of the prolonged setting time.

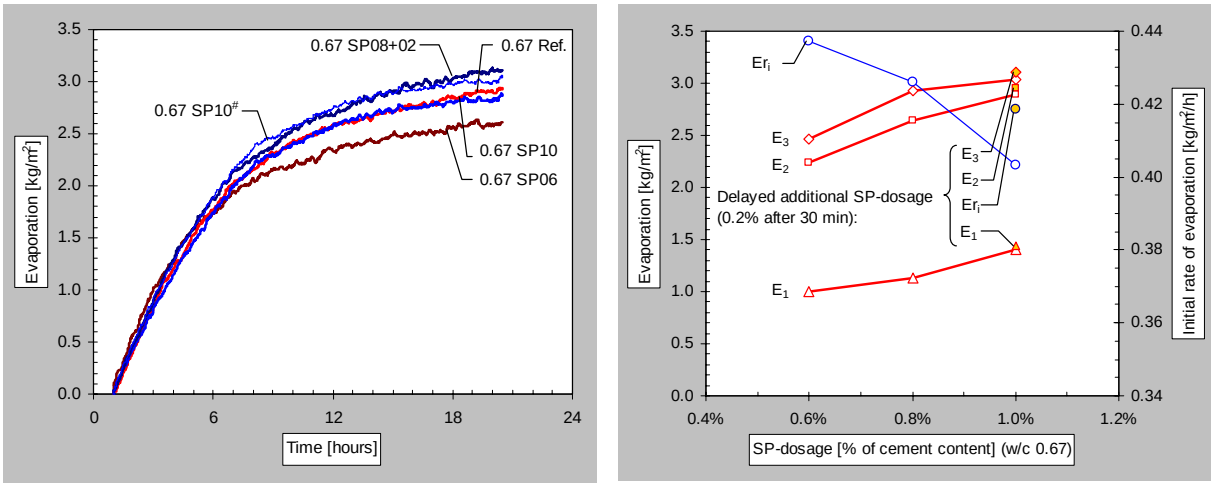

(a) *(b)*

Figure 97. Effect of the SP-dosage on evaporation for concrete with w/c 0.67: (a) comparison of evaporation curves – SP10# refer to a modified evaporation curve due to high RH; and (b) comparison of the rate of evaporation and the evaporation at time t_1, t_2, and t_3.

Temperature development

Figure 98 and Figure 99 shows the effect the SP-dosage had on the hydration of the reference concrete with w/c-ratio 0.67. An increased SP-dosage delayed the hydration slightly, and the length of the dormant period (see Figure 100) was increased with about one hour. In the same way, but opposite, a reduced SP-dosage lead to a somewhat earlier cement reaction.

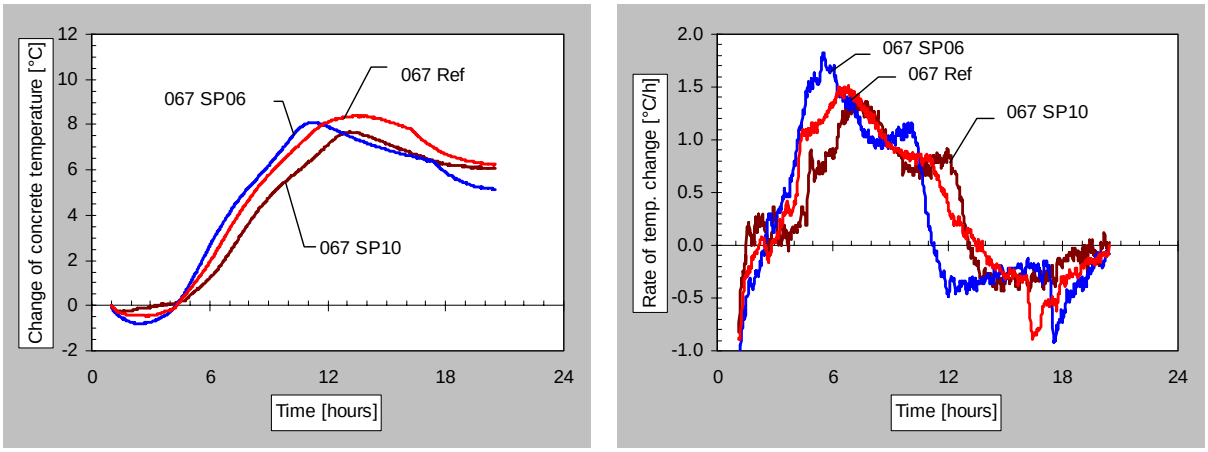

(a) *(b)*

Figure 98. Effect of SP-dosage on temperature development of reference concrete with w/c 0.67: (a) comparison of temperature change; and (b) comparison of the rate of temperature change.

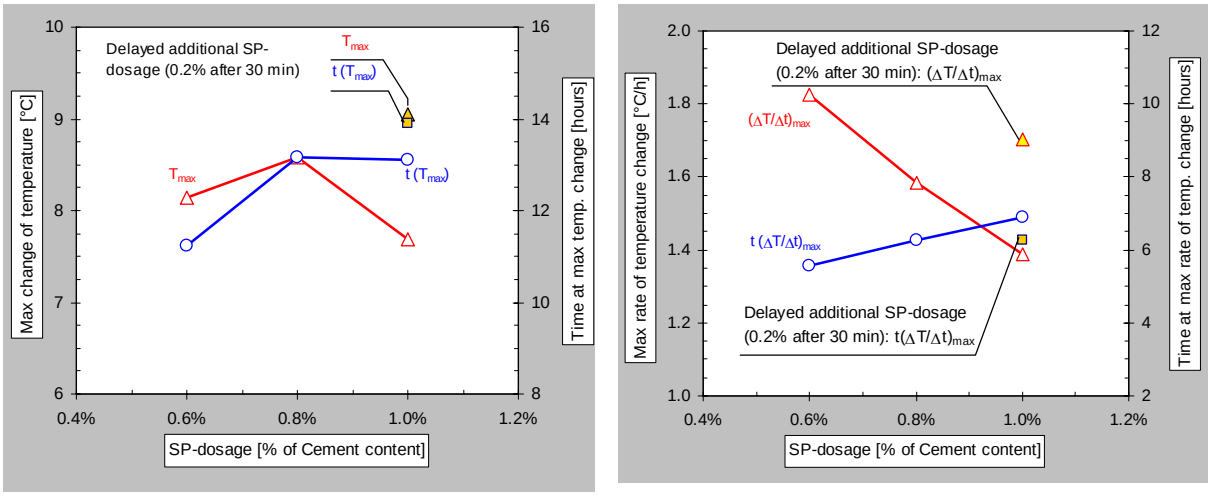

(a) *(b)*

Figure 99. Effect of SP-dosage on hydration of reference concrete with w/c 0.67: (a) comparison of max temperature change and point of time; and (b) comparison of max rate of temperature change and point of time.

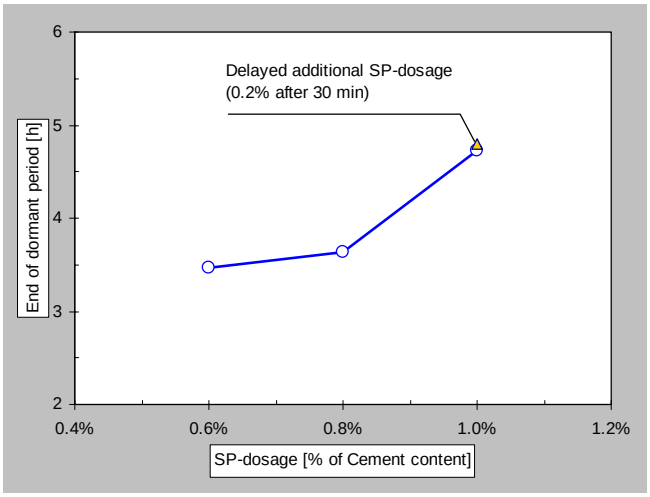

Figure 100. Effect of SP-dosage on hydration of reference concrete with w/c 0.67, comparison of the end of the dormant period.

Pore pressure change

The influence of the SP-dosage on the pore pressure development is presented in Figure 101 and Figure 102. The effect the SP-dosage had on the pore pressure development was analogous to that it had on the hydration: a low dosage accelerated the pressure development; a high dosage had a retarding effect. The rate of the pressure development seemed not to be influenced.

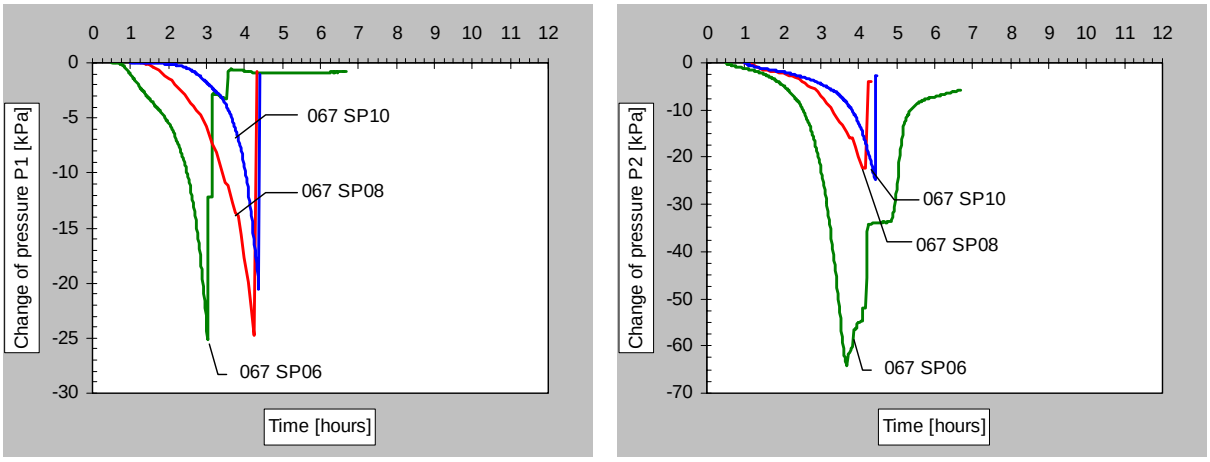

(a) *(b)*

Figure 101. Effect of SP-dosage on pore pressure change: (a) pressure P1 at a depth of 60 mm; and (b) pressure P2 at a depth of 20 mm

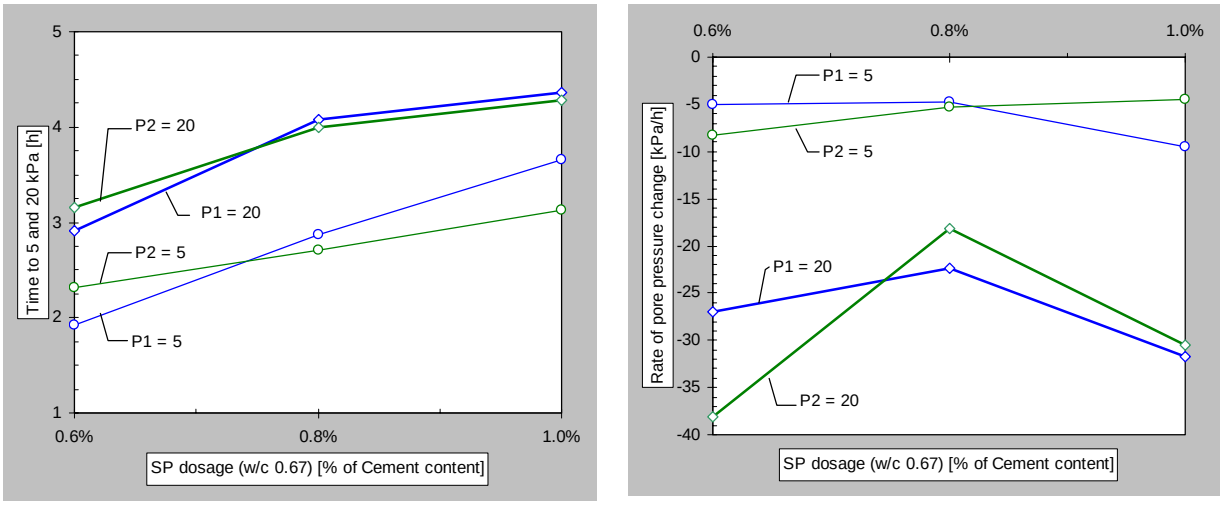

(a) *(b)*

Figure 102. Effect of SP-dosage on pore pressure change for the reference concrete with w/c 0.67: (a) Time to 5 and 20 kPa; and (b) the rate of pressure change at 5 and 20 kPa.

Cracking tendency

The superplasticizer dosage seemed to have a large influence on the average crack area. As can be seen in Figure 103, when the SP-dosage was reduced to 0.6% the crack area was reduced by a factor of 5.0 (the relative crack area was only 0.2) and with the high SP-dosage (1.0%) the crack area increased by a factor of 1.54. For the case with a delayed additional SP-dosage (0.2% after 30 min) the crack area was also increased (by a factor of 2.0). However, it should be pointed out that for the case with a SP-dosage of 1.0% the relative humidity was slightly higher compared to the other tests: for the case with the high dosage, the average RH was 35%; for the case with the delayed dosage, average RH was 27%; for the case with the low dosage, the average RH was 30%; and for the reference concrete (SP 08), the average RH was 30%

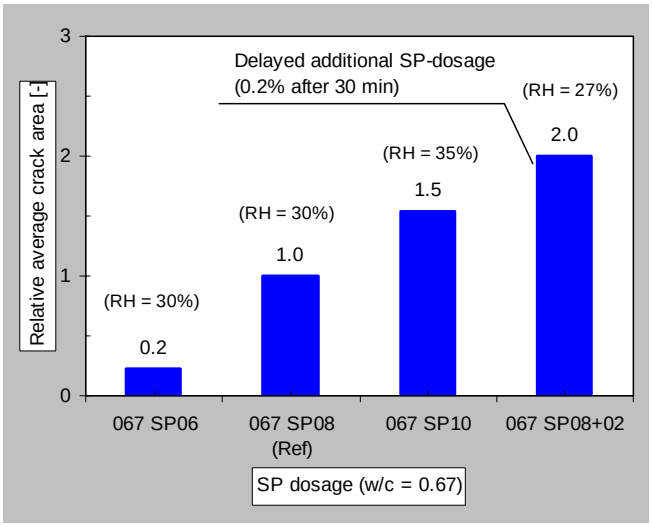

Figure 103. Effect on the SP-dosage on the average crack area for the reference concrete with w/c 0.67 (the crack area has been normalised against the reference concrete).

4.2.8 Accelerator and retarder

Evaporation

The effect the accelerator and the retarder had on the evaporation can be seen in Figure 104. The curve for 067 RE02 in Figure 104 have been modified to account for the higher relative humidity during the test, the modified curve is denoted 067 RE02$^{\#}$. The effect of the accelerator and retarder on the evaporation is comparable to the effect the SP-dosage had. For the concrete with accelerator the evaporation was reduced with 16% and for the concrete with retarder the evaporation increased with 5%. The accelerator seemed to reduce the initial rate of evaporation, see Figure 104(b).

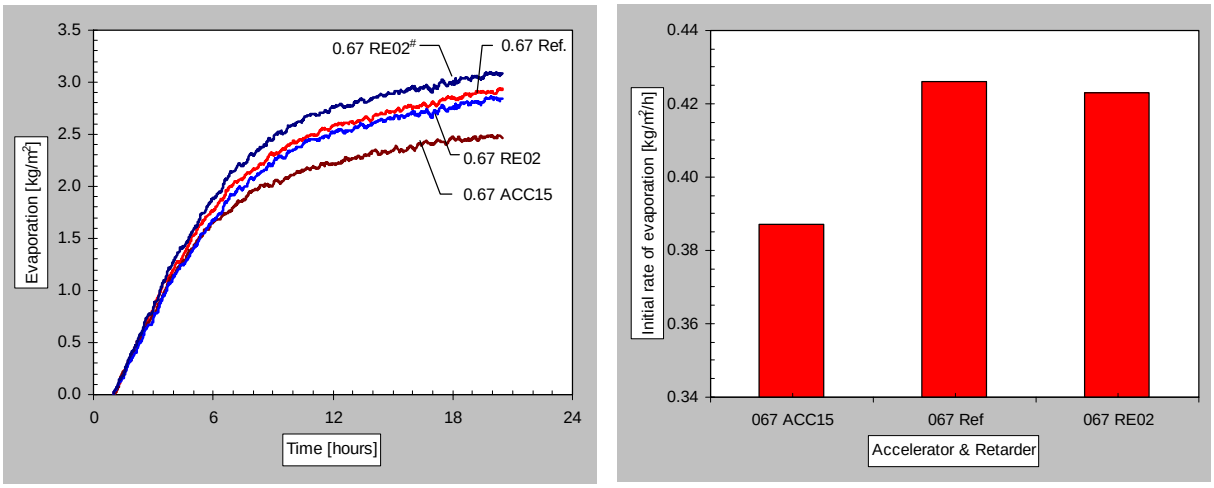

(a) *(b)*

Figure 104. Effect of accelerator (ACC) and retarder (RE) on evaporation for concrete with w/c 0.67: (a) comparison of evaporation curves – RE02$^{\#}$ refer to a modified evaporation curve due to high RH; and (b) comparison of the rate of evaporation.

Temperature development

The effect the accelerator and the retarder had on the hydration parameters (the temperature development is presented in Figure 105 to Figure 107. As can be seen in Figure 105(b) and Figure 107, the accelerator had no effect on the early hydration and did not shorten the length of the dormant period while the retarder increased the dormant period slightly. However, as soon as the hydration has started the accelerator led to a much more rapid hydration rate, as can be seen in Figure 105(b) with the two peaks.

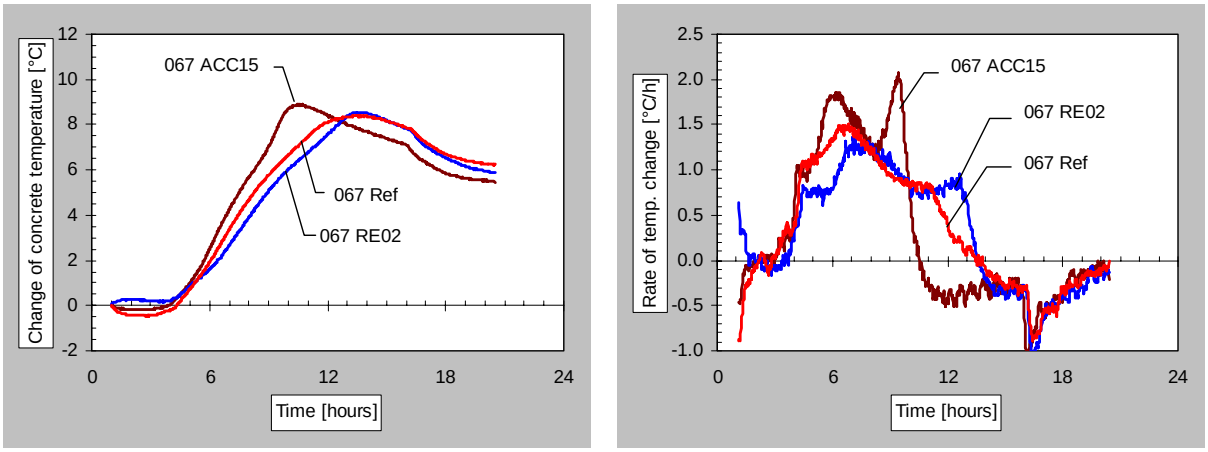

(a) *(b)*

Figure 105. Effect of accelerator (ACC) and retarder (RE) on temperature development of reference concrete with w/c 0.67: (a) comparison of temperature change; and (b) comparison of the rate of temperature change.

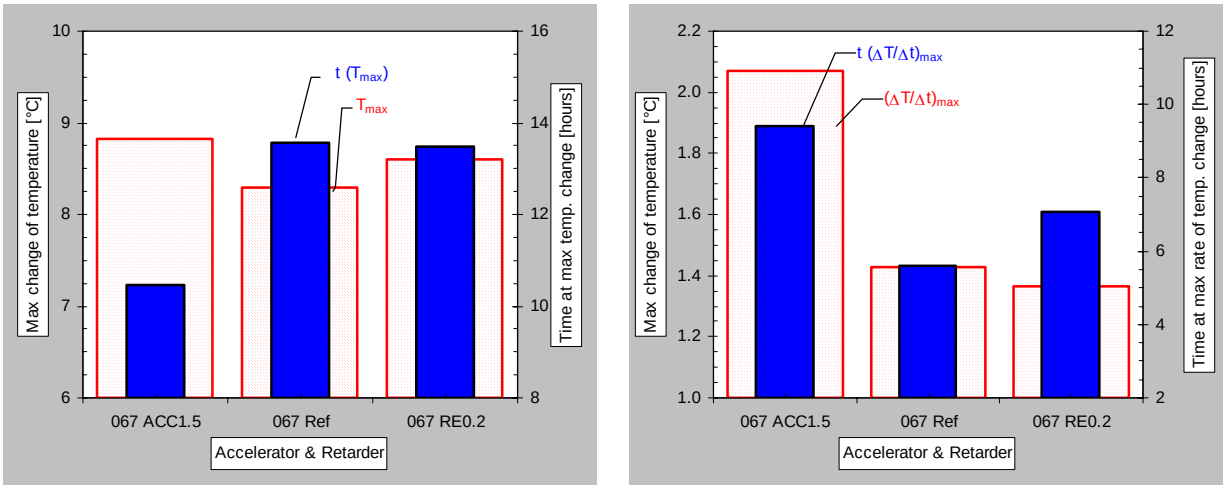

(a) *(b)*

Figure 106. Effect of accelerator (ACC) and retarder (RE) on hydration of reference concrete with w/c 0.67: (a) comparison of max temperature change and point of time; and (b) comparison of max rate of temperature change and point of time.

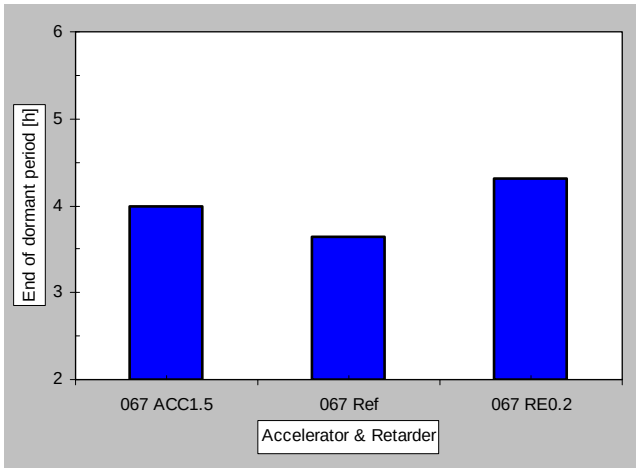

Figure 107. Effect of accelerator (ACC) and retarder (RE) on hydration of reference concrete with w/c 0.67, comparison of the end of the dormant period.

Pore pressure change

The effect the accelerator and retarder had on the pore pressure development is presented in Figure 108 and Figure 109. The effect were equivalent to the effect on the hydration in the way that the accelerator lead to an earlier pressure change and that the retarder delayed this. Even though the accelerator and retarder had no effect on the length of the dormant period it did influence the pressure development. Similar results were found in the CDD experiments.

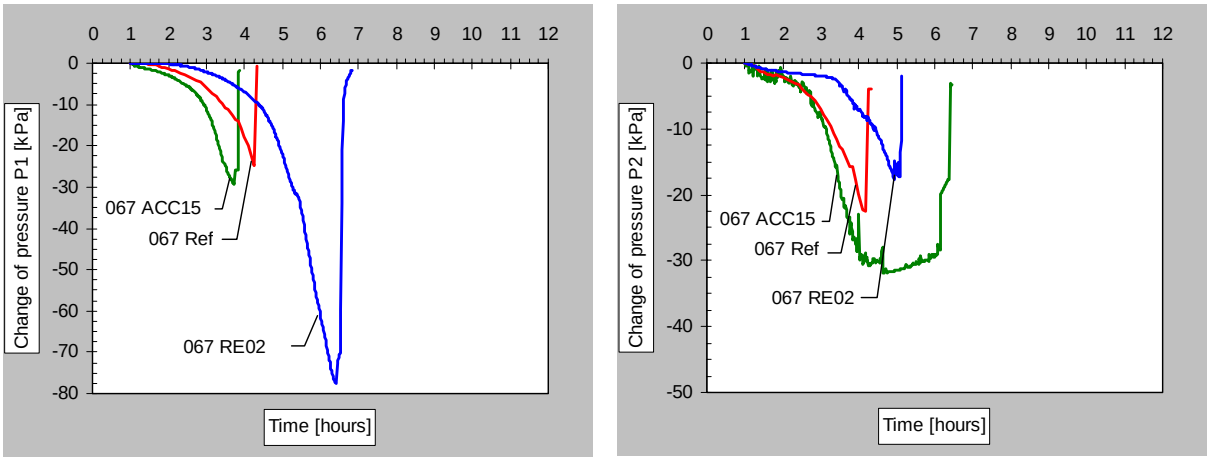

(a) *(b)*

Figure 108. Effect of accelerator (ACC) and retarder (RE) on pore pressure change: (a) pressure P1 at a depth of 60 mm; and (b) pressure P2 at a depth of 20 mm

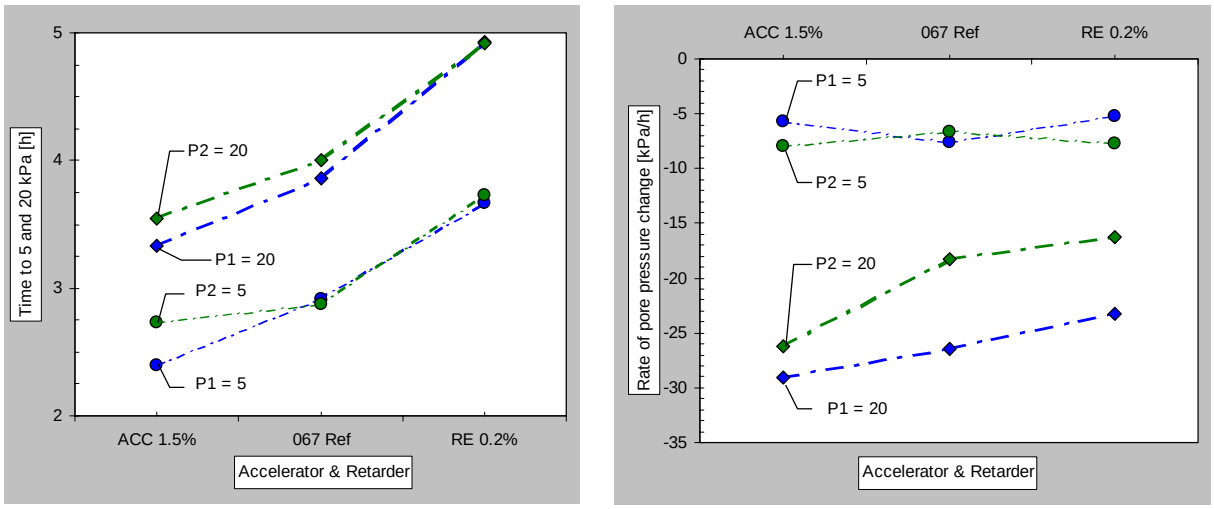

(a) *(b)*

Figure 109. Effect of accelerator (ACC) and retarder (RE) on pore pressure change for the reference concrete with w/c 0.67: (a) Time to 5 and 20 kPa; and (b) the rate of pressure change at 5 and 20 kPa.

Cracking tendency

Similar to the effect of the SP-dosage, accelerating and retarding the concrete had a considerable effect on the crack area, as can be seen in Figure 110. For the concrete with accelerator, the crack area was reduced by a factor of 2.0 (relative crack area was 0.5) and for

the concrete with retarder, the crack area increased by a factor of 1.3. However, the relative humidity was somewhat higher for the concrete with retarder compared to the other concretes, which could have resulted in a larger crack, are. For the accelerated concrete, the average RH was 31%; for the reference concrete, the average RH was 30%; and for the retarded concrete the average RH was 36%.

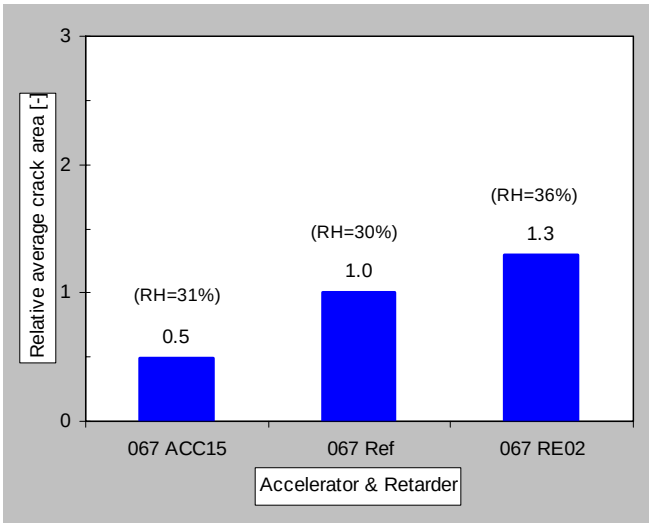

Figure 110. Effect of accelerator (ACC) and retarder (RE) on the average crack area for reference concrete with w/c 0.67 (the crack area has been normalised against the reference concrete).

4.2.9 Shrinkage reducing admixture

Evaporation

The effect of shrinkage reducing admixture (SRA) on the evaporation can be seen in Figure 111 and Figure 112. The effect of the SRA starts to be notable at about three hours and after this point the evaporation and the rate of evaporation was significantly less for the concretes containing SRA. The main effect of the SRA is that it reduces the surface tension of the water (or pore solution) and in this manner has an positive effect on shrinkage as it reduces the capillary tension caused by a reduction in pore radius. However, the SRA also influences the rate of drying and the concretes containing SRA had a significantly lower weight reduction than the reference concretes and the mechanism is notable as soon as the hydration starts. With the SRA there was a slightly reduction of the initial rate of evaporation whereas the final rate of evaporation was only half of that of the references, see Figure 112.

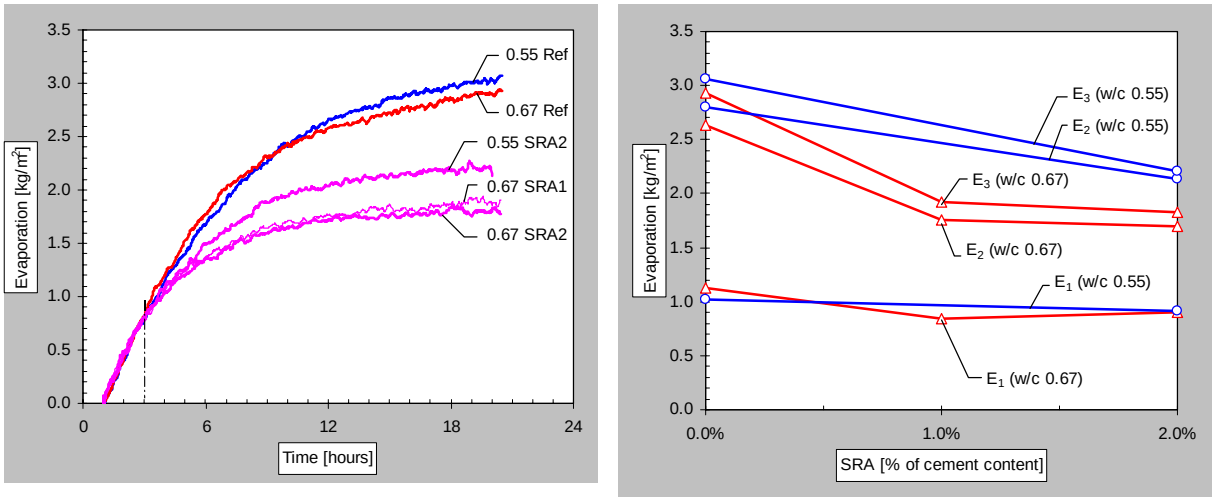

(a) *(b)*

Figure 111. Effect of shrinkage reducing admixture (SRA) on the evaporation for concrete with w/c 0.55 and 0.67: (a) comparison of evaporation curves; and (b) comparison of the evaporation at time t_1, t_2, and t_3.

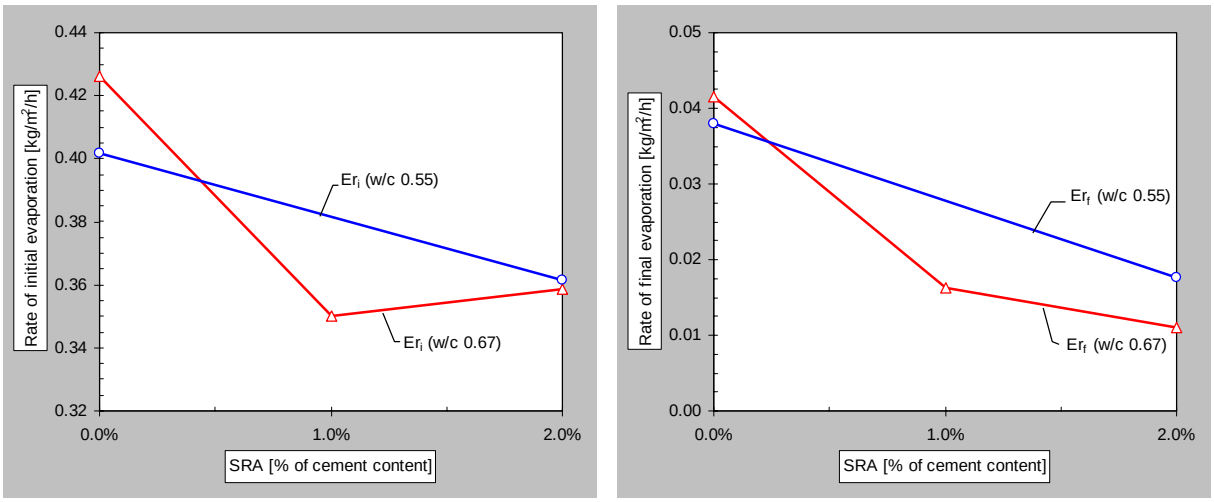

(a) *(b)*

Figure 112. Effect of shrinkage reducing admixture (SRA) on the rate of evaporation for concrete with w/c 0.55 and 0.67: (a) the initial rate of evaporation and (b) the final rate of evaporation.

Temperature development

The effect the shrinkage reducing admixture had on the temperature development can be seen in Figure 113 and Figure 114 where the hydration parameters are presented. There was no significant effect on the maximum temperature development and the rate of the temperature development. However, there was a small influence on the time for the temperature peak and on the length of the dormant period (see Figure 114). This, however, could be a result of the lower rate of evaporation and a reduced cooling effect due to the evaporation.

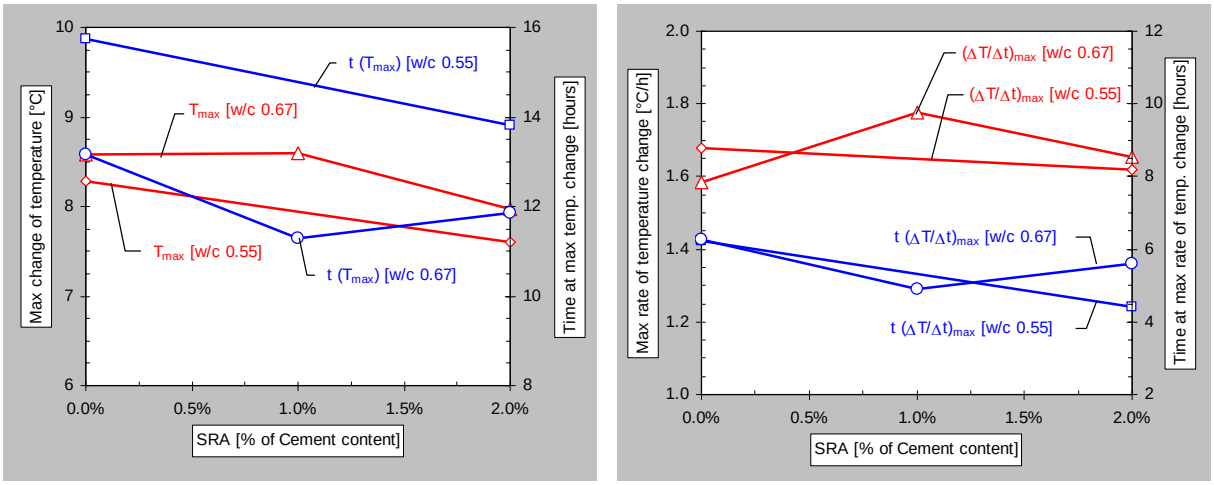

(a) *(b)*

Figure 113. Effect of shrinkage reducing admixture (SRA) on hydration of reference concrete with w/c 0.55 and 0.67: (a) comparison of max temperature change and point of time; and (b) comparison of max rate of temperature change and point of time.

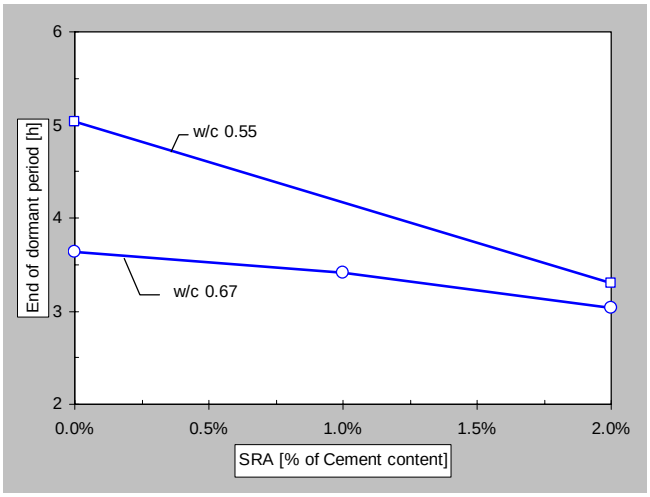

Figure 114. Effect of shrinkage reducing admixture (SRA) on hydration of reference concrete with w/c 0.55 and 0.67, comparison of the end of the dormant period.

Pore pressure change

The pore pressure development for the concretes with shrinkage reducing admixture (SRA) can be viewed in Figure 115. From the test result it was not possible to draw any conclusions on the effect of the SRA, as this did not appear to have any influence on the time of the pressure change or on the rate of the pressure change.

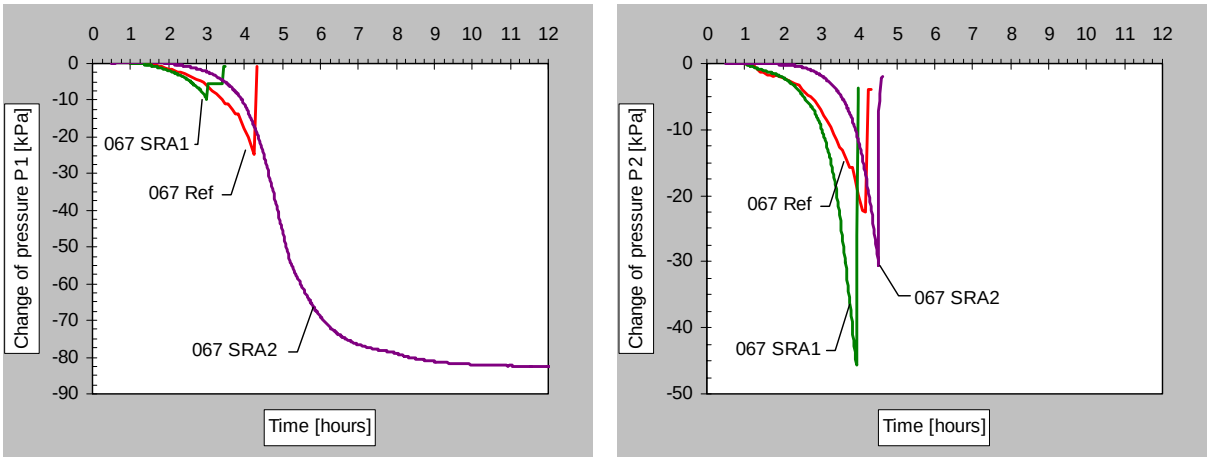

(a) *(b)*

Figure 115. Effect of shrinkage reducing admixture (SRA) on pore pressure change for the reference concrete with w/c 0.67: (a) pressure P1 at a depth of 60 mm; and (b) pressure P2 at a depth of 20 mm.

Cracking tendency

The shrinkage reducing admixture (SRA) had a positive effect on the crack area. As can be seen in Figure 116, for both the investigated concretes (w/c 0.55 and 0.67) the crack area was reduced with SRA: with 2% SRA in the concrete with w/c 0.55 the crack area was reduced be a factor of 2.3 (relative crack area was 0.44); with 1 % and 2% SRA in the concrete the crack area was reduced by a factor of 2.0 respectively 3.8 (relative crack area 0.51 respectively 0.26).

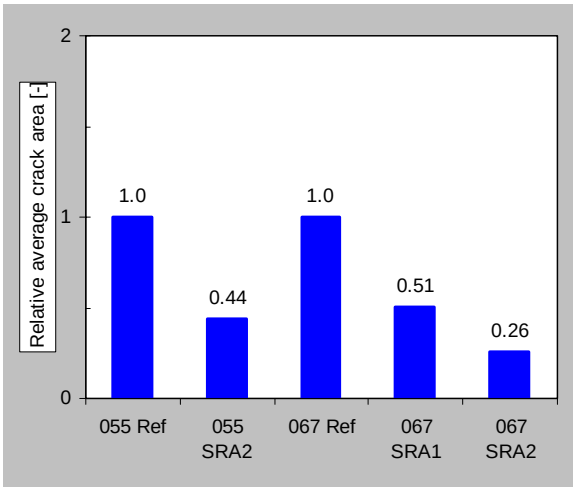

Figure 116. Effect of shrinkage reducing admixture (SRA) on the average crack area for the reference concrete with w/c 0.55 and for the reference concrete with w/c 0.67 (the crack area has been normalised against the reference concretes).

4.2.10 Air entraining agent

Evaporation

The effect the air entraining agent had on the evaporation can be seen in Figure 117. The curve for 067 AEA05 in Figure 117 have been modified to account for the low relative humidity during the test, the modified curve is denoted 067 AEA05#. For the reference concrete, the average RH was 30%; for the concrete with 0.5% air entraining agent the average RH was 24%; and for the concrete with 1.0% air entraining agent the average RH was 29%. The air entraining agent had no effect on the total amount of evaporation, but there appeared to be a small influence on the rate of the evaporation as this was reduced.

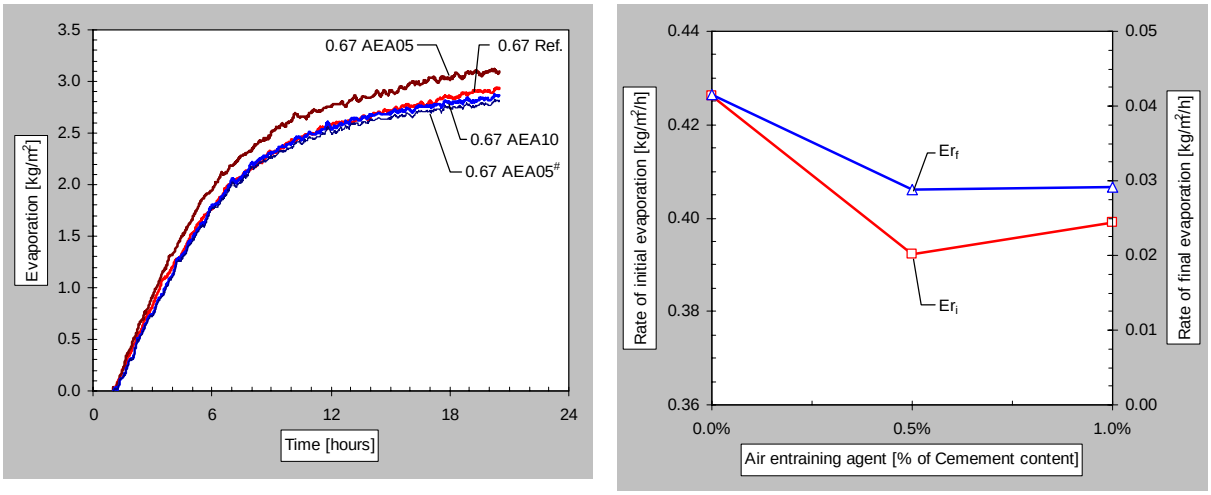

(a) *(b)*

Figure 117. Effect of air entraining agent on the evaporation: (a) comparison of evaporation curves – AEA05# refer to a modified evaporation curve due to low RH; and (b) comparison of the evaporation at time t_1, t_2, and t_3.

Temperature development

The effect the air entraining agent had on the temperature development can be seen in Figure 118 and Figure 119 where the hydration parameters are presented. As can be seen, and as expected, there was no significant effect on the hydration.

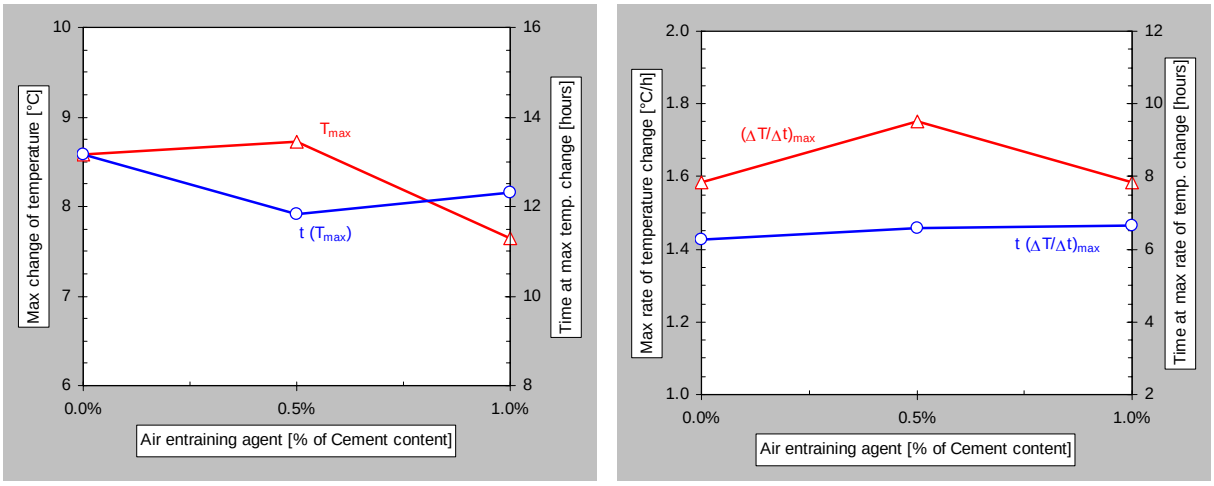

(a) *(b)*

Figure 118. Effect of air entraining agent on hydration of reference concrete with w/c 0.67: (a) comparison of max temperature change and point of time; and (b) comparison of max rate of temperature change and point of time.

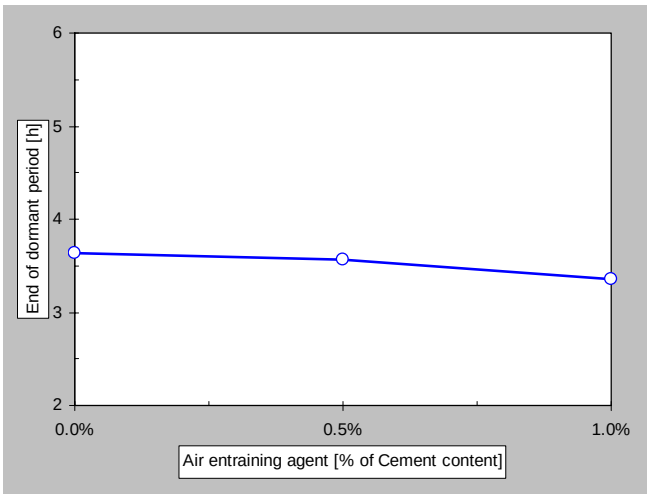

Figure 119. Effect of air entraining agent on hydration of reference concrete with w/c 0.67, comparison of the end of the dormant period.

Pore pressure change

The pore pressure development for the concrete with air entraining agent is presented in Figure 120. The effect was not clear from the test result but it looks as if as the pore pressure developed slightly earlier for the concrete with air and that the rate of the pressure development was increased.

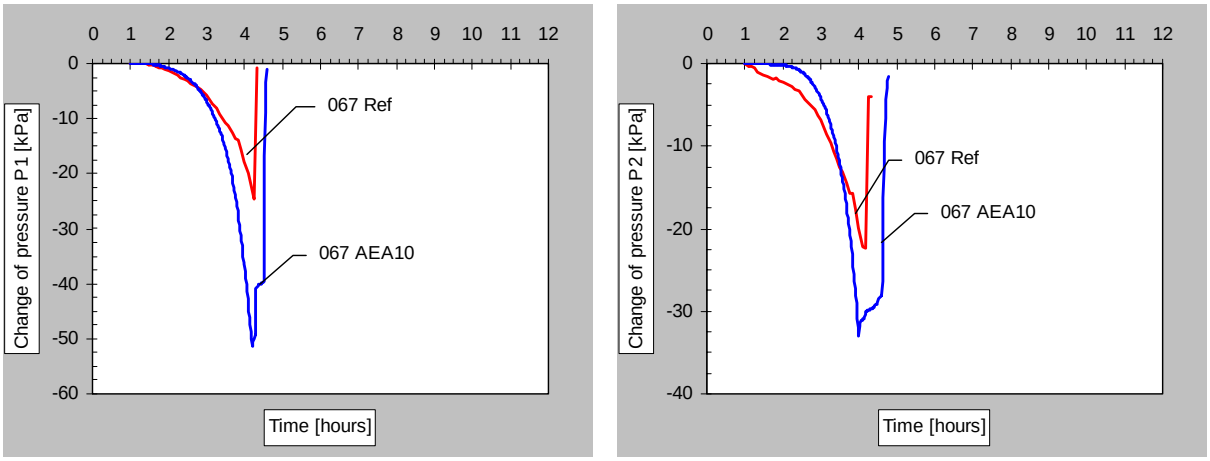

(a) *(b)*

Figure 120. Effect of air entraining agent (1.0%) on pore pressure change for the reference concrete with w/c 0.67: (a) pressure P1 at a depth of 60 mm; and (b) pressure P2 at a depth of 20 mm.

Cracking tendency

The effect of air entraining agent on the crack area can be seen in Figure 121. As can be seen, the air entraining agent had a positive effect on the average crack area as this was reduced, the crack area was on average (for the two concretes with air entraining agent) reduced by a factor of 1.9 (relative crack area 0.54).

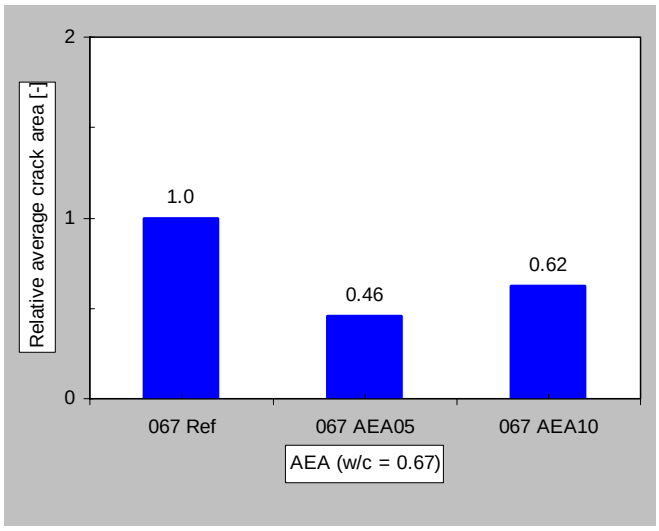

Figure 121. Effect of air entraining agent on the average crack area for the reference concrete with w/c 0.67 (the crack area has been normalised against the reference concretes).

4.2.11 Fibres

Evaporation

The effect fibres had on the hydration can be seen in Figure 122. As expected, the fibres had no effect on the evaporation with the exception for the glass fibres, which reduced the total evaporation. Moreover, there was no significant effect on the initial rate of evaporation but the final rate of evaporation was reduced for all the concretes with fibres (by a factor of: 0.95 for the PP-fibres; 0.89 for the nylon fibres; and 0.87 for the glass fibres).

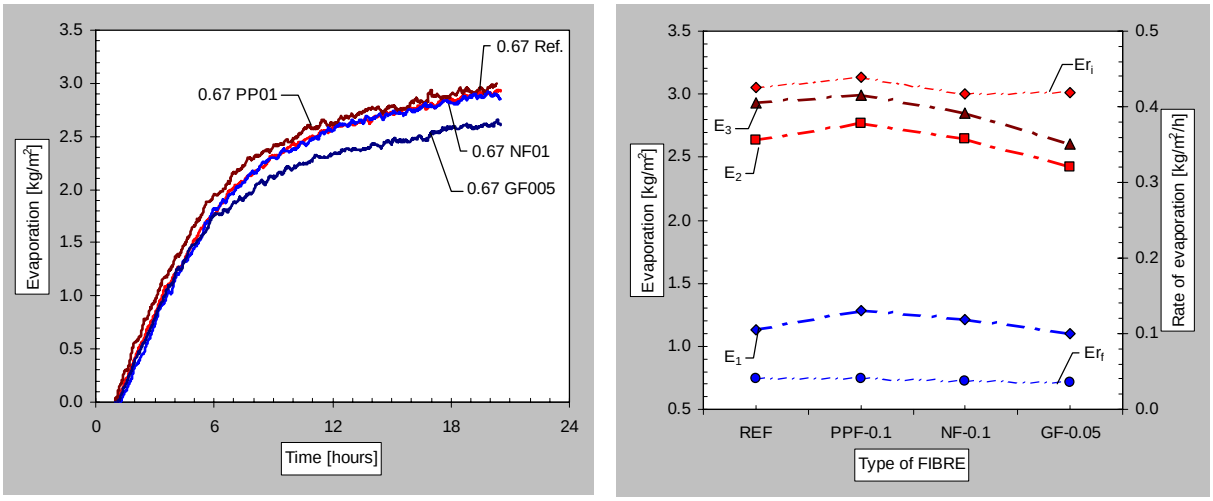

(a) *(b)*

Figure 122. Effect of fibres on the evaporation (a). (b) Comparison of the evaporation at time t_1, t_2, and t_3.

Cracking tendency

The effect the different fibres had on the average crack area can be seen in Figure 123. Fibres significantly reduces the crack area. With an addition of 0.1 volume percent of either polypropylene or nylon fibres the crack area was reduced with a factor 3.6 respectively 3.8 (relative crack area 0.28 respectively 0.26). With an addition of 0.05 volume percent of glass fibres the crack area was reduced with a factor of 2.6 (relative crack area 0.39).

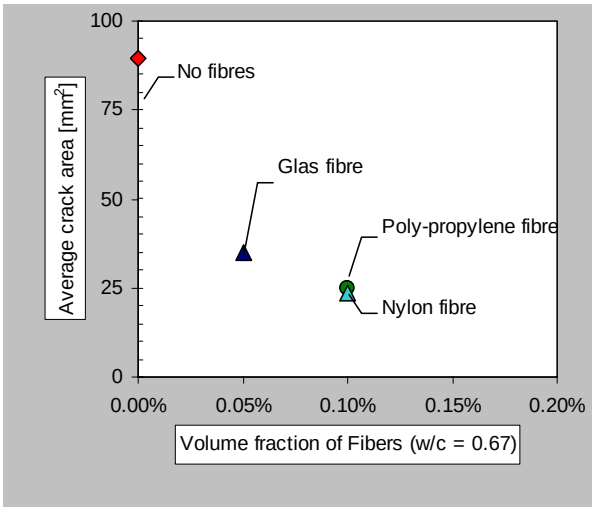

(a)

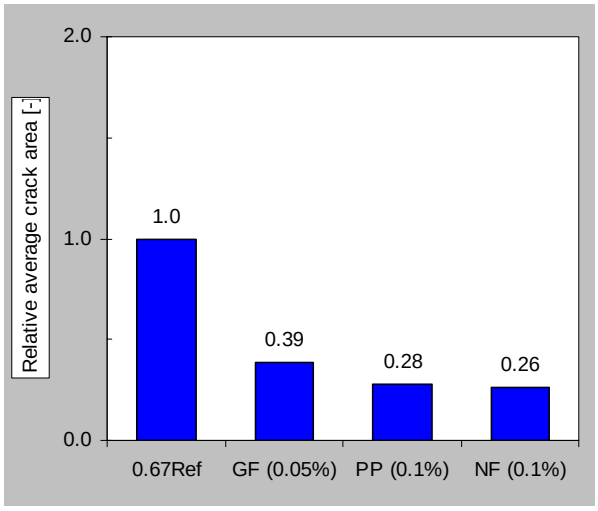

(b)

Figure 123. Effect of addition of fibres on the average crack area for the reference concrete with w/c 0.67: (a) crack area with the addition 0.05% glass fibres and 0.10% poly-propylene and nylon fibres; and (b) relative crack area compared to the reference.

4.2.12 Curing membranes

Evaporation

The effect of curing membranes on the evaporation can be seen in Figure 124 and Figure 125. The curing membranes were sprayed on the concrete surface approximately 50 minutes after mixing and 10 minutes before the measurements started. As can be seen in Figure 124, the most effective membrane was the wax-based (Sika Antisol-E), which significantly reduced the evaporation - the initial rate of evaporation was reduced with a factor of two and the total loss of water by a factor of three. The acrylic-based membranes did not perform as well as the wax based. Of the two tested it was only Sika Top-71 that showed any significant reduction in the evaporation - the initial rate of evaporation was reduced with a factor of 1.2 and the total loss of water by a factor of 1.4. In Figure 125, the shrinkage reducing admixture (SRA) have been included for comparison

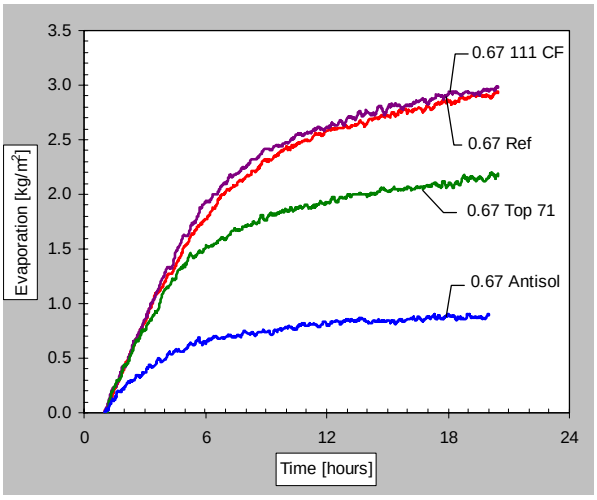

(a)

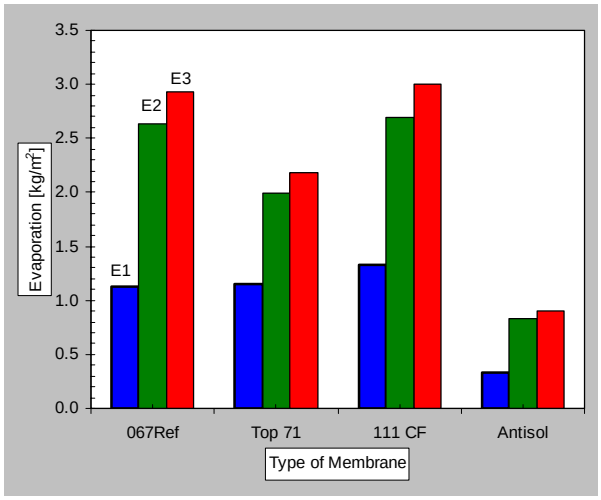

(b)

Figure 124. Effect of curing membrane on the evaporation: (a) evaporation curves; and (b) comparison of the evaporation at time t_1, t_2, and t_3.

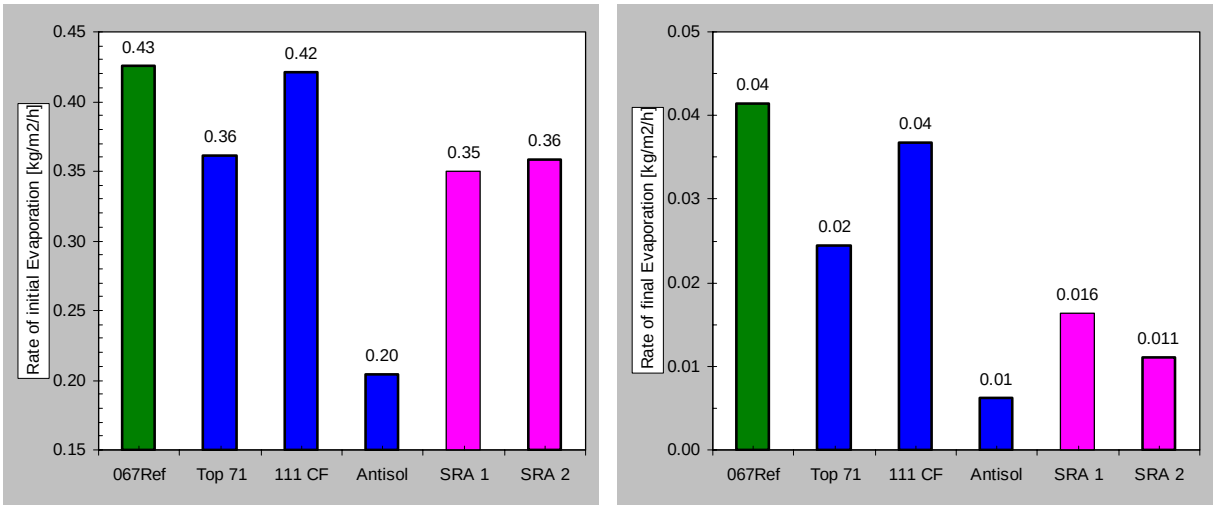

(a) *(b)*

Figure 125. Effect of curing membrane on the evaporation (and comparison with shrinkage reducing admixture, SRA): (a) initial rate of evaporation; and (b) final rate of evaporation.

Temperature development

The effect the membranes had on the temperature development can be seen in Figure 126 and Figure 127. For the concretes with membranes, both the maximum temperature change and maximum rate of the temperature change was increased. Furthermore, the temperature peak occurred earlier and for the concrete with the wax-based membrane the hydration was significantly accelerated (the dormant period was shortened). The effect on the temperature development was a secondary effect caused by the reduced evaporation.

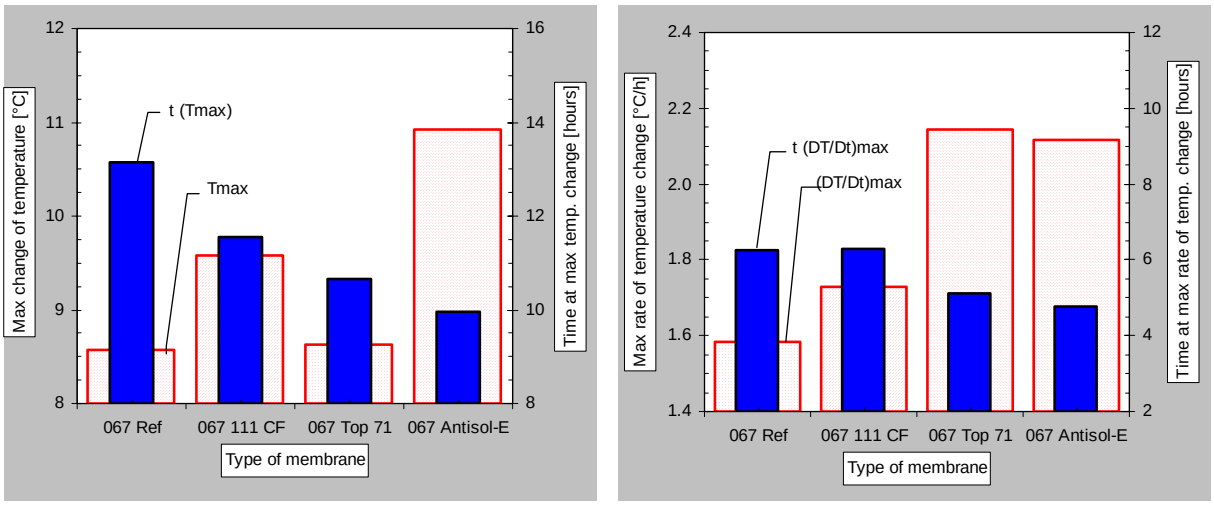

(a) *(b)*

Figure 126. Effect of curing membrane on hydration of reference concrete with w/c 0.67: (a) comparison of max temperature change and point of time; and (b) comparison of max rate of temperature change and point of time.

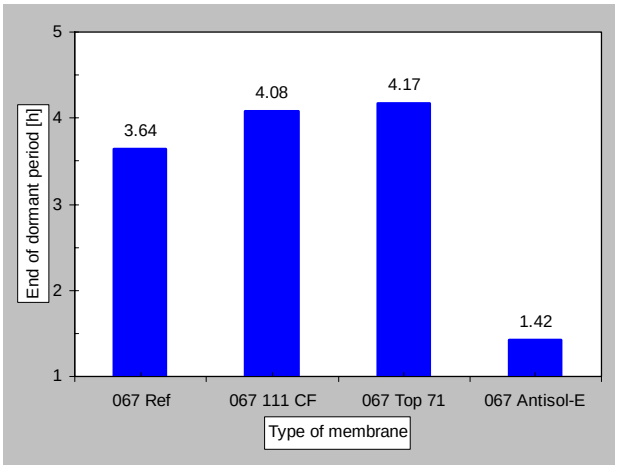

Figure 127. Effect of curing membrane on hydration of reference concrete with w/c 0.67, comparison of the end of the dormant period.

Cracking tendency

The effect the curing membranes had on the crack area can be seen in Figure 128. As can be seen, all of the membranes led to a reduced crack are. The most effective membrane was the wax based for which almost no cracks appeared, and those that did appear had a short length and a small crack width. Both of the acrylic based membranes reduced the crack area, the most effective was SIKA Top-71. With the wax based membrane the crack area was reduced by a factor of 50 (relative crack area 0.02).

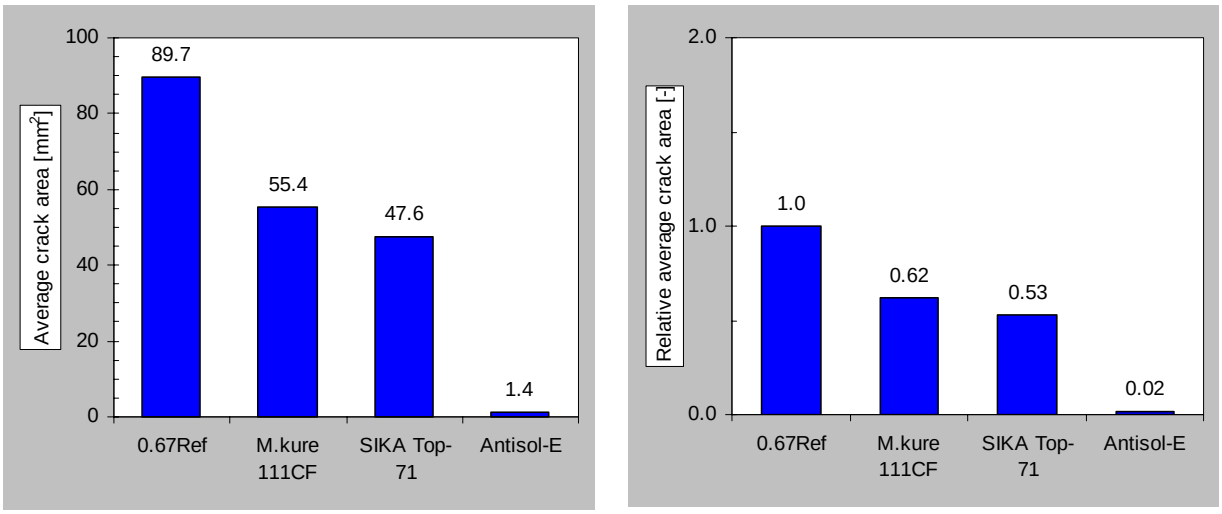

(a) *(b)*

Figure 128. Effect of curing membranes on the average crack area for the reference concrete with w/c 0.67: (a) Crack area with three different types of membranes, two acrylic based (MasterKure 111CF and Sika Top-71) and one wax based membrane (Sika Antisol-E); and (b) Relative crack area compared to the reference.

4.3 Sealed specimens

The temperature and pore pressure development was also measured on some sealed specimens. In Figure 129 a comparison of sealed and un-sealed (the ring test) conditions for the reference concrete with w/c 0.67 is made. As can be seen, for the un-sealed specimen, the temperature development, Figure 129(a), was delayed by the initial cooling effect caused by the evaporation. Furthermore, for the sealed specimen the pore pressure development, in Figure 129(b), started to build up at about four hours in comparison to the other specimen where it started at two hours. Similar, results can be seen for the reference concrete with w/c 0.45, see Figure 130, and for concrete with w/c 0.67 with rapid hardening cement (CEM I 52,5 R), see Figure 131 and Figure 132.

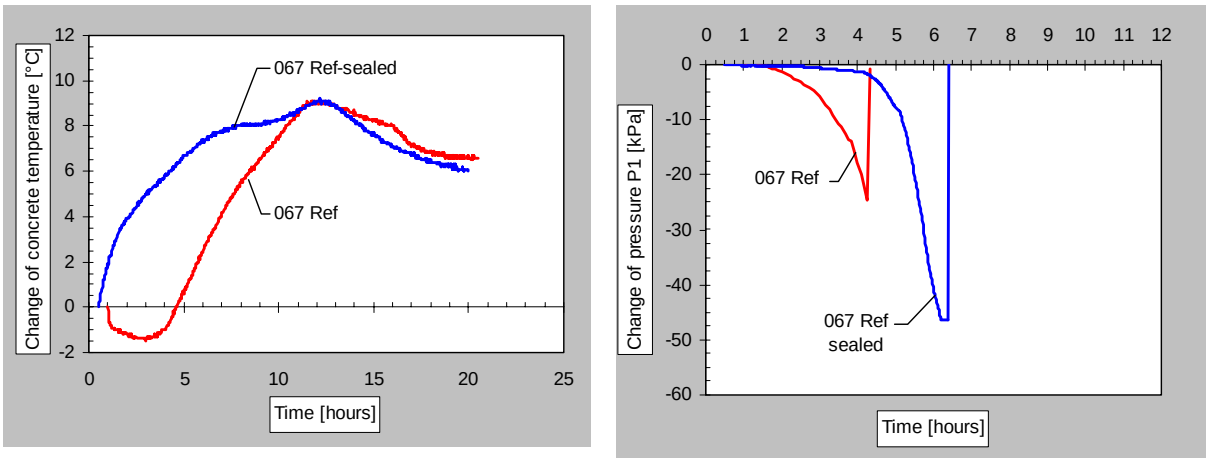

(a) *(b)*

Figure 129. Effect of curing conditions (sealed and un-sealed specimens) for the reference concrete with w/c 0.67: (a) change of concrete temperature; and (b) pore pressure change P1 at a depth of 60 mm.

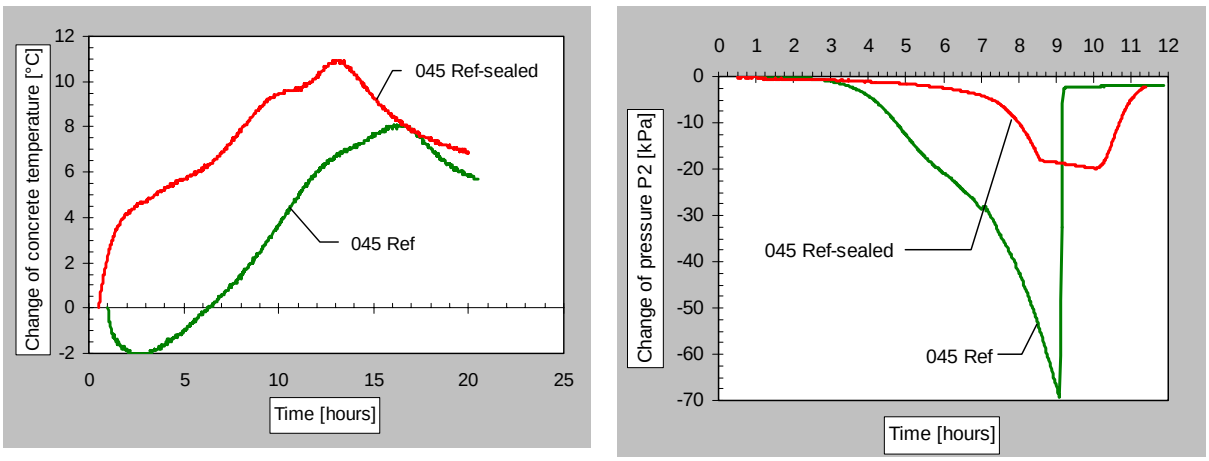

(a) *(b)*

Figure 130. Effect of curing conditions (sealed and un-sealed specimens) for the reference concrete with w/c 0.45: (a) change of concrete temperature; and (b) pore pressure change P2 at a depth of 20 mm.

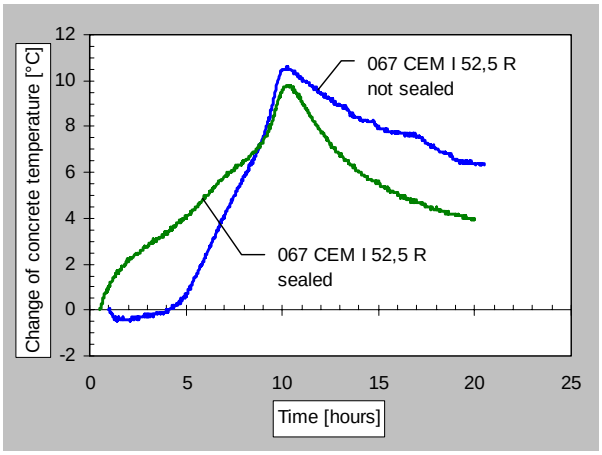

Figure 131. Effect of curing conditions (sealed and un-sealed specimens) for the concrete with w/c 0.67 with CEM I 52,5 R: change of concrete temperature.

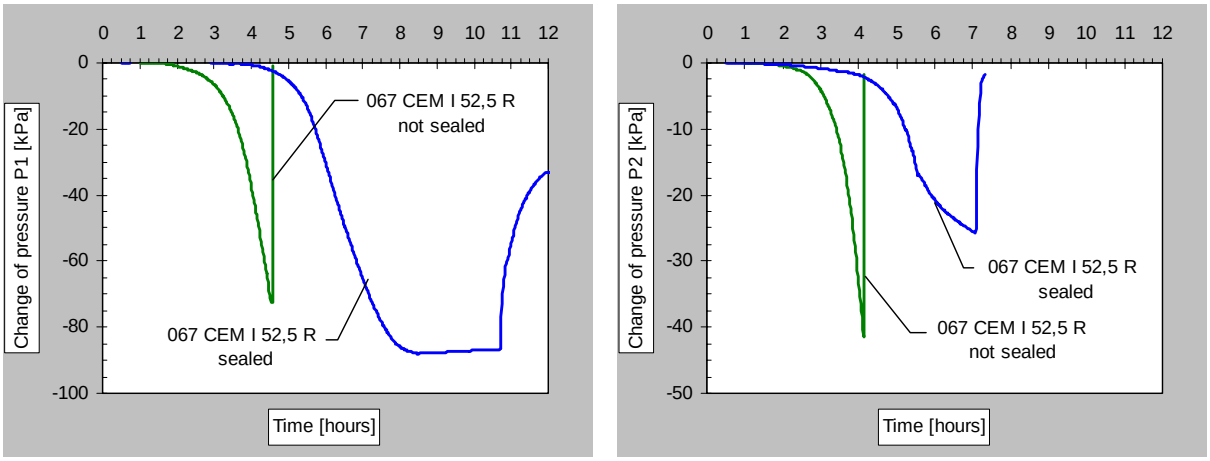

(a) *(b)*

Figure 132. Effect of curing conditions (sealed and un-sealed specimens) for the concrete with w/c 0.67 with CEM I 52,5 R: (a) pore pressure change P1 at a depth of 60 mm; and (b) pore pressure change P2 at a depth of 20 mm.

The relationship between the change in capillary pore pressure, deformation, and temperature (the initial temperature rise was a result of the concrete having a lower temperature than the climate room) can be seen in Figure 133, were the measurement results from two of the reference concretes are presented (w/c 0.45 and 0.67). As can be seen, as long as the concrete is plastic the deformation develops with almost a linear relationship and, during this period, the temperature and capillary pore pressure undergoes only small changes, which are linear. However, at one stage (at about five to six hours) the rate of the deformation is slowed down, indicating a 'setting' of the concrete, and a plateau is reached. At this point in time, it can be seen that both the capillary pore pressure and the temperature reach an accelerating phase, which indicates that the dormant period is ended and that the cement hydration accelerates. Final set is reached at about ten hours, which for the deformation is manifested in a second plateau slightly ahead of the temperature peak.

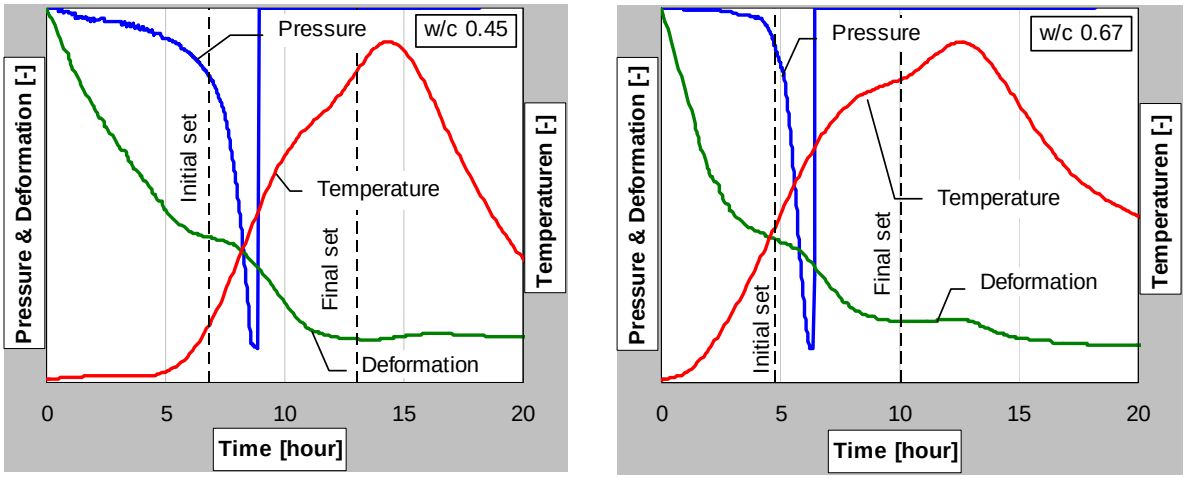

Figure 133. Comparison of measurements of pressure, deformation, and temperature (the initial temperature rise was a result of the concrete having a lower temperature than the climate room): (a) for reference concrete with w/c 0.45; and (b) for reference concrete with w/c 0.67.

4.4 Optimized concretes

Based on the experience gained during this study two 'optimized' concretes were developed and tested in the ring test. The optimized mixes were based on the reference mixes but had the following changes mad in their compositions:
Optimized w/c 055: aggregates 5/45/50% ("0-4mm"/"0-8mm"/"8-16mm"); reduced superplacticizer dosage, 1.0% SP of cement content; 2.0% shrinkage reducing admixture of cement content; and 0.1 vol-% polypropylene fibres.
Optimized w/c 067: aggregates 5/45/50% ("0-4mm"/"0-8mm"/"8-16mm"); 2.0% shrinkage reducing admixture of cement content; and 0.1 vol-% polypropylene fibres.

For the test to be as tough as possible it was decided to have a low relative humidity (average RH was 22%).

The result from the evaporation test can be seen in Figure 134(a), the initial rate of the evaporation was for both concretes 0.40 kg/m^2/h and there was no difference in the total amount of evaporation. The average crack area for the optimized concretes can be seen in Figure 134(b) together with the reference concretes. As can be seen, the concrete with w/c 0.55 was the one that performed best, with almost no cracks (a crack area of 2 mm^2).

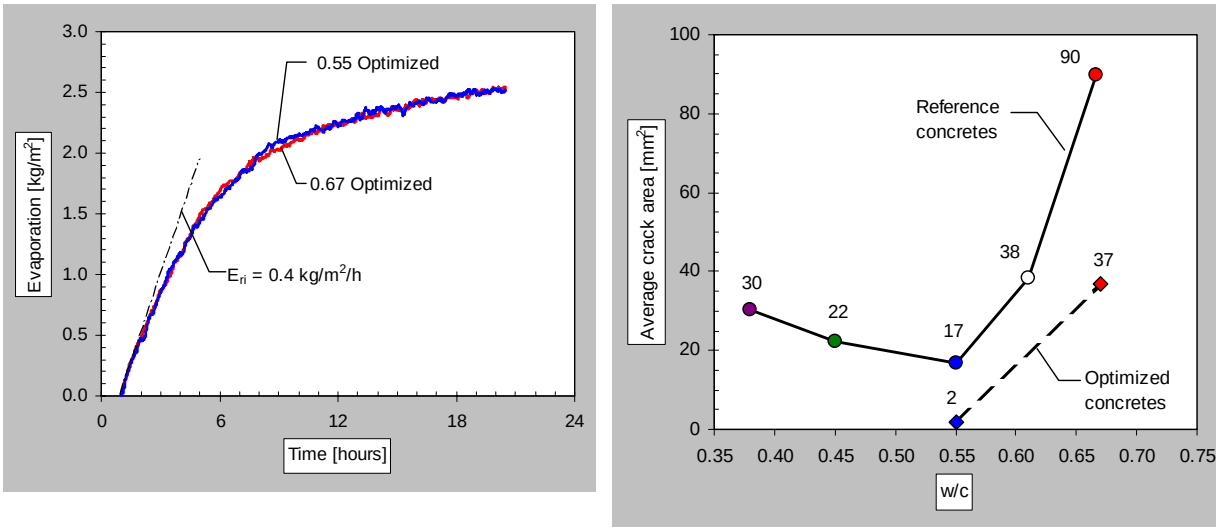

(a) *(b)*

Figure 134. Results for the optimized concrete: (a) evaporation from optimized concretes tested with an average RH of 22%; and (b) average crack area of the optimized concrete compared to the reference concretes.

5 Field study

5.1 Description of field study

In order to verify the laboratory results a field study was undertaken in which the cracking tendency was evaluated both the ring test specimens and on larger slab elements that were cast outside and exposed to the environment.

The experimental setup used in the field study can be seen in Figure 135, as well as in Figure 136 and Figure 137. The slab specimens were 3.0 by 1.7 meters and had a thickness of 95 mm. In order to introduce restraint a 21 mm thick form board (1.2 by 2.5 meters) was placed on top of a gravel bed resulting in an inner slab with a thickness of 74 mm. The measurement of crack area was conducted in the same manner as for the ring test specimens (described in chapter 3.2.2).

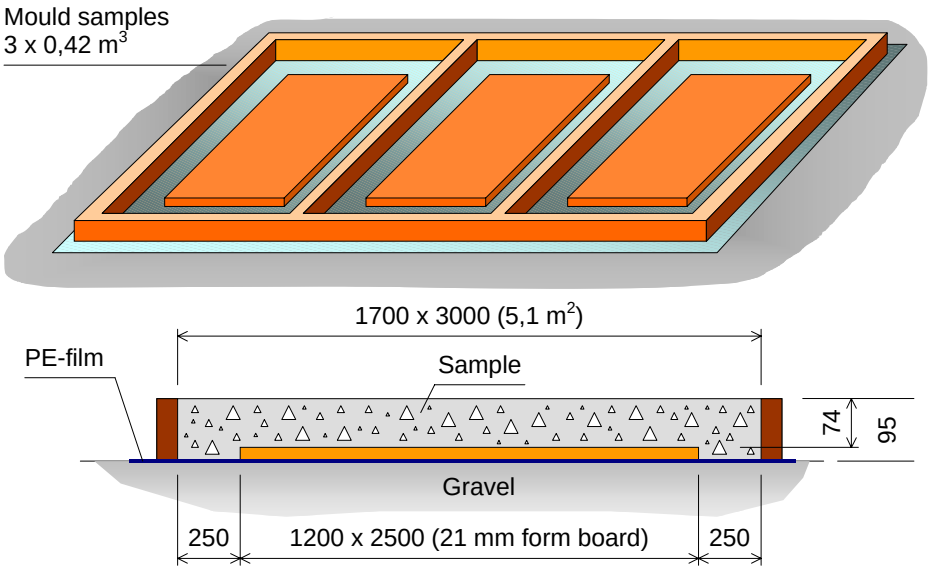

Figure 135. Experimental setup and geometry of the slab specimens used in the investigation.

Figure 136. Casting of slab elements for the field study.

Figure 137. Ring test specimens in the field study.

The parameters investigated in the field study were:

1. The effect of the wax based curing membrane (SIKA Antisol-E) on reference concrete with w/c 0.67 – denoted 067 Antisol-E.
2. The effect of shrinkage reducing admixture (dosage, 2% of cement content) in reference concrete with w/c 0.67 – denoted 067 SRA2.
3. The effect of additional SP-dosage (0.2% added in the truck) to reference concrete with w/c 0.67 – denoted 067 SP08+02.

4. The effect of fibres (0.1 vol-% polypropylene fibres) in reference concrete with w/c 0.67 – denoted 067 PP01.
5. The effect of adding extra water (12 liters added in the truck) to reference concrete with w/c 0.67 – denoted 067 W12.
6. The effect of w/c-ratio, comparing reference concretes 0.67 Ref and 0.55 Ref.

The filed study was divided into three separate casting occasions, always with one slab and ring test specimen made with the reference concrete with w/c 0.67, according the following list:

I. Slab 1 with 067 SRA2, slab 2 with 067 Antisol-E, and slab 3 with 067 Ref.

II. Slab 1 with 067 PP01, slab 2 with 067 SP08+02, and slab 3 with 067 Ref.

III. Slab 1 with 055 Ref, slab 2 with 067 W12, and slab 3 with 067 Ref.

All the concrete used in the field study was produced in a central drum mixer, with a capacity of 6 m^3, at Färdig Betongs' Ringön plant in Göteborg. The materials used were the same as in the laboratory study, with the exception of the coarse aggregate material (8-16mm).

5.2 Results and discussion

The weather conditions during the field study has been analysed and are shown in Figure 138 and Figure 139. In the figures average values for periods of six hours are presented: temperature in Figure 138(a); sun radiation in Figure 138(b); air velocity in Figure 139(a); and relative humidity in Figure 139(b). It can be seen that temperature was highest during field study II, which also had the lowest relative humidity and highest air velocity. During field study III the temperature and relative humidity were significantly lower and also the air velocity was lower.

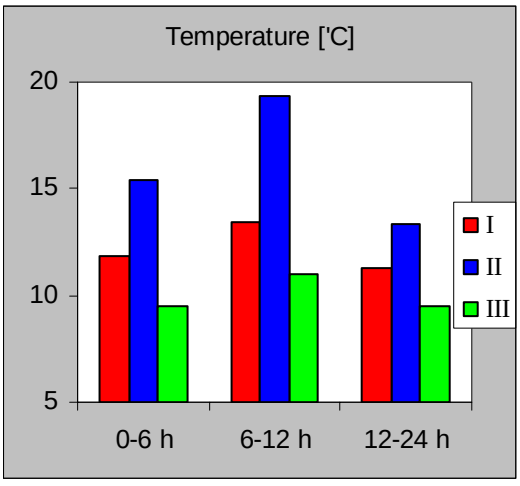

(a)

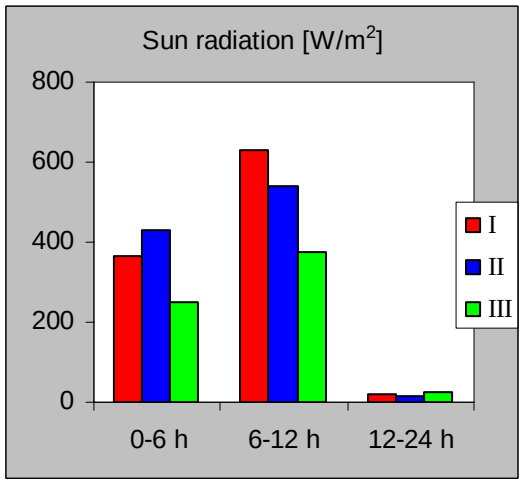

(b)

Figure 138. Weather data: (a) temperature and (b) sun radiation (average date for periods of six hours).

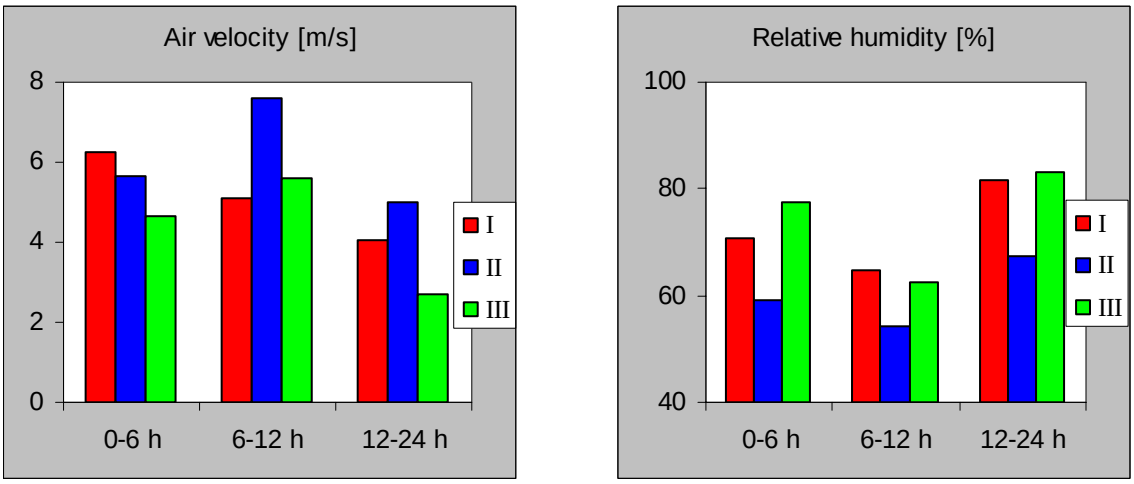

(a) *(b)*

Figure 139. Weather data: (a) air velocity and (b) relative humidity (average date for periods of six hours).

Some examples of the cracks that occurred in the field study can be seen in Figure 140 and Figure 141 and the results of the crack area measurements are presented in Figure 142 to Figure 144.

Figure 140. Picture showing a slab with a large crack.

Figure 141. Picture showing a close-up a large crack.

For field study I, Figure 142, it can be seen that the shrinkage reducing admixture (SRA) and the wax membrane (SIKA Antisol-E) significantly reduced the crack area compared to the reference concrete. Moreover, the same trends can be observed for both slab and ring test specimens. For field study II, Figure 143, it can be seen that the polypropylene fibres significantly reduced the crack area while the additional SP-dosage increased it. Also for this case there is a good correlation between the slab and the ring test specimens. For field study III, Figure 144, it can be seen that the reference concrete with w/c 0.55 has a smaller crack area compared to the reference with w/c 0.67. Furthermore, adding extra water increased the crack area. Again there is a good correlation between the slab and the ring test specimens. Furthermore, when comparing the reference concrete (067 Ref) which were present in all three filed studies it can bee seen that when the weather conditions were favourable (field study III) the crack area was significantly lower, approximately only one tenth compared to filed study I and II.

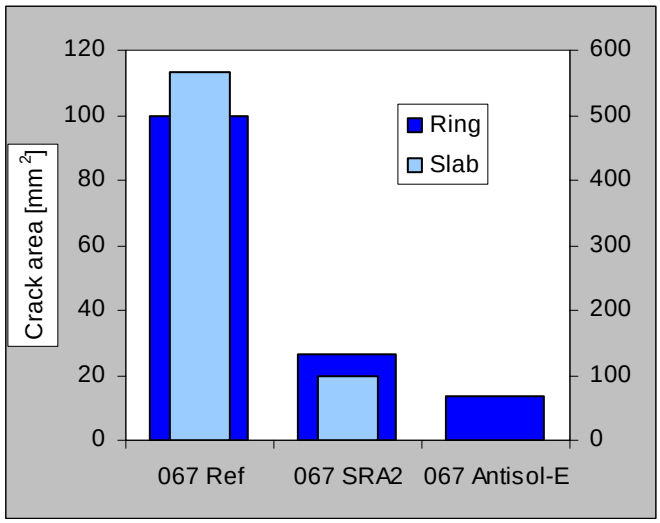

Figure 142. Comparison of crack area for field study I.

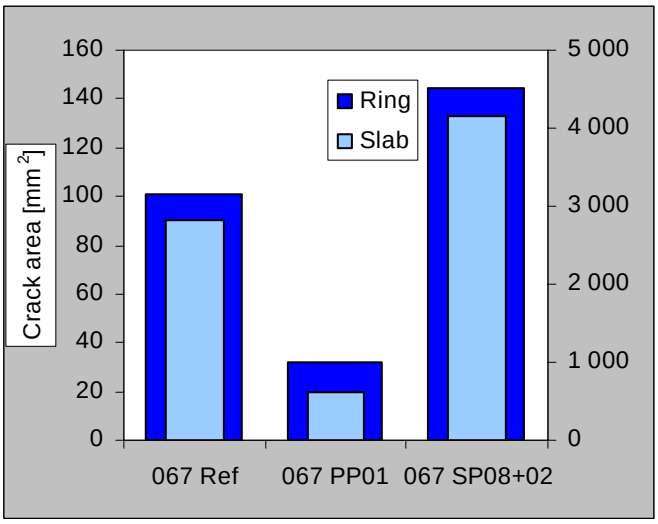

Figure 143. Comparison of crack area for field study II.

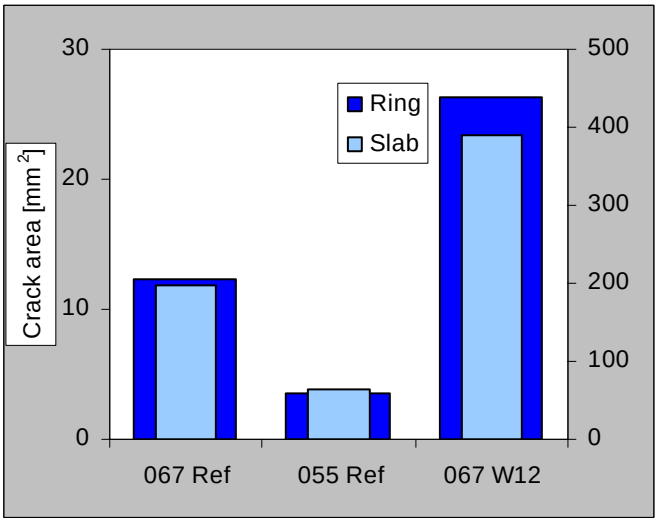

Figure 144. Comparison of crack area for field study III.

Figure 145 shows a comparison between the results from the laboratory tests and the field study. The figure shows the relative crack area (using 067 Ref as reference) for all the investigated mixes. The relative crack areas of Figure 145 has been analysed by calculating the Pearson's correlation coefficient (using Excel) and the result of the correlation analysis is presented in Table 7. As can be seen, the correlation is strong (close to one) between the ring tests performed in the laboratory and the field study (both the ring test and the slab specimens). Furthermore, there is also a high correlation between ring test specimens of the filed study and the slab specimens.

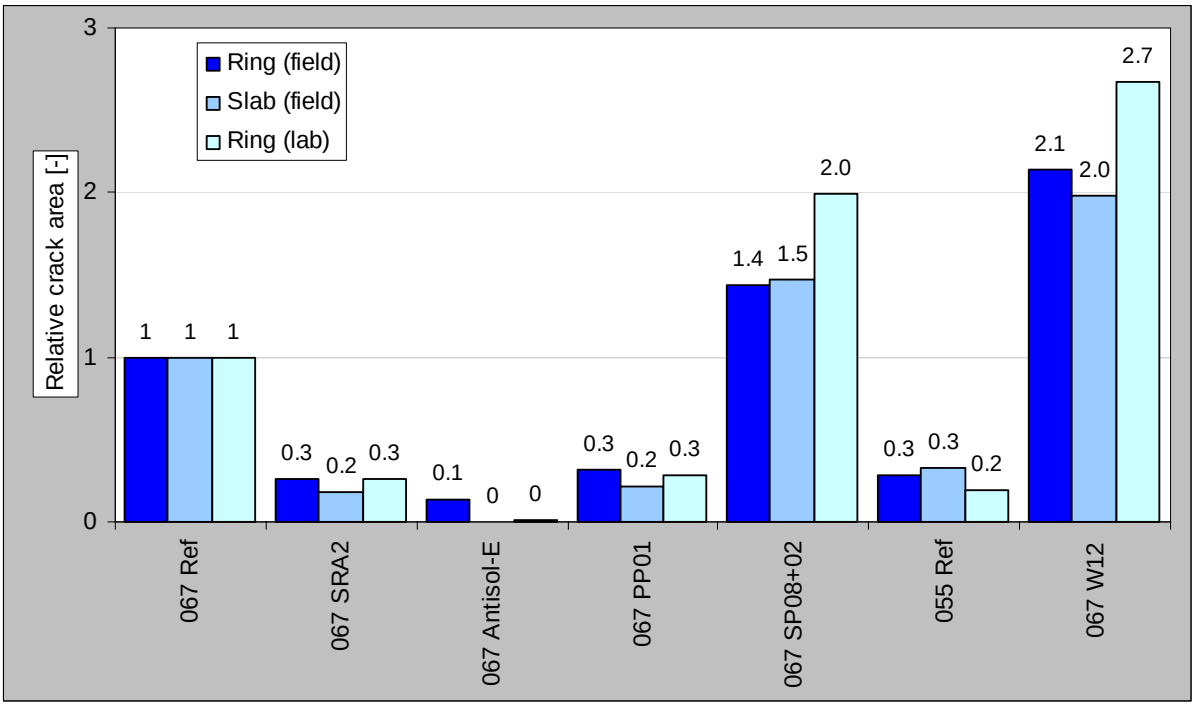

Figure 145. Comparison of the relative crack area between the filed study (the ring-tests and the slabs of) and the ring-tests of the laboratory study.

Table 7. Correlation matrix between the ring tests performed in the lab and the ring test and slab specimens used in the field study (a value >0.8 indicates a strong correlation).

	Ring test lab	**Ring test field**	**Slab test field**
Ring test lab	1		
Ring test field	**0.99**	1	
Slab test field	**0.98**	**0.99**	1

6 Conclusions and recommendations

6.1 Conclusions

An experimental investigation of early age deformation and cracking tendency was made on a number of self-compacting concretes, having w/c-ratio between 0.38 and 0.67, and the influence of various mix parameters as well as three different curing membranes were investigated. Autogenous deformations were measured and the cracking tendencies were investigated in a restraint ring specimen. Furthermore, evaporation, temperature, and pore pressure was measured in the ring specimens. In addition, a filed study was conducted, were slab and ring-test specimens were cast and placed in the filed. A high correlation was found between the results of the ring-tests performed in the laboratory and the field study and between the ring-test specimens and the slab specimens.

When combining the measurements of linear autogenous deformation, capillary pore pressure, and temperature (see Figure 133), it was found that as long as the concrete is plastic the deformation developed with almost a linear relationship and, during this period, the temperature and capillary pore pressure underwent only small changes, which were linear. However, at one stage (at about five to six hours) the rate of the deformation was slowed down, indicating a ‘setting’ of the concrete, and a plateau was reached. At this point in time, it could be seen that both the capillary pore pressure and the temperature reached an accelerating phase, which indicated that the dormant period was ended and that the cement hydration accelerated. Final set was reached at about ten hours, which for the deformation was manifested in a second plateau slightly a head of the temperature peak. That hydration (apart from the rate of evaporation) also plays an important role for how the capillary pressure developed was shown by how accelerator and retarder changed the time of the pressure drop (Figure 108): for an accelerated concrete the pressure started to drop earlier in comparison to a reference; for a retarded concrete, on the other hand, the pressure drop was delayed. It was found that for a sealed specimen, the rate depended primarily on the rate of hydration, while it for an unsealed specimen depended on the rate of evaporation and hydration, see Figure 129 to Figure 132. For a concrete with evaporation the capillary pressure developed earlier than for a sealed specimen.

The results from the measurements of linear autogenous deformation by the CDD show that:

- Increased cement content (lower w/c) increases the rate of and total chemical shrinkage and thereby the autogenous deformation.
- Increased coarse aggregate content decreased the magnitude and rate of autogenous deformation. The effect was more apparent at higher content of coarse aggregate, which might be explained by the coarser particles ability to create a restraining matrix. As the packing of the aggregates were improved, water was “released” to the mix and parallels can be made to increased water content where more water decreases the magnitude and rate of autogenous deformation.

- Increased water content decreased the magnitude and rate of autogenous deformation in the plastic and semi-plastic stage, which can be explained by better dispersed fine particles and increased interparticle distances (decreases the interparticle forces). At w/c 0.67 the larger surplus of water probably had only a small or no effect on the cement hydration. No large significant changes in times could be observed, but an increased water content tends to delay the rigid period.
- The addition of FA caused the concrete to swell in the plastic period. The early swelling increased with lower w/c, which can be explained by that the dosage of FA is based on the cement content, the FA addition increases with decreased w/c. In the semiplastic period the deformation were similar to those without FA. The effect of FA in the rigid period is not clear, but at high w/c the FA seemed to have a reducing effect of the rate of deformation, and at low w/c the opposite was observed. Moreover, it is well known that a concrete with FA addition tends to be retarded at early stages ("dormant" period), especially at low w/c.
- Addition of silica fume increased the magnitude and rate of autogenous shrinkage in all periods, and the effect increased with increased silica dosage. Silica fume decreased the plastic time period, and the effect increased with increased silica dosage. No changes in semiplastic time could be observed.
- Increased SP dosage increased the magnitude of autogenous shrinkage, which can be explained by the better cement dispersion. SP dosage increased the rate of shrinkage at the plastic and semiplastic period. After setting, the effect was the opposite, where the rate of shrinkage decreased with SP dosage.
- In the plastic period (before initial setting), accelerator (ACC) increased the magnitude and rate of shrinkage, and retarder (RE) hade the opposite effect, which could be expected. In the semiplastic period, ACC and RE showed no significant effect of magnitude and rate of shrinkage. ACC and RE showed no significant effect on the time of the periods, but RE tended to delay the time to initial setting.
- Addition of shrinkage reducing admixture (SRA) decreased the magnitude and rate of autogenous shrinkage for all concretes, and the effect increased with increased SRA dosage. In the semiplastic period the effect of SRA was not as pronounced as in the plastic and rigid period. SRA showed no effect on the times of the periods, which agrees with the supplier (SIKA) information.

The conclusions that can be drawn from the restraint ring tests are that:

- The rate of evaporation for the investigated, self-compacting, concretes varied between 0.37 and 0.44 kg/m^2/h (the low values for w/c $\leq$0.45), this can be compared with the evaporation from a free water surface of 0.50 kg/m^2/h for the test conditions used in this study.
- Rate of evaporation was not always the governing factor: for concrete with reduced aggregate content the rate of evaporation was reduced but the crack area increased.
- Reduced coarse aggregate content increased autogenous deformation, and the rate of the pressure change, while the evaporation was reduced.
- A rapid development of the pore pressure is not necessarily negative as long as the concrete has a hydration to match this; the concrete must gained sufficient strength and deformability.

- Delaying/retarding the hydration, with increased SP-dosage or by adding a retarder, increased both the autogenous deformation (the CDD experiments) and the crack area. Furthermore, it also delayed the pore pressure development.
- Accelerating the hydration, with a lower SP-dosage or by adding an accelerator, decreased both the autogenous deformation (the CDD experiments) and the crack area. Furthermore, the development of the pore pressure started earlier.
- Silica fume lead to increased autogenous deformation (the CDD experiments) and increased crack area in the ring test, even though the evaporation was reduced. Accelerated hydration and increased the rate of the pore pressure change. Furthermore, the cracks were initiated earlier.
- Fly ash lead to an initial swelling in the CDD experiments but in the ring tests the crack area increased. For the 0.67 concrete the evaporation increased while it was reduced for the 0.55 concrete. It is possible the fly ash had a retarding effect on the 0.67 concrete (increased evaporation). For the 0.55 concrete the evaporation was reduced. Furthermore, the cracks were initiated earlier.
- The slow hardening cement lead to a significantly larger crack area and for this type of cement the evaporation increased, mainly as a result of the delayed hydration. The rapid hardening cement also lead to increased crack area.
- The concrete with the high w/c-ratio (0.67) had the highest crack area. Furthermore, there seems to exist an optimum w/c-ratio for the investigated reference mixes, which indicates that the w/c-ratio should be in the region of 0.55, see Figure 61. This is also supported by other investigations: Bjøntegaard et al. (1998) tested concrete with w/b between 0.30 and 0.45 and found that the crack area increased with a decreasing w/b-ratio; Person (2003) tested concrete with w/b between 0.35 and 0.53 and found that the concrete with w/b 0.43 and higher performed better.
- By optimizing the concrete composition it was possible to significantly reduce the cracking (even at tough climate conditions).

6.2 Recommendations

To avoid excessive early age cracking due to evaporation the currently most reliable method seems to be to ensure a proper curing, for example by covering the surface to prevent evaporation or with a good curing membrane (e.g. a wax based membrane). However, experience shows that some types of concrete (i.e. concrete with very low w/c-ratio and with addition of micro silica) are prone to cracking even though proper curing has been ensured. Moreover, in some situations it might not be possible, or practical, to cover the surface with a plastic sheet or to apply a curing membrane. For such concretes and situations the only option is to minimize the cracking, or risk of cracking, by reducing the shrinkage potential by proper mix design – for example by a high coarse aggregate content and with addition of shrinkage reducing admixture. A second barrier is to add fibres, which do not prevent cracks from forming but rather reduce the crack widths to acceptable limits.

To minimize the risk of excessive early age cracking due to evaporation the following recommendations can be made:

If cracks are to be avoided, the following mix parameters were found to have a positive effect (reduces the crack area):

1. A w/c-ratio around 0.55 (optimum – not safe to be above 0.6).
2. Shrinkage reducing admixture (reduced evaporation as well as autogenous shrinkage).
3. High coarse aggregate content (reduced both the cracking area and the autogenous deformation).
4. Fibres (if cracks are formed the fibres limits the crack width).
5. Reduced SP-dosage.
6. Air entraining agent.

The following mix parameters were found to have a negative effect (increase the crack area):

1. High w/c-ratio (>0.6) or low w/c-ratio (<0.4).
2. Silica fume.
3. Fly ash (could perhaps be positive if it was used to reduce the required water content).
4. Cement type (its fineness and rate of hydration).
5. Reduced coarse aggregate content.
6. Delayed hydration (for example by adding more SP or a retarder or using slow hardening cement).
7. Adding extra water (increased evaporation and delayed early hydration, bur reduced autogenous shrinkage).
8. A rapid evaporation, which cools the concrete and have a retarding effect on the hydration.

7 References

ACI 209-92, (1997): *Prediction of Creep, Shrinkage, and Temperature Effects in Concrete Structures*, American Concrete Institute, Farmington Hills.

Bjøntegaard Ø., Hammer T.A., Sellevold E.J., (1998): *Cracking in High Performance Concrete before Setting*, Proceedings to the Int. Symposium on High-Performance and Reactive Powder Concretes, Sherbrooke.

Gartner E.M., Young J.F., Damidot D.A., Jawed I., (2002): *Hydration of portland cement*. Chapter three in Structure and performance of cements (ed. Bensted and Barnes) Spoon Press, London.

Hanehara S., Yamada K., (1999): Interaction between cement and chemical admixture from the point of cement hydration, absorption behaviour of admixture, and paste rheology, *Cement and Concrete Research,* Vol 29, pp 1159–1165.

Holt E.E., (2001): *Early age autogenous shrinkage of concrete*. Technical Research Centre of Finland, VTT Publications 446, 184 p.

Jensen O. M., Hansen F., (1995): A dilatometer for measuring autogenous deformation in hardening Portland cement paste, *Materials and Structures*, Vol 28 (181), pp 406-409.

Jensen O. M., Hansen F., (2001): Autogenous deformation and RH-change in perspective, *Cement and Concrete Research*, Vol 31, pp. 1859-1865.

Johansen R., Dahl P.A. (1993): *Control of plastic shrinkage of cement*, Paper presented at the 18th Conference on Our World in Concrete and Structures, Singapore.

Kasai Y., Yokoyama K., Matsui I., (1972): Tensile Properties of Early Age Concrete, *Mechanical Behavior of Materials, Society of Materials Science*, Vol. 4, Japan, pp 288 - 299.

Langana B.W., Wengb K., Ward M.A. (2002): Effect of silica fume and fly ash on heat of hydration of Portland cement*, Cement and Concrete Research,* Vol 32, pp 1045–1051.

Locher F.W., Richartz W., Sprung S. (1976): Erstarren von Zement (in German), *Zement Kalk Gips,* Vol 29 (10), pp 435-442.

Mindess S., Young J.F, Darwin D., (2003): *Concrete*, Second edition, Pearson Education Inc.

Neville A.M., (2000): *Properties of Concrete*, fourth edition. Pearson Educion Limited.

NORDTEST (1995): *NT BUILD 433 - Concrete: Cracking Tendency -Exposure to Drying During the First 24 Hours*. NORDTEST, Espoo, Finland, 1995.

Okamura H., (1997): Self-compacting high-performance concrete, *Concrete International*, Vol 19 (7), pp 50-54

Person B., (2003): *Plastisk krympning hos självkompakterande betong utan byggfukt* TVBM-7176, Avd. Byggnadsmaterial Lunds tekniska högskola, Lund 2003.

Powers T. C., (1968): *Properties of Fresh Concrete*. John Wiley & Sons, Inc. 664 p.

Radocea A., (1992): *A Study on the Mechanisms of Plastic Shrinkage of Cement-Based Materials*, doctoral dissertation, CTH Göteborg, Sweden, 1992, 125 pp.

Ravina D., (1986): Early longitudinal dimensional change of fly ash mortar exposed to trying conditions, *Cement and Concrete Research*, Vol 16, pp 902-910.

RILEM Technical Committee 181-EAS: *Early Age Cracking in Cementitious Systems* - Report of RILEM Technical Committee 181-EAS, edited by A. Bentur, (RILEM Publications, France), Vol 1, 350 pp.

Wittmann F.H., (1976): On the Action of Capillary Pressure in Fresh Concrete, *Cement and Concrete Research*, Vol. 6, pp. 49 - 56.

Appenix A

Concrete Digital Dilatometer (CDD) test

CONCRETE DIGITAL DILATOMETER (CDD):
LINEAR MEASUREMENT OF AUTOGENOUS DEFORMATION IN FRESH AND HARDENING CONCRETE

Key words: Concrete, shrinkage, autogenous

1 SCOPE

This test method covers determination of concrete autogenous deformation. It has the ability to start measure before setting, when concrete is fresh. The method is a modification of the CT1 digital dilatometer for pastes and mortars.

As the use of high-performance and self-compacting concrete has increased, problems with early-age shrinkage and cracking have become problematic. Conditions as reduced water-cement ratio, reduced maximum aggregate size, increased amount of fines and increased binder content all contribute to this problem. Compared with drying shrinkage that generally occurs from the outside surface of the concrete inward, autogenous shrinkage develops uniformly through the concrete member, but can be more likely to cause cracking, because it develops more rapidly and occurs when the cement paste is young and has poorly developed mechanical properties.

2 FIELD OF APPLICATION

With the concrete digital dilatometer test, the fresh and hardening concrete linear autogenous deformation is evaluated.

The test is only to be applied for laboratory use.

Maximum coarse aggregate size is 16 mm.

Concrete digital dilatometer (CDD) test is preferable to be combined with:

- Cracking tendency ring test (NT BUILD 433) for concrete
- Digital dilatometer (CT1) test for cement paste.

3 REFERENCES

CT1 digital dilatometer: Jensen O. M., Hansen F., “A dilatometer for measuring autogenous deformation in hardening Portland cement paste”, Materials and Structures, Vol 28 (181), pp 406-409, 1995.

Sampling procedure: EN 12350-1, ASTM C172 or NT BUILD 191.

Cracking tendency test: NT BUILD 433

4 NOTATIONS

4.1 Definitions

Linear deformation; the relative change in length due to shrinkage or expansion, referred to the specimen origin length.

Autogenous deformation; the unrestrained, time-depending, bulk deformation of fresh and hardening sealed concrete at a constant temperature.

Shrinkage; when the deformation is a contraction, it may be referred to as shrinkage, e.g. autogenous shrinkage.

Chemical shrinkage; under sealed conditions, the cement paste hydration products occupy less space than the original reactants. Chemical is the major of factors causing the autogenous shrinkage.

4.1 Symbols

l_0 length of specimen at the time of casting (when start measuring), in millimeters [mm].

Δl change in length of specimen at time t, in micrometers [µm].

t time after mixing (when start measuring), in hours and minutes [hh:mm].

ε relative change in length, defined positive for shrinkage (swelling if negative), in microstrain [µm/m].

T concrete cross section temperature, in degree Celsius [ºC]

5 METHOD OF TEST

5.1 Principle

The concrete digital dilatometer is a test method for evaluation of linear autogenous deformation of fresh and hardening concrete at sealed conditions and constant ambient temperature.

The concrete is cast in a vapour proof steel coil reinforced flexible polyurethene (PU) tube mould with inner diameter 82 mm and specimen length ~400 mm. The mould is placed in a mechanical stable measuring rig, where the unrestrained, time-depending, bulk deformation is recorded by a digital gauge (1/1000 mm) at thermal controlled ambient conditions (20ºC) for a period of 24 hours or more.

The method is illustrated in *Figure 1*.

5.2 Apparatus

Required equipment and apparatus for a typical test is:

- Thermal controlled room or chamber with an air temperature of 20±1ºC.
- 2 or 3 complete CDD setup (mould consisting PE-tube, end-caps, fixture and hose-clamps and measuring rig), as shown in *Figure 1*.
- 1 set (2 off) of recording temperature sensors.
- Table vibrator.
- Ruler or gauge graded in 1/1 mm.
- Stopwatch, measuring 1/1 sec (if manual reading of change in length).

5.3 Preparation of test specimen

5.3.1 Mould

The first end-cap (moving end) is to be fitted to the PE-tube with a house-clamp. The mould is to be placed in a vertical support rack (e.g. a piece of duct) to ensure stability during casting.

5.3.2 Mix

Concrete constituents volume is be calculated by 1/1000 liter. Dry materials (aggregate) are preferable.

5.3.3 Mixing

Suitable concrete mixing method, mixer and volume is to be selected and documented. No standards are available.

5.3.4 Sample

The sample size is 2.2 liter and is to be collected in accordance with EN 12350-1, ASTM C172 or NT BUILD 191.

Maximum coarse aggregate size is 16 mm.

5.3.5 Casting

The specimen must completely fill the mould. If needed, compaction by vibration.

If temperature sensors; place one in the center and one at the surface of the mould cross section.

The second end-caps (fixed end) are to be fitted to the PE-tube with a house-clamp.

5.4 Procedure

5.4.1 Starting the test

a) The specimen is to be placed in the measuring rig.

b) The mould is to be adjusted and fixed to the rig so the digital gauge contact point is in start position.

c) Reference length l_0 (mould length excl. the end-caps, i.e. specimen length) is to be measured by 1/10 mm.

d) The digital gage is to be re-zeroed and its recording phase (time t and length change Δl) to be started.

e) If temperature sensors; start temperature T recording.

The test must be performed in a thermal controlled room or chamber with an air temperature of 20±1ºC.

The starting procedure (a-d) is to be performed within 20-30 minutes from adding water to the mix. This time is to be noted. The initial measures are sensitive and it is recommended to let the sample set (or rest) in the rig for 10 minutes before starting the measurements.

5.4.2 During the test

If manual reading, continuously record the time t, length change Δl and concrete temperature T. Enough sampling frequency is to be selected for smooth curve of shrinkage development.

Visual observation of specimen straightness; possible curviness is to be measured and noted.

5.4.3 Finishing the test

Recording phase (t, Δl and T) stops. Values are to be transferred to computer for calculation and evaluation.

5.5 Expression of results

The shrinkage, ε, for each test specimen is to be calculated as:

$$\varepsilon = \frac{\Delta l}{l_0} \cdot 10^6 \text{ [in parts per million, e.g. µm per m]}$$

The results are to be calculated as a mean value of two or tree tests, and are to be given in microstrain with two significant digits.

The shrinkage shall be corrected for the recorded concrete cross section temperature (T). Adequate thermal expansion coefficient to be applied.

The development of shrinkage (ε) with time (t) is to be presented graphically.

6 TEST REPORT

The report is shall include necessary information from among the following:

a) Document id (name, nr, test method, etc).
b) Date and time.
c) Performer id (name and address).
d) Test object id.
e) Purpose of test.
f) Concrete id (producer, recipe, etc).
g) If relevant, concrete and/or air temperature.
h) Method of sampling.
i) Time from water addition to start sampling.
j) Reference length (l_0), i.e. specimen length.
k) Storage conditions.
l) Test results (t, Δl and T).
m) Relevant visually observations (e.g. sample curviness) and personal judgments and interpretations.
n) Any deviation from the test method.
o) Graphic presentation shrinkage (ε) development with time (t).
p) Inaccuracy and/or uncertainty of test results.
q) Date and signature.

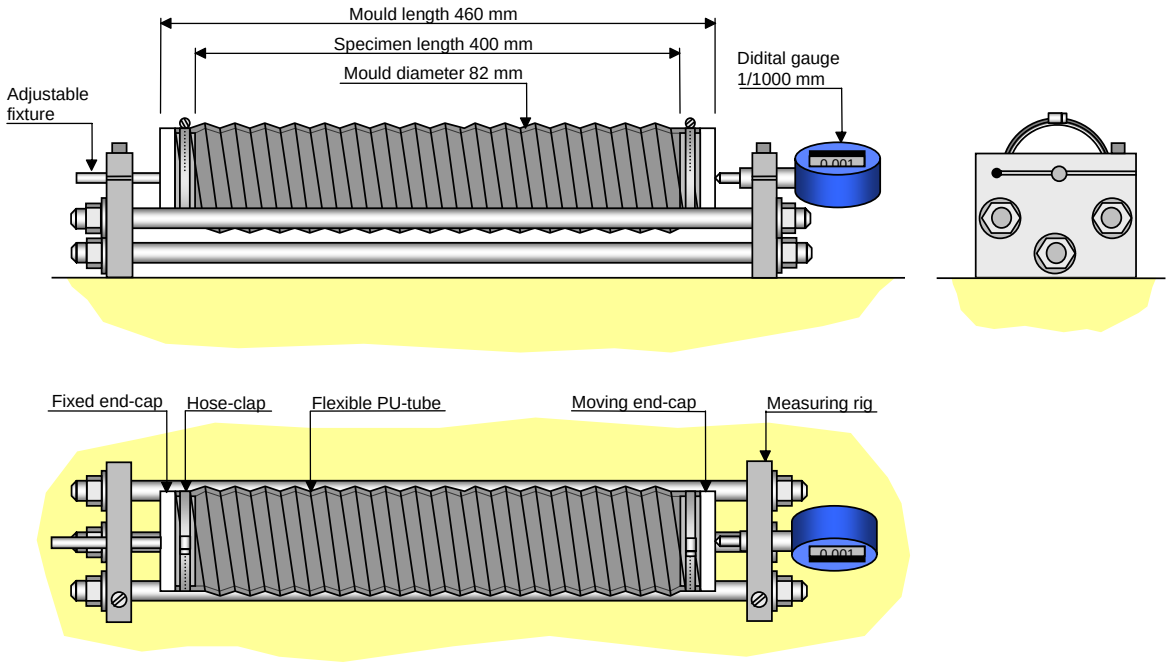

Figure 1. Principe of the Concrete Digital Dilatometer (CDD) for autogenous measurement.

Appenix B

Cracking tendency ring test

CONCRETE CRACKING RING TEST:
CRACKING TENDENCY MEASUREMENT DUE TO DRYING DEFORMATION THE FIRST 24 HOURS

Key words: Concrete, cracking, shrinkage, drying

1 SCOPE

This test method covers determination of concrete cracking tendency at early ages. The test is performed on 3 restrained ring shaped specimen, exposed to an air stream of defined velocity, temperature and relative humidity, the first 24 hours after casting.

The principle of the test is that the concrete sample is cast around a restraining inner steel ring, causing a development of tangential stresses, that if sufficiently high may lead to cracking. The evaluation is based on characterization of the cracks in terms of average total area by the three samples.

The method is a modification of the Nordtest method “NT BUILD433”.

Problems with early-age shrinkage and cracking have become problematic. Conditions as reduced maximum aggregate size, increased amount of fines, presence of retarding admixtures, increased binder content and deficient covering and curing all contribute to this problem.

Most likely the cracking caused by drying shrinkage also are consisting autogenous shrinkage. Compared with autogenous shrinkage that generally develops uniformly through the concrete member, drying shrinkage occurs from the outside surface of the concrete inward, both causing cracks that develops rapidly and occurs when the cement paste is young and has poorly developed mechanical properties.

2 FIELD OF APPLICATION

With the “Concrete cracking ring test”, the plastic and hardening concrete cracking tendency can be used for an evaluated of different type of concrete exposed to early drying.

The test is only to be applied for laboratory use where the method information is relative and cannot predict the extent of cracking which might occur under prevailing conditions.

Maximum coarse aggregate size is 16 mm.

Concrete cracking ring test is preferable to be combined with:

- Volume or linear measurement of autogenous deformation, e.g. Concrete Digital Dilatometer (CDD) test for concrete.

3 REFERENCES

Sampling procedure: EN 12350-1, ASTM C172 or NT BUILD 191.

Cracking tendency test: NT BUILD 433

4 NOTATIONS

4.1 Definitions

Shrinkage; when the deformation is a contraction, it may be referred to as shrinkage, e.g. autogenous or drying shrinkage.

Autogenous shrinkage; the unrestrained, time-depending, bulk deformation of fresh and hardening sealed concrete at a constant temperature.

Chemical shrinkage; under sealed conditions, the cement paste hydration products occupy less space than the original reactants. Chemical is the major of factors causing the autogenous shrinkage.

Drying shrinkage; when water evaporates from the fresh and hardening concrete, tensile stress build up in the capillaries causing the concrete to contract. In early stages, drying shrinkage can be defined as plastic shrinkage.

4.1 Symbols

n number of cracks of each specimen.

l length of each crack, in millimeter [mm].

w each crack average width, in millimeter [mm].

A average total crack area calculated from two ore more samples, in sqr millimeter [mm^2].

t time after mixing, in hours [h].

Δm sample weight loss due to drying, in kilogram [kg].

E sample evaporation, in kilogram per sqr meter [kg/m^2].

v air velocity, in meter per second [m/s].

RH air relative humidity, in percentage [%].

T_a air temperature, in degree Celsius [ºC]

T_c concrete temperature, in degree Celsius [ºC]

5 METHOD OF TEST

5.1 Principle

When water evaporates from the fresh concrete the concrete tends to contract, and as contraction is restrained, tangential tension develops cross section of the ring specimen. The extent of cracking depends on both the magnitude of the tensile forces and on the strain capacity of the concrete.

The concrete is cast between two concentric steel rings with diameter 300 and 600 mm with a depth of 80 mm, see *Figure 1*. The steel rings have ribs attached to provide crack initiation and are fixed to a stiff base plate with a smooth surface. After casting, the ring specimens are positioned under air funnels with a 10 mm opening between the concrete surface and the funnel along the circumference of the outer ring. The funnel is shaped to provide equal wind velocity across the concrete surface of 4.5 m/s. The test is to be performed at stabile and constant environmental conditions, where one of the samples is to be placed on a balance.

The cracking tendency is evaluated from crack length and average width measurements on the concrete top surface.

5.2 Apparatus

Required equipment and apparatus for a typical test is:

- Thermal and humidity controlled room or chamber with a constant air temperature of T=20±1ºC and relative humidity of RH=40±3%. The conditions magnitude is not absolute, but they are preferable.
- 3 complete mould setup for ring specimen, as shown in *Figure 1*.
- 3 set of air funnels, including fan and ducting, as shown in *Figure 1*.
- Balance (load cell) with manual reading or automatic recording of weight changes.
- Devices and instrumentation for manual reading or automatic recording of:
  - air velocity
  - temperature and relative humidity of air
  - concrete temperature.
- Ruler or measuring wheel graded in 1/1 mm.
- Water level.
- Stopwatch, measuring 1/1 sec.

5.3 Preparation of test specimen

5.3.1 Mould

The inner and outer steel rings are fixed on a stiff base steel plate with a smooth surface. The steel rings are to be covered with a thin layer of form oil and the base plate is not be oiled.

5.3.2 Mix

Concrete constituents by dry weight shall be recorded. Max coarse aggregate size is 16 mm.

5.3.3 Mixing

Suitable concrete mixing method, mixer and volume is to be selected and documented. No standards are available.

5.3.4 Sample

The sample size is 17 liter (x3) and is to be collected in accordance with EN 12350-1, ASTM C172 or NT BUILD 191.

5.3.5 Casting

The concrete shall be sampled from the mixer immediately after the end of mixing period. The casting of 3 ring specimens shall be accomplished within 30-45 minutes after water addition.

The specimen must completely fill the mould (to the top of the inner and outer steel ring). If needed, compaction by vibration. Top surface are to be smoothed in equal manner.

5.4 Procedure

5.4.1 Starting the test

a) One of the specimens is to be placed on the balance.

b) Each specimens horizontal position are to be ensured (if unsure, use a water level).

c) One concrete temperature sensors is to be placed in the center of the mould cross section.

d) The air funnels are to be placed in such a way that the opening between the concrete surface and the funnel edge is uniform (10 mm) along the whole circumference of the outer steel ring.

e) The fans are to be started 55 minutes after water addition. Velocity over the concrete surface are to be ensured (4.5 m/s)

f) The recording phase (time t, concrete temperature T_c, specimen weight loss Δm, air temperature and humidity T_a and RH) to be started, 60 minutes after water addition.

The test is be performed in a thermal humidity stable and controlled room or chamber with an air temperature of 20±1ºC. and relative humidity of 40±3%

The starting procedure (a-d) is to be performed within 60 minutes from water addition, if not this time is to be noted.

5.4.2 During the test

If manual reading, continuously record the time t, concrete temperature T_c, specimen weight loss Δm, air temperature and humidity T_a and RH. Enough sampling frequency is to be selected for smooth curve of temperature and weight loss development (less then 1/2 hours interval).

Visual observation of specimens throughout the 24 hours can be made in order to describe the crack development. The type, orientation and time of occurrence of cracks can then be noted.

5.4.3 Finishing the test

Recording phase (t, T_c, Δm, T_a and RH) stops. Values are to be transferred to computer for calculation and evaluation.

5.4.3 Crack measurements

The ring specimens shall normally be examined after 24 hours exposure, and surface cracks with an approximate radial orientation shall be identified and marked in an adequate way. The average widths (w) and length (l) of each crack are to be measured and recorded. The width measurements shall be performed by the use of the magnifying glass and readings by interpolation to the nearest 0.02 mm. It is recommended that a lower crack limit is 0.05 mm. The main crack pattern of each ring can be recorded by photo or sketched by drawing.

The standard procedure also includes recording of weight loss and temperature development. These parameters give useful information about the evaporation of water, and serve as a control for identical tests as well.

5.5 Expression of results

The total crack area for each ring shall be calculated as accumulated sum of each average crack width multiplied by its length. The average total crack area (A) is expressed by the average areas for 3 rings, rounded to the nearest 0.1 mm, as:

$$A = \frac{\sum_{j=1}^{3}(\sum_{i=1}^{n}(l_i \cdot w_i))}{3} \text{ [mm}^2\text{]}$$

The water evaporation (E) is calculated by the quote of weight loss (Δm) and ring surface area, as:

$$E = \frac{\Delta m}{0.212} \text{ [kg/m}^2\text{]}$$

The development of concrete temperature (T_c) and evaporation (E) with time (t) is to be presented graphically.

6 TEST REPORT

The report is shall include necessary information from among the following:

a) Document id (name, nr, test method, etc).

b) Date and time.

c) Performer id (name and address).

d) Test object id.

e) Purpose of test.

f) Concrete id (producer, recipe, etc).

g) Identification of the test equipment and instruments used.

h) Method of sampling.

i) Time from water addition to start/stop sampling and crack measuring.

j) Air velocity (v), temperature (t_a) and humidity (RH) during the test.

k) Test results: number of cracks (n), total crack area (A) and graphical presentation of concrete temperature and evaporation (t, T_c and E).

l) Relevant visually observations and personal judgments and interpretations.

m) Any deviation from the test method.

n) Inaccuracy and/or uncertainty of test results.

o) Date and signature.

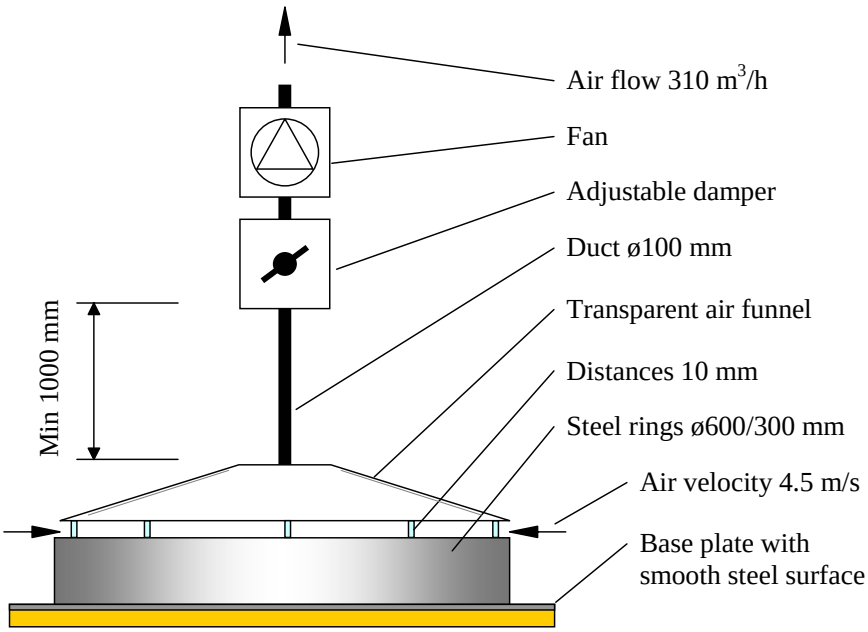

Test arangement

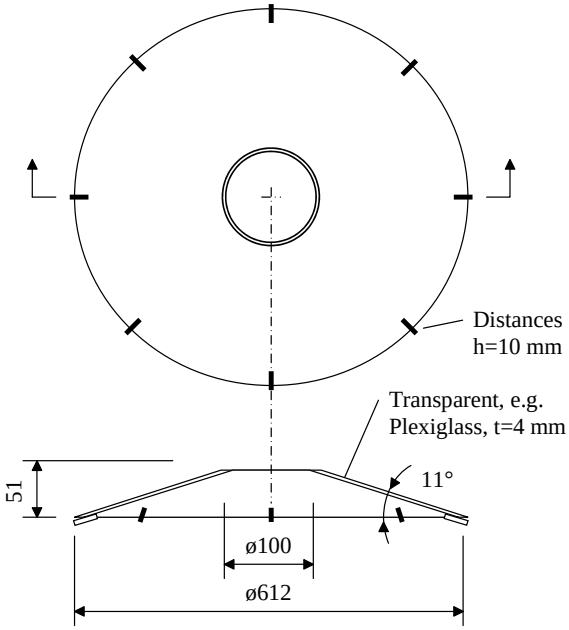

Transparent air funnel

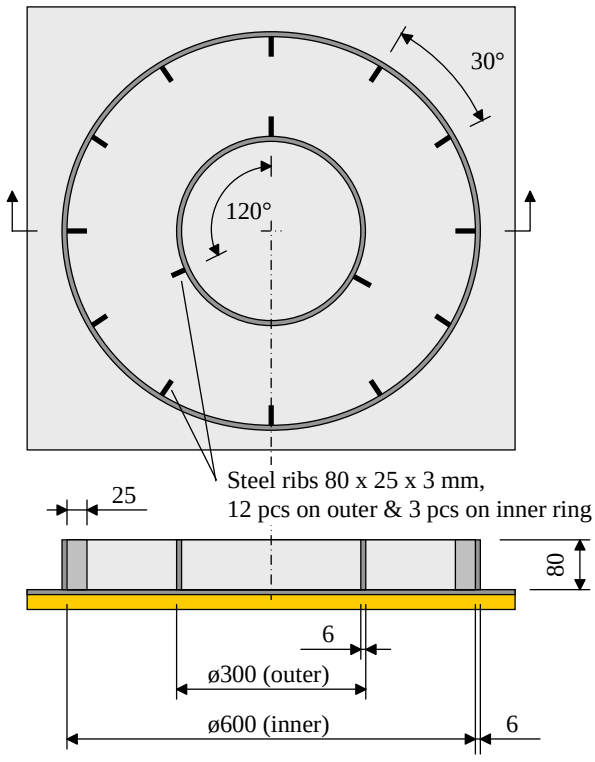

Ring mould setup

Figure 1. Principe of the concrete cracking ring test for cracking tendency measurement.